Advanced Drug Delivery Reviews 143 (2019) 177–205

Contents lists available at ScienceDirect

Advanced Drug Delivery Reviews

journal homepage: www.elsevier.com/locate/addr

Application of Förster Resonance Energy Transfer (FRET) technique to elucidate intracellular and *In Vivo* biofate of nanomedicines

Tongkai Chen [a,1], Bing He [b,d,1], Jingsong Tao [c,1], Yuan He [c], Hailiang Deng [b], Xueqing Wang [b,**], Ying Zheng [c,*]

[a] *Institute of Clinical Pharmacology, Guangzhou University of Chinese Medicine, Guangzhou 510405, China*
[b] *Beijing Key Laboratory of Molecular Pharmaceutics and New Drug Delivery System, School of Pharmaceutical Sciences, Peking University, Beijing 100191, China*
[c] *State Key Laboratory of Quality Research in Chinese Medicine, Institute of Chinese Medical Sciences, University of Macau, Macau, China*
[d] *State Key Laboratory of Natural and Biomimetic Drugs, Peking University, Beijing 100191, China*

ARTICLE INFO

Article history:
Received 29 December 2018
Received in revised form 25 February 2019
Accepted 8 April 2019
Available online 12 June 2019

Keywords:
Förster Resonance Energy Transfer (FRET)
Nanomedicines
Integrity
Biofate
Micelles
Polymeric Nanoparticles
Lipid-based nanoparticles

ABSTRACT

Extensive studies on nanomedicines have been conducted for drug delivery and disease diagnosis (especially for cancer therapy). However, the intracellular and *in vivo* biofate of nanomedicines, which is significantly associated with their clinical therapeutic effect, is poorly understood at present. This is because of the technical challenges to quantify the disassembly and behaviour of nanomedicines. As a fluorescence- and distance-based approach, the Förster Resonance Energy Transfer (FRET) technique is very successful to study the interaction of nanomedicines with biological systems. In this review, principles on how to select a FRET pair and construct FRET-based nanomedicines have been described first, followed by their application to study structural integrity, biodistribution, disassembly kinetics, and elimination of nanomedicines at intracellular and *in vivo* levels, especially with drug nanocarriers including polymeric micelles, polymeric nanoparticles, and lipid-based nanoparticles. FRET is a powerful tool to reveal changes and interaction of nanoparticles after delivery, which will be very useful to guide future developments of nanomedicine.

Abbreviations: Ag_{10}NPs, Silver decahedral nanoparticles; AgNPs, Ag nanoparticles; ABt and BDP, a molecular probe bearing the arylboronate group; CNTs, Carbon nanotubes; AuNCs@Chi, chitosan oligosaccharide lactate-functionalized Au nanoclusters; AuNPs, Au nanoparticles; AuNCs, Au nanoclusters; BODInD-Cl, semi-cyanine-BODIPY hybrid dye; BODIPY, 4,4-difluoro-4-bora-3a,4a-diaza-s-indacene; BRET, bioluminescence resonance energy transfer; BTTPF, a near-infrared-emissive conjugated polymer; CNHs, Carbon nanohorns; CoMoCAT SWCNTs, Co and Mo catalyzed single-wall carbon nanotubes; $(CPT)_2$-ss-Mal, two camptothecin molecules connected by a reduction-labile maleimide thioether bond; Cy, Cyanine; Cy3-HSA, cyanine 3-labeled human serum albumin; Cy5.5LP, lipophilic cyanine 5.5; Cy7.5LP, lipophilic cyanine 7.5; DA-TAT-PEG-PCL, 2,3-dimethylmaleic anhydride linked TAT and then conjugated to PEG-PCL; DiD, 1,1'-dioctadecyl-3,3,3'3'-tetramethylindocarbocyanine perchlorate; DiI, 1,1'-dioctadecyl-3,3,3',3'-tetramethylindocarbocyanine perchlorate; DiO, 3,3'-dioctadecyloxacarbocyanine perchlorate; DiR, 1,1'-dioctadecyl-3,3,3',3'-tetramethylindotricarbocyanine iodide; DMPE, Dimyristoyl phosphatidyl ethanolamine; ETH 2439, 9-dimethylamino-5-[4-(16-butyl-2,14-dioxo-3,15-dioxaeicosyl)- phenylimino] benzo [a] phenoxazine; FAM, fluorescein amidite; FITC, fluorescein isothiocyanate; FLIM, fluorescence-lifetime imaging microscopy; FP730, fluorescent protein; FRET, Förster Resonance Energy Transfer; H_2P, a-5-(2-aminophenyl)-a-15-(2-nitrophenyl)-10,20-bis(2,4,6-trimethylphenyl)-porphyrin; HRP, Horseradish Peroxidase; HRP-AuNCs, Horseradish peroxidase decorated Au nanoclusters; LNCs, lipid nanocapsules; mPEG-PLGA, methoxy poly(ethylene glycol)-b-poly(lactic-co-glycolic acid); $NaGdF_4$@UCNPs, up-conversion nanoparticles consist of $NaGdF_4$; NBD, 7-nitro-2,1,3-benzoxadiazole; NEs, nanoemulsions; NH_2-$NaYF_4$@SiO_2 UCNPs, silicon dioxide up-conversion nanoparticles consist of NH_2-$NaYF_4$; NIR, near infrared; NMOF-PVA, nanoscale metal-organic framework-poly (vinyl alcohol); NPCS, N-palmitoyl chitosan; OLA, oleic acid; OPV, oligo-phenylenevinylene; oxSWCNHs, oxidized Single-walled carbon nanohorns; PCL, poly(ε-caprolactone); PECT, poly(ε-caprolactone-co-1,4,8-trioxa[4.6]spiro-9-undecanone)-b-poly-(ethylene glycol)-b- poly(ε-caprolactone-co-1,4,8-trioxa[4.6]-spiro-9-undecanone) triblock copolymer; PEEP-PCL, poly(ethyl ethylene phosphate)-co-poly(ε-caprolactone); PEG-$(Cys)_4$-PDLLA, polyethylene glycol-$(Cysteine)_4$-poly(D,L-lactic acid); PEG-CA_8, polyethylene glycol-block-dendritic oligomer of cholic acid copolymers; PEG-Cys_4-CA_8, polyethylene glycol-block-dendritic oligomer of cysteine and cholic acid copolymers; PEG-DSPE, poly(ethylene glycol)-(distearoyl-snglycero-3-phosphoethanolaminen); PEG-PCL, poly(ethylene glycol)-co-poly(ε-caprolactone); PEG-PLA, poly(ethylene glycol)-b-poly(D,L-lactic acid); PEG-PLGA, polyethylene glycol-block-poly (D, L-lactide-coglycolide); PEG-PPLG, polyethylene glycol-block- poly (γ-propargyl-L-glutamate); PEG-PPS, polyethylene glycol-block-poly(propylene sulfide); PEG-PS, polyethylene glycol-block-polystyrene; PEO, poly (ethylene oxide); PEO-PS, poly(ethylene oxide)-block-polystyrene; PGA, poly (glycolic acid); PLA, poly (lactic acid); PLGA, poly (lactic-co-glycolic acid); PR, ionizable block; QDs, quantum dots; RB, Rhodamine B; SDBS-graphenes, Sodium dodecylbenzene sulfonate dispersed graphenes; SWCNTs, single-wall carbon nanotubes; TAT-PEG-PCL, trans-activating transcriptional activator conjugated to PEG-PCL; TMR, tetramethyl rhodamine; TO@UiO-66, thiazole orange loading "UiO-66" metal-organic framework; UCNPs, up-conversion luminescent nanoparticles.

* Correspondence to: Y. Zheng, Institute of Chinese Medical Sciences, University of Macau, China
** Correspondence to: X. Wang, Department of Pharmaceutics, School of Pharmaceutical Sciences, Peking University, China
E-mail addresses: wangxq@bjmu.edu.cn (X. Wang), yzheng@umac.mo (Y. Zheng).
[1] These authors contributed equally to this work.

https://doi.org/10.1016/j.addr.2019.04.009
0169-409X/

Contents

1. Introduction

In the past two decades, there has been explosive increase in publications, patents, and clinical trials related to the development of novel nanomedicines for drug delivery, imaging, and diagnosis, such as liposomes, micelles, polymeric nanoparticles, and quantum dots etc. With the extremely small particle size, nanomedicines have very high surface area for reaction and unique physiochemical properties, which provide potentially wide applications to deliver drugs with improved efficacy (e.g. long circulation *in vivo*) and reduced toxicity (e.g. stimuli-responsive targeting). Despite the rapid advancement of the nanotechnology, only few nanomedicines have entered into clinical trials and finally approved by FDA. Therefore, many articles have been published raising doubts about the 'overpromising' benefits of nanotechnology [1]. They further pointed out that the high production cost, extreme difficulty in industrial scale up, as well as the poor fundamental understanding of their interactions with biological systems, are the main challenges for the successful development of nanomedicines to bedside applications. Bourquin and coworkers have raised concerns regarding the limited number of specific, reliable, and standard analytical methods for intracellular-, tissue-, and organ-based quantification of drug nanomaterials, as lack of quantification is the main hurdle to elucidate biodistribution, clearance, and long-term fate of clinically relevant nanomaterials [2]. To address this issue, Förster Resonance Energy Transfer (FRET)-based approaches [3,4] have been successfully utilized to study the interaction of nanomedicines with biological environments to guide nanomedicine development [3,5], as well as for the visualisation of molecular signalling for biological systems [6]. Besides classical FRET-based approaches, other fluorescent probes such as near-infrared fluorophores and polymer aggregation-caused quenching (ACQ) probes [7–9], aggregation-induced emission (AIE) probes [10,11], or combination of these probes with FRET techniques [12] have also been designed to elucidate the integrity and biofate of nanomedicines after being delivered into circulation.

Resonance energy transfer was firstly observed by Francis Perrin in the early 20th century. Then in the year 1948, Theodor Förster further proposed an equation to quantify the energy transfer efficiency between fluorophores with a known distance [13], and this is where the name FRET came from. FRET chromophores represent a unique class of environment-responsive fluorophores, with the advantage of high sensitivity, good selectivity, non-radioactive, and non-invasiveness. Since FRET was first introduced as a physical process in the 1940's, this fluorescence phenomenon has been extensively explored to study biological processes. Ma and coworkers summarised three main reasons for the utilisation of FRET in biological research [14]: FRET, as a 'spectroscopic ruler', is most sensitive to changes in the distance between the donor and acceptor fluorophores, the distance range where FRET occurs matches well with the dimensions of proteins and polynucleotides, and FRET has evolved to provide real time imaging for living cells especially when FRET is combined with microscopy as FRET fluorescence-lifetime imaging microscopy (FRET-FLIM) or with atomic force microscopy (AFM) as AFM-FRET [15]. Although several excellent reviews from experts of biophysics, biology, materials science, and imaging have covered basic principles of FRET [16,17], extension to the multiple acceptors for simultaneous detection of multiple interactions [6], application for protein studies [14], as well as FRET applications on supramolecular systems [18], there still lacks a critical review and discussion from a pharmaceutical point of view to understand the effects of nanocarrier composition

and properties on the intracellular and *in vivo* biofate of drug nanocarriers (e.g. micelles, polymeric or lipid-based nanoparticles, nanocrystals, and nanoemulsions), which will be valuable for formulation and nanomedicine design in the future. Therefore, the aim of this review is to introduce the recent applications of FRET in understanding the intracellular and *in vivo* biofate of nanomedicines, including construction, stability, drug release behaviour, disassembly kinetics, elimination, and the nano-bio interactions with lipids, proteins, and cells within microenvironments *in vivo*. Herein, we firstly present the basic principle of FRET and the commonly used donor and acceptor fluorophores in drug nanocarriers. We next describe the design strategy and application of FRET in nanomedicine, their release and interaction within cells during the uptake and transport process, their integrity, *in vivo* release, and pharmacokinetics after being delivered by various delivery routes in mouse and zebrafish.

2. Theory of FRET

2.1. Conditions for FRET to occur

FRET involves a nonradioactive, resonant transfer of electronic excitation energy from a donor fluorophore in the excited state to an acceptor molecule in the ground-state, depending upon the near-field interaction between them [19]. FRET requires a very particular set of prerequisites for its occurrence. The primary requirement for FRET is the integral overlap between the fluorescence emission spectrum of the donor molecule and the fluorescence excitation spectrum of the acceptor molecule, in order to generate enough energy for dipole–dipole coupling (Fig. 1). An overlap of more than 30% is the minimum condition for an efficient, accurate, and reliable detection of FRET [20]. The secondary requirement for FRET is a close distance (1-10 nm) between the donor molecule and the acceptor molecule (Fig. 1).

If a pair of fluorophores has met the specific criteria of FRET, the donor's excitation may lead to the acceptor's emission (F_{FRET}), while simultaneously quenching the fluorescence of the donor (F_D). As shown in Fig. 1, in order for FRET to occur, several constraints must be met. For instance, the donor's emission has to excite the acceptor, in which case F_D should overlap partially with the excitation spectrum of the acceptor fluorophore (ε_A). Briefly, the quantification of overlap can be expressed

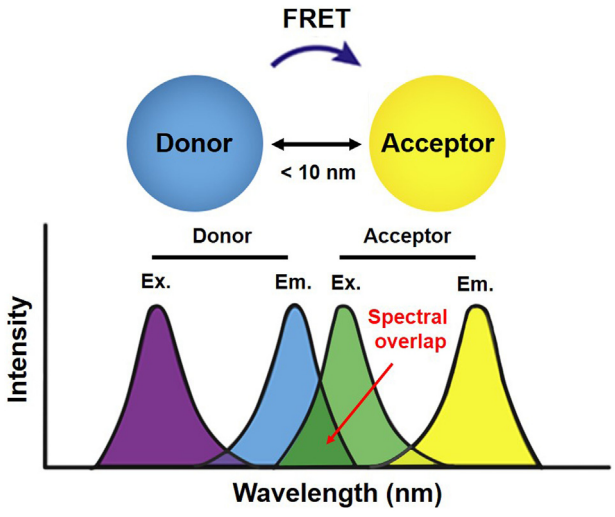

Fig. 1. Specific requirements for the detection of FRET signals. The spectra of donor molecule emission (*Em.*) are overlapped with the spectra of acceptor molecule excitation (*Ex.*). The efficiency of FRET appears to be the highest when the energy transferred from *Em.* to *Ex.* is fallen within 10 nm in a parallel orientation. Adapted with permission from [21]. Copyright (2017) Elsevier.

by J (normalised spectral overlap integral; units $M^{-1}cm^{-1}nm^4$; Eq. 1) [22].

$$J(\lambda) = \frac{\int_0^\infty F_D(\lambda)\varepsilon A(\lambda)\lambda^4 d\lambda}{\int_0^\infty F_D(\lambda)d\lambda} \quad 1$$

FRET efficiency (E) is calculated by dividing the excitation of donor that caused FRET by the total excitation of donor plus the actual distance between fluorophores (r) to the power of six (see Eq. 2) [23].

$$E = \frac{R_0^6}{R_0^6 + r^6} \quad 2$$

R_0 (or known as Förster distance) indicates the distance at which E is equal to 50% of the excitation of donor that results in energy transfer to the acceptor (see Eq. 3) [24].

$$R_0 = 0.0211\left(J\Phi_D\kappa^2 n^{-4}\right)^{1/6} \quad 3$$

where κ^2 is estimated as 2/3 of the free (unbound) dyes, n represents the refractive index between donor and acceptor molecules, depending on the composition, size, and structure of the nanocarrier and the location of donor and acceptor molecules.

Due to the close relationship between FRET efficiency and donor-acceptor pair distance, FRET has been used in a wide variety of fields [25–27]. In the field of nano-drug delivery, FRET can offer a comprehensive information of nanomedicines including nanomedicine design *in vitro* stability, intracellular drug release as well as their *in vivo* biofate during nano-bio interaction processes [28–30].

2.2. Donor-acceptor selection

Classic FRET fluorophores are listed in Table 1. These fluorophores are originally used as membrane tracers, such as 3,3′-dioctadecyloxacarbocyanine perchlorate (DiO), 1,1′-dioctadecyl-3,3,3′, 3′-tetramethylindocarbocyanine perchlorate (DiI), 1,1′-dioctadecyl-3,3,3′3′-tetramethylindocarbocyanine perchlorate (DiD), and 1,1′-

Table 1
Summary for fluorophores discussed in this review

Fluorophore	Wavelength range of excitation (nm)	Wavelength range of emission (nm)	λ_{ex}[a] (nm)	λ_{em}[b] (nm)	ε[c] ($L\cdot mol^{-1}\cdot cm^{-1}$)
DiO	350-550[d]	475-650[d]	484[f]	501[f]	154,000[g]
DiI	400-605[d]	530-700[d]	549[f]	565[f]	148,000[g]
DiD	495-700[d]	600-800[d]	644[f]	665[f]	264,000[g]
DiR	500-830[d]	720-900[d]	750[f]	779[f]	270,000[g]
Cy3	402-610[d]	499-740[d]	555[e]	570[e]	150,000[e]
Cy5	400-700[d]	600-800[d]	646 [e]	662[e]	250,000[e]
Cy5.5	510-750[d]	635-800[d]	673[e]	707[e]	209,000[e]
Cy7	500-850[d]	700-850[d]	750[e]	773[e]	199,000[e]
Cy7.5	546-900[d]	750-890[d]	788[e]	808[e]	223,000[e]
Alexa Fluor 488	400-600[d]	475-680[d]	490[f]	525[f]	72,000[g]
Alexa Fluor 546	360-674[d]	530-700[d]	556[f]	573[f]	112,000[g]
BODIPY-FL	400-550[d]	470-640[d]	503[e]	509[e]	80,000[e]
BODIPY-TR	448-600[d]	515-700[d]	589[e]	616[e]	69,000[e]
FITC	300-540[d]	480-675[d]	490[g]	525[g]	78,000[g]
Coumarin 6	350-505[d]	450-750[d]	467	502	\
Rhodamine B	440-585[d]	520-760[d]	555[f]	580[f]	\

[a] Excitation peak.
[b] Emission peak.
[c] Peak extinction coefficient.
[d] Data obtained from https://searchlight.semrock.com.
[e] Data obtained from https://www.lumiprobe.com.
[f] Data obtained from https://www.biotech.iastate.edu.
[g] Data obtained from https://www.thermofisher.com.

dioctadecyl-3,3,3′,3′-tetramethylindotricarbocyanine iodide (DiR). Due to their short excitation wavelengths and poor tissue penetration, DiO and DiI are mostly applied *in vitro* at cellular level. DiD and DiR, active in the near infrared (NIR) region, possess the advantages of minimal interference of absorbance and fluorescence from biological samples and improved tissue penetration depth, due to which they are widely used *in vivo* (e.g. mouse and zebrafish models).

Cyanine (Cy) dyes (e.g. Cy3, Cy5, Cy5.5, Cy7, and Cy7.5) offer higher fluorescence stability, better separation from autofluorescence and less cell damage than other common dyes such as fluorescein isothiocyanate (FITC), Coumarin 6, and Rhodamine B. However, their fluorescence spectra and quantum yield are influenced by undesirable aggregation, non-specific protein binding, and unwanted photobleaching [31,32]. In addition, due to their positive charge [33], Cy dyes tend to accumulate in specific organelles (e.g. mitochondria) resulting in a negative FRET phenomenon.

A number of alternatives to the bulky Cy dyes are commercially available, such as Alexa Fluor 488 and Alexa Fluor 546, which possess increased solubility, environmental stability, and brightness.

Various 4,4-difluoro-4-bora-3a,4a-diaza-s-indacene (BODIPY) dyes (e.g. BODIPY-FL and BODIPY-TR) have been widely developed because of their photostability and sharp absorption and emission spectra [34]. However, the properties of high hydrophobicity and Stokes shifts of these dyes might be a problem in FRET measurements.

FRET pairs of these dyes applied *in vitro* and *in vivo* are listed in Table 2. Generally, the environment that nanomedicines encounter in cells and *in vivo* is more complex than that *in vitro*. At cellular level, endocytic organelles (with different pH, enzymes, and so on) must be taken into consideration in the selection of appropriate FRET fluorophores. Fluorophores with excellent sensitivity, desirable tissue penetration depth, and low fluorescence background are preferred for their applications *in vivo*, such as DiD/DiR, Cy5.5/Cy7, and Cy5.5/Cy7.5. Recently, increasing attention has been paid to the use of upconversion nanomaterials [35], quantum dots (QDs) [36], polymer dots [37], carbon dots [38] and AIE dots [39,40] as FRET pairs, which will be described in section 3.1.3.

2.3. FRET measurements

There are many different methods to measure FRET, such as sensitised emission, acceptor photobleaching, fluorescence-lifetime imaging microscopy (FLIM), spectral imaging, and polarisation anisotropy imaging [19]. At present, fluorescence spectrometer, fluorescence microscopy, confocal laser scanning microscopy (CLSM), *in vivo* imaging system (IVIS), and spectrum imaging system are commonly utilised to evaluate the FRET efficiency *in vitro* and *in vivo*. In this section, sensitised emission, acceptor photobleaching, and FLIM-FRET will be introduced briefly.

2.3.1. Sensitised emission

The fundamental principle of intensity-based FRET measurements is primarily based on the response of the acceptor emission to the donor emission. For intramolecular FRET-based sensor, image acquisition is performed on the fluorescence signals of donor and FRET, and subsequently calculated as the FRET ratio. The calculation of FRET ratio is relatively similar to the formula of FRET efficiency (E) (see Eq. 4).

$$E = \frac{F_{FRET}}{F_{FRET} + F_D} \quad (4)$$

The acquisition and processing of *in vivo* FRET images is relatively complex, which is attributed to the concentration and localisation of donor and acceptor molecules as well as the correction for acceptor excitation bleaching and donor emission bleed-through. Thus, multiple controls and correction factors are required for the calculation of a corrected FRET image [55]. Nevertheless, there are some advantages of this method, especially its applicability in a wide variety of fields and different types of microscopes. Moreover, this method could be applied to live-cell imaging for studying dynamic cellular events, due to its rapid image acquisition, depending upon the microscope configuration.

2.3.2. Acceptor photobleaching

The most direct method for FRET detection is through acceptor photobleaching. The fluorescence emission of donor is enhanced by the selective depletion of acceptor via photodestruction, presuming that the absorption of acceptor could be abolished through photobleaching. A high fluorescence intensity of donor emission could be used as a reliable indicator, by comparing the images of donor emission before and after acceptor photobleaching. Here, FRET efficiency E is dependent upon the donor fluorescence intensity, in the presence (I_{DA}) and in the absence of the acceptor (I_D), as depicted in Eq. 5.

$$E = 1 - \frac{I_{DA}}{I_D} \quad (5)$$

This may be obtained prior to and after acceptor photobleaching with the same sample to prevent donor concentration changes, as fluorophore concentration affects the intensity. This approach has been used with a wide variety of microscopes. However, acceptor photobleaching possesses several disadvantages. It is highly destructive, requires longer analysis times, and it is only applicable on fixed sample preparations. Moreover, the donor may be depleted by this method. Despite these limitations, acceptor photobleaching is the first key step in FRET imaging, owing to its rapid information acquisition to compare the differences between experimental samples.

2.3.3. FLIM-FRET

FLIM is a method for measuring the lifetime of fluorescence, by using time-domain or frequency-domain methods [56]. Meanwhile, in FRET, the lifetime of the donor fluorescence is reduced concomitantly with the donor quenching in the presence of suitable acceptor. Here, E is dependent upon the ratio of the donor fluorescence lifetimes in the presence (τ_{DA}) and absence of the acceptor (τ_D) (Eq. 6).

$$E = 1 - \frac{\tau_{DA}}{\tau_D} \quad (6)$$

FLIM-FRET overcomes the difficulties that are related to intensity-based approaches and are suitable for measurement of live cells with a good time-resolution. The significant advantages of FLIM-FRET include, but are not limited to, the requirement of only donor imaging, independence of sample concentration, and high stability against photobleaching. Nonetheless, the fluorescence lifetime of FLIM-FRET may be influenced by several environmental factors, including pH, refractive index of the solution, and the presence of ions. FLIM is time-consuming and requires specialised instruments for both time- and frequency-domain measurements. In addition, numerous fluorophores display multi-exponential decay curves in live cells, which necessitates complex data analysis.

Table 2
Common donor-acceptor FRET pairs for drug delivery

In vitro	*In vivo*
DiO/DiI [5,28,41,42]	DiO/DiI [28,43]
DiI/DiD [44,45]	DiD/DiR [46]
Cy3/Cy5 [47]	DiI/DiD [44]
FITC/Rhodamine B [48]	Cy5.5/Cy7 [49]
Coumarin 6/DiI [30]	Cy5.5/Cy7.5 [50]
Alexa Fluor 488/Alexa Fluor 546 [51]	DiO/Rhodamine B [52]
Alexa Fluor 488/Cy5 [53]	Coumarin 6/DiI [30]
BODIPY-FL/BODIPY-TR [54]	\

3. Design strategy and application of FRET in nanomedicine

FRET has been used to assess microcosmic interactions at nanoscale due to its high sensitivity to the donor's fluorescence intensity, excited state lifetime, and distance between fluorophores. Over the past two decades, owing to the increased production of fluorophores and the rapid development of fluorescent microscopy, FRET has made it possible to deeply investigate biological processes including protein-protein interactions [57], conformational alterations of stimulated receptor and membranes [58,59]. With the development of new materials, especially nanomaterial-based fluorophores, FRET has been intensely utilised in the field of nanomedicine to monitor the interaction of nanomedicines with biological environments as well as to visualise the biofate of nanomedicines in biological systems. Indeed, biomedical research in nanomedicine is a multi-disciplinary area, and as a bridge, it links up material/chemistry and biology/medicine. FRET is becoming more and more important in this area.

3.1. FRET design in nanomedicine possesses distinct properties

Compared to classical FRET in biological applications, its participation in nanomedicine opens a new avenue in nano-bio interaction investigations and expands the choices of fluorophores [3]. Thus, the design and use of FRET in nanomedicine offers its own distinct advantages.

3.1.1. FRET in analysis of structural features

Fluorophores can be directly conjugated with polymeric materials to explore the structural features of nanomedicines. In the development of nanomedicines, the assembly of polymers causes a reduction of intermolecular distances. When using a single fluorescent molecule or multiple FRET pairs as probes, the reduced distance can trigger homo-FRET or hetero-FRET [60,61], in which the altered spectrum and fluorescence lifetime can be used as an 'ON/OFF' switch to detect the structural dynamics of nanomedicines in the fabrication process (Fig. 2A). Conversely, when the nanomedicine enters the body and encounters different tissue microenvironments, their integrities could also be monitored with FRET (Fig. 2B) [62]. Recently, development of microenvironment-sensitive nanomedicines have paid much attention to their 'intelligent' characteristics, which increases the targeting efficiency of nanomedicines by responding with high sensitivity to extrinsic mediators (e.g. light, sound, and magnetism) or intrinsic effects (e.g. enzyme, pH, and reducibility) [63–66]. As a sensitive 'ON/OFF' reporter, FRET is now gradually becoming the standard technique for the evaluation of 'intelligent' nano delivery systems.

Efficient drug loading and release are the key points for successful development of nanomedicines. By physically loading appropriate fluorescent pairs, FRET can be utilised to evaluate the dynamic processes during drug loading and release (Fig. 2C) [51]. Besides, FRET between fluorescent drug and nanocarrier can also be employed in monitoring drug loading and release by conjugating nanocarriers with fluorescent labels (Fig. 2D) [12,67]. In this context, an enhanced FRET efficiency indicates successful drug loading, while reduced FRET efficiency is associated with drug release.

Furthermore, based on the high sensitivity of FRET efficiency for the assessment of intermolecular distance and orientation, it is reasonably inferred that FRET can identify and distinguish fine structures in nanomedicines (Fig. 2E), such as homogeneous mixtures, core-shell or multilayer structured nanomedicines. Some pioneering work has been conducted in this field [68].

3.1.2. FRET in the investigation of nano-bio interactions

Nanomedicines and biological molecules can be simultaneously labelled with FRET pairs to detect nano-bio interactions. Compared to the pharmacological actions of small molecular drugs, protein regulatory pathways of nanomedicines are more complicated [69]. FRET can be used as an efficient tool for the accurate analysis of protein complexes and the discovery of potential targeting receptors. As shown in Fig. 2F, FRET efficiency can be assessed by conjugating fluorophores, forming FRET pairs, to nanomedicines and specific proteins, respectively [70]. If the labelled protein binds to nanomedicines with high affinity, the acceptor fluorescence intensity and therefore FRET efficiency increases, thus indicating that the protein is a target of the nanomedicine. Interestingly, this FRET strategy can also be used for the study of known protein-protein interactions [71]. In this context, nanomaterials usually act as an amplifier to increase the fluorescence signal derived from the protein-protein interaction. This method is often used for the design of biosensors to test the trace biological components [72,73]. Similar to nano-protein interactions, the impact of nanomedicines on lipid membranes can also be analysed by FRET (Fig. 2G). However, the selected hydrophobic probes are usually dissolved and flow in lipid bilayers but are not fixed to a certain location as in protein labelling [74]. In addition, partial environment-sensitive lipid dyes are used and combined with FRET to investigate the effect of nanomedicines on membrane conformation [75].

3.1.3. Application of novel nanomaterial-based fluorophores

Compared to canonical FRET in the biomedical field, more nanomaterial-based fluorophores are being incorporated into nanomedicine for studying their *in vitro* or *in vivo* fate [76]. In contrast to the usually implemented small molecular probes, some nanomaterials can act as both drug carriers and fluorophores, due to their specific nanostructures. These nanomaterials are mainly developed from inorganic materials, such as semiconductor quantum dots (QDs) [77], metal organic frameworks, and up-conversion luminescent nanoparticles (UCNPs), etc [78–80]. Table 3 summarises the common fluorescent nano entities and their FRET-based biomedical applications. As a typical example, QDs have been comprehensively utilised in nanomedicine study because of their high extinction coefficients and brightness [77]. By varying their size and composition, QDs can have a wide range of wavelengths, narrow photoemissions, and multiple functionalisation sites, making them very suitable for imaging analysis including FRET.

Additionally, it is worth noting that some nanomedicines endow FRET with other distinct properties, in which the acceptor's fluorescent intensities are significantly amplified (Fig. 2H) or attenuated (Fig. 2I) due to the effects of nano-structures. For instance, some metal nanostructures have been observed to enhance the fluorescence intensity of organic fluorophores or QDs, a phenomenon termed metal-enhanced fluorescence. Li et al. [81] designed a sensor for target cell imaging based on silver decahedral nanoparticles (Ag_{10}NPs), which largely enhanced the fluorescence intensity of FITC. Hong and co-workers [82] have reported similar functions for gold substrates. Some nanomaterials can also attenuate fluorescence signals as "superquenchers", which are generally used to reduce background signals (e.g. graphene oxide, gold nanoparticles) [83]. For example, Li et al. [84] reported a graphene-based molecular beacon (MB) for homogeneous DNA detection. In this system, graphene oxide significantly reduced the background fluorescence of MB, further improved signal-to-background ratio and, consequently, sensitivity of DNA detection. In summary, these specific nanomaterials can deliver drugs as carriers while expanding the selection of FRET pairs and increase the accuracy of FRET technology for the evaluation of diagnosis and therapeutic applications of nanomedicine.

3.2. The FRET technology works in multiple stages of nanomedicine delivery process

As one of the important discoverers of FRET, Förster demonstrated that the transfer efficiency in FRET depends on the inverse of the sixth-power of the distance between the donor and acceptor [105], which indicates energy transfer between fluorophores is highly

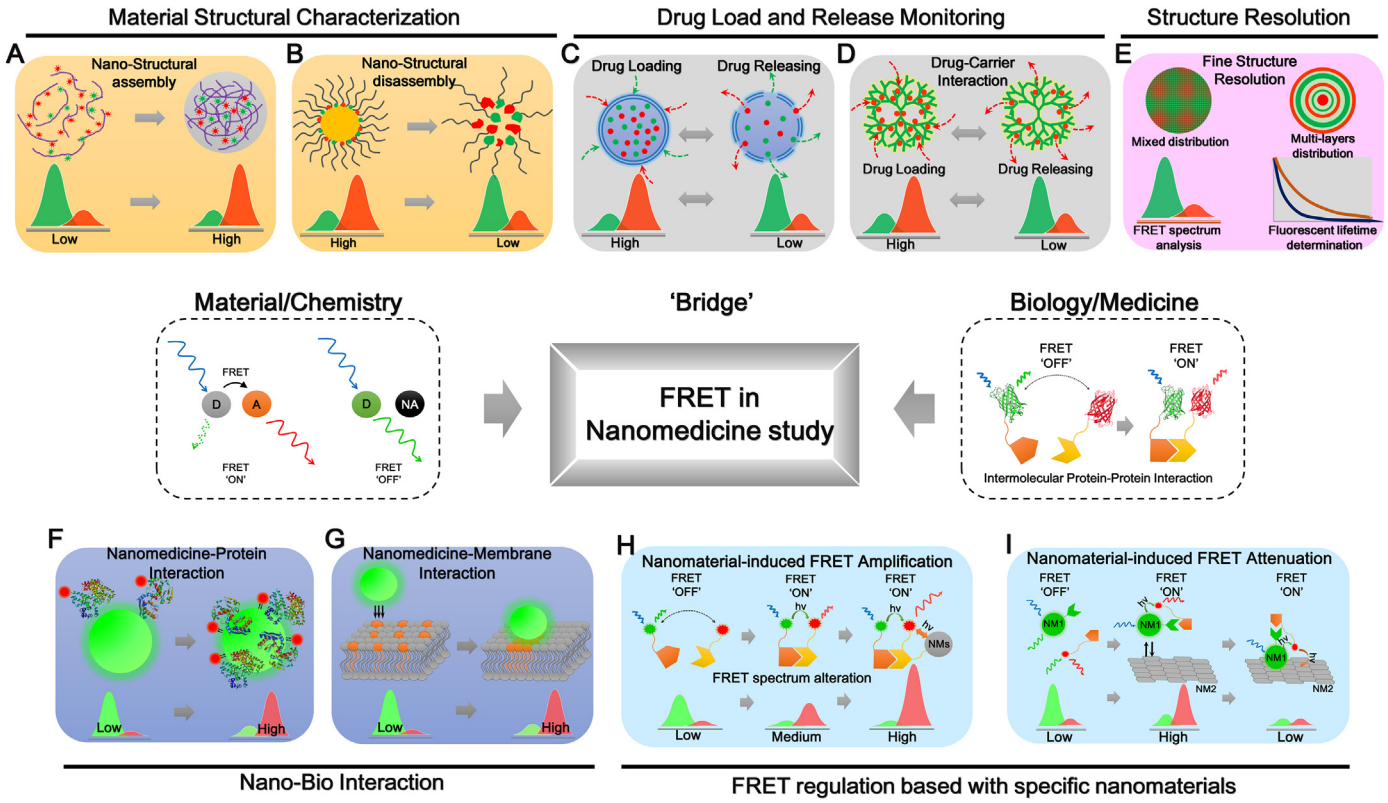

Fig. 2. Nanomedicine is an interdisciplinary field which links up material/chemistry and biology/medicine, endowing the FRET design in nanomedicine possessing its own distinct properties. (A) The fluorophores in FRET pair can be conjugated with polymeric materials in nanomedicines to monitor the nano-structure assembly. The spectrum enhancement of acceptor fluorescence indicates the successful construction of nanomedicines. (B) Vise versa, FRET strategy can also be used to investigate whether nanomedicines maintain the structure integrity in biological environment. Once the nanomedicines disassemble, the FRET efficiency will significantly reduce owing to the increase of distance among polymers. (C, D) The drug loading and release behaviors in nanomedicines can be monitored by labeling the loaded drug with appropriate fluorophore in FRET detection to illuminate the drug loading and release rate (C) and material-drug interaction (D). (E) The microcosmic structures of nanomedicines can be resolved by FRET because different nanostructure shows distinguished FRET efficiency and fluorescent lifetime. (F, G) When nanomedicines and biological ingredients, like proteins (F) and membrane (G), are labeled with different fluorophore to form FRET pair, the nano-bio interactions can be explored by means of the FRET efficiency determination. (H, I) Some nanomaterials can directly regulate the characteristics of energy transfer via their own elemental feature and nanostructure. Based on the difference of nanomaterials, the energy transfer and the resulted fluorescent signal can be amplified (H) or attenuated (I), which endow nanomedicines with multiple functions.

sensitive to micro spacing. Importantly, it means that the changes in intermolecular distance in nanomedicine study can be characterised via FRET, as long as these molecules are labelled with appropriate fluorophores in FRET pairs. Notably, these distance-associated processes encompass both the synthesis and biodistribution of nanomedicines. Therefore, as a versatile strategy, FRET can be applied in multiple scenarios in nanomedicine research.

3.2.1. Nanomedicine construction

Most nanomedicines, especially those constructed by 'bottom-up' strategies, are assembled by polymeric unimers through weak interactions, including hydrophobicity, electrostatic attraction, π-π interaction, hydrogen bonding, etc [108]. When the polymers are labelled with FRET probes, the construction process of nanomedicines can be monitored by assessing the energy transfer efficiency that is closely related to the distance between molecules (Fig. 3A). For example, Magnusson et al. [106] designed a micellar nanoparticle based on DNA conjugates for the recognition of nucleic acid sequence. In this nano system, two partially complementary oligonucleotides were separately labelled with fluorescein and black hole quencher 1 (BHQ-1) as a FRET pair. The fluorescence was quenched when the oligonucleotides combined, which indicated the successful construction of nanoparticles. By addition of a complementary strand and sequence-specific unshielding of the ligand, FRET was disrupted, and fluorescence could be detected (Fig. 3B).

Besides, FRET can also be used to identify microscopic structures. Mandal et al. [109] reported a method of studying micelle-to-vesicle morphologic transitions based on ultrafast FRET. Rhodamine 6G and Coumarin 153 were chosen as a FRET pair in their work. The increasing timescale of FRET indicated the increasing distance between donor and acceptor which led to a further identification of the conversion of microstructures during micelle-to-vesicle transitions. In particular, in recent years, biomimetic nanocarriers based on natural biomembranes have been found to display long circulation and targeting effects [110]. Lipid fusion is an indispensable method for the functional modification of materials during the fabrication of these nanocarriers. FRET is an efficient tool for the monitoring and evaluation of membrane fusion by using liposoluble fluorophores as FRET pairs. For instance, Sato et al. [111] engineered a novel biomimetic nanocarrier by realising membrane fusion of exosomes with liposomes, and the efficiency of exosome and liposome fusion was quantitatively evaluated with a FRET assay using a set of NBD- and rhodamine-labelled lipids.

3.2.2. Nanomedicine stability

In addition to the 'static' characterisation of the nanomedicine preparations as previously described, the dynamic process of synthesis can also be investigated via FRET-based strategies (Fig. 3A). As an example, Azcárate and co-workers [112] used FRET to monitor the stability of polymer-coated QDs dispersed in solvents with different polarities *in vitro*. In their work, QDs emitting 550 nm were chosen as donors and coated with a polymer containing a quencher molecule and a

Table 3
The common fluorescent nanomaterials and their biomedical applications via FRET

FRET-associated nanomaterials	Composition	Morphological characterization	Examples				
			Nanoparticles	Spectrum characterization	FRET pairs	Application	Ref.
Quantum dots (QDs)	Semiconductor nanocrystals, mainly consisting of II-VI group elements	Quasi-zero-dimensional colloidal nanocrystals	CdSe–ZnS QDs	λex: 450 nm, λem: 560 nm	QSY-9,	For the design of a maltose biosensor	[85]
			QD_{490}	λex: 405 nm, λem: 490 nm	ETH 2439	For the design of a ratiometric potassium Sensor	[86]
			CdTe QDs	λex: 380 nm, λem: 530 nm	AuNPs	For the detection of a tumour marker (carcinoembryonic antigen)	[87]
Metal organic frameworks (MOFs)	Coordination network consisting of metal ions or clusters coordinated to organic ligands	Porous nanoparticles with densely packed oriented structure	NMOF-PVA	λex: 340 nm, λem: 420 nm	ABt, BDP	For the design of a ratiometric peroxynitrite sensor	[88]
			TO@UiO-66	λex: 510 nm, λem: 560 nm	CuO nanoparticles	For the detection and imaging of H_2S in living cells	[89]
Upconversion nanomaterials (UCNPs)	Lanthanide nanocrystals	Nano-size crystalline host matrix containing Lanthanide ions	$NaGdF_4$@UCNPs	λex: 980 nm, λem: 365 nm	Azobenzene	For the bioimaging of tumours	[90]
			lanthanide-doped @UCNPs	λex: 980 nm, λem: 365 nm	2'-nitrobenzyl photocage group	For the design of a metal ion probe in cells and zebrafish (Zn^{2+})	[91]
			NH_2-$NaYF_4$@SiO_2 UCNPs	λex: 980 nm, λem: 543 nm	AuNPs	For the detection of acetamiprid	[92]
Au nanoparticles (AuNPs)	Colloidal gold	nano-size colloidal gold nanoparticles	50 nm AuNPs	Fluorescence quenching	UCNPs	For the design of an organophosphorus pesticides nanosensor	[93]
			20 nm AuNPs	Fluorescence quenching	Cy3, Cy3B	For the detection of the protein cardiac troponin T	[94]
			13 nm AuNPs	Fluorescence quenching	Rhodamine B	For the detection of Mercury (II) in aqueous solution	[95]
Au nanoclusters (AuNCs)	Gold atoms stabilized by small molecules or polymers	Gold atom clusters with ultra-small size (<2 nm)	AuNCs@Chi	λex: 405 nm, λem: 535 nm	Cy1	For the detection of H_2S	[96]
			HRP-AuNCs	λex: 365 nm, λem: 650 nm	HRP-AuNCs	For hydrogen peroxide sensing	[97]
Ag nanoparticles (AgNPs)	Nanoparticles consisting of silver or silver oxide	Silver nanocrystals with various shapes	Silver triangular nanoplates	Fluorescence quenching	QDs	For the design of a virus antigen sensor	[98]
			Ag_{10}NPs	Fluorescence enhancing	FITC, BHQ-1	For target cell imaging	[81]
Carbon nanotubes (CNTs)	Cylindrical carbon molecules	Cylindrical nanostructure	CoMoCAT SWCNTs	Fluorescence quenching	Nile blue A	Expected to be used for molecular diagnostics and *in vitro* and *in vivo* imaging	[99]
			SWCNTs	Fluorescence quenching	CdSe-ZnS QDs	-	[100]
Graphenes	Reticular carbon molecules	Two-dimensional carbon crystal with one atom thickness	SDBS-graphenes	Fluorescence quenching	FAM	For the detection of thrombin	[101]
			Graphene oxide	λex: 400 nm, λem: 547 nm	AuNPs	For the design of an immuno-biosensor for pathogen detection (rotavirus)	[102]
Carbon nanohorns (CNHs)	Conoid carbon molecules	A high-aspect ratio subset of fullerenes with closed cage structure	CNHs	Fluorescence quenching	H_2P	-	[103]
			oxSWCNHs	Fluorescence quenching	FAM	For the detection of thrombin	[104]

secondary emitting molecule (Alexa Fluor 647). FRET occurred when polymers correctly assembled on the surface of the QDs, owing to the appropriate donor-accepter distance. When polymers were stripped from the QDs, FRET was disrupted and the fluorescence signal of QDs could be detected easily. Notably, the design of environment-sensitive nanomedicines aims to maximise the therapeutic effect of the loaded drugs. These 'intelligent' nanomedicines can respond to the microenvironment, and then release drugs at a specific spatio-temporal site, protecting drugs against degradation, and avoiding side effects [113]. Intriguingly, FRET can directly monitor the dynamics of drug release. Miteva and co-workers [51] investigated the intracellular drug release of micelles by co-loading dsDNA molecules separately labelled with the FRET pair Alexa Fluor 488 and Alexa Fluor 546 in micelles. They used FRET signals to visualise the process of drug release at the cellular level. FRET signal was higher when the pair of fluorescent molecules was entrapped in micelles, and it decreased when the fluorescent molecules were released.

3.2.3. Biofate

Efficient delivery to target organs or cells is a key point of biomedical applications of nanomedicines. Thus, exploration of the fate of nanomedicines during the delivery process is essential for the assessment of therapeutic efficiency. As shown in Fig. 3A, from macroscopic to microcosmic, the process of nano delivery mainly involves three stages, including tissue distribution, cellular transport, and molecular interaction [114]. Nanomedicines have different biological behaviours at each stage due to the changed microenvironments [115]. Similar to the 'static' characterisations (such as the evaluation of structural

A

FRET in Nanomedicine Study

Characterization

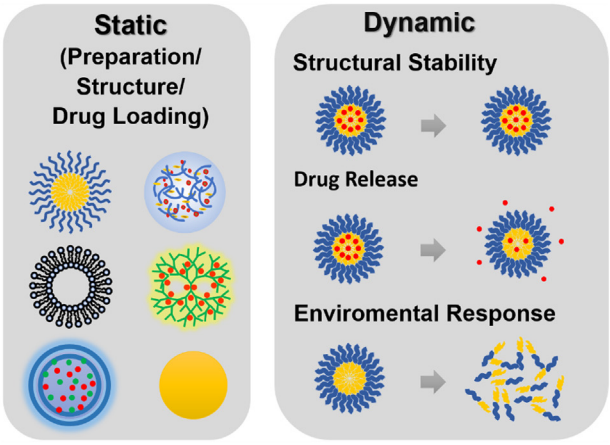

Molecular Interaction

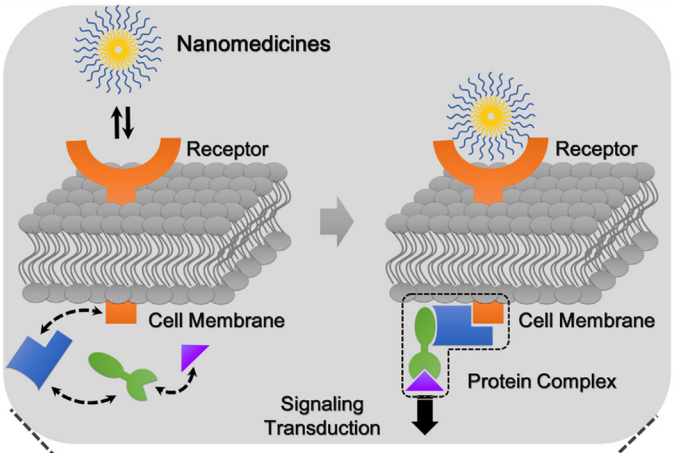

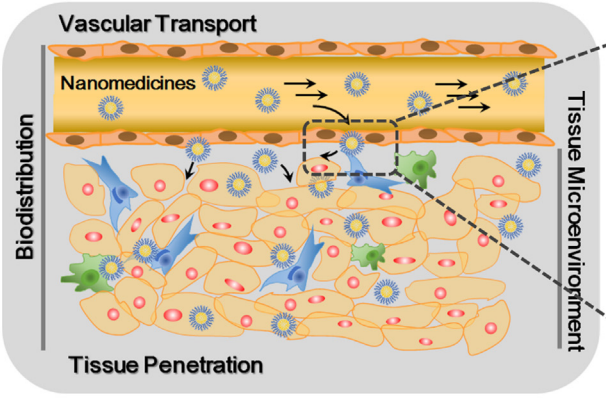

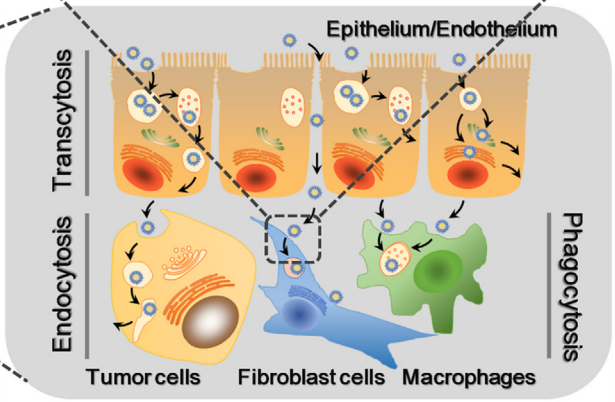

Tissue Distribution

Cellular Transport

B

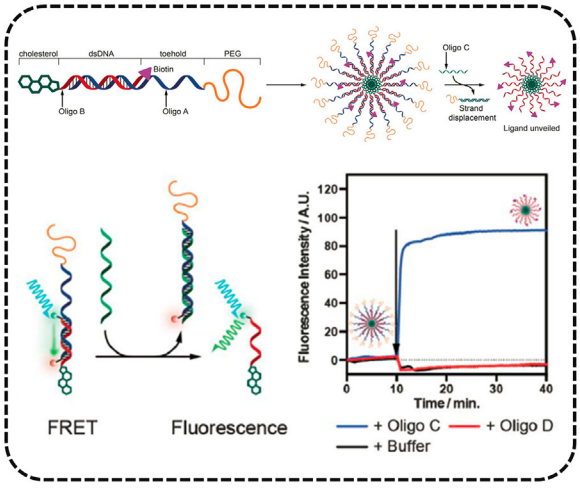

C

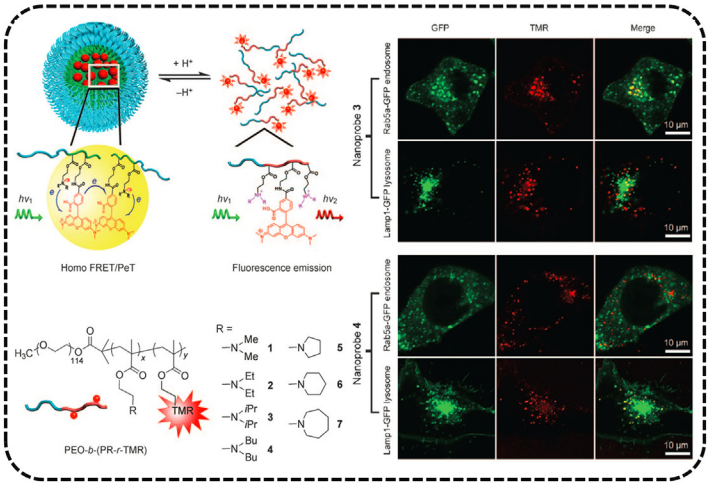

characteristics or the drug loading of nanomedicines), 'dynamic' characterisations (such as the evaluation of the structure stability, drug release or the environmental response of the nanomedicines) *in vitro* along with the structural changes of nanomedicines in tissues and cells can be detected by FRET. However, more factors need to be carefully considered when using FRET to examine the biofate of nanomedicines, because physiological environments in tissues and cells are more complicated than those encountered *in vitro*. Abundant research in nanomedicine has focused on FRET to improve its accuracy and sensitivity for better diagnostic and therapeutic applications [116,117]. For instance, Bouchaala et al. [118] described a methodology for monitoring the integrity of lipid nanocarriers *in vivo* by FRET. Cy 5.5 and Cy 7.5 were selected as a FRET pair and were co-encapsulated in lipid nanocarriers. The use of near infrared fluorescent dyes enhanced the tissue penetration of FRET signals and allowed the monitoring of the biofate of nanocarriers *in vivo*.

Additionally, in cellular studies, most nanomedicines enter cells via vesicle-mediated pathways and undergo a pH gradient as they move from endosomes to lysosomes. FRET is highly sensitive to these changes in cellular environments. As a typical example, Wang et al. [107] utilised a series of 'ultra-pH-sensitive' (UPS) nanoparticles containing FRET-paired fluorophores to detect the maturation of endosomes in HeLa cells. The fluorescence of the donor was quenched when UPS nanoparticles were in the micelle state and recovered after micellar disassembly at a responsive pH. In this nano system, FRET signals reflect the structural change in nanoparticles, revealing the maturation process of endosomes (Fig. 3C). Nevertheless, these few examples do not cover the multiple applications of FRET to the complex and diverse biofates of nanomedicines. Therefore, we will further expand and highlight these studies in the following sections.

3.3. General design strategies of FRET in nanomedicine

Based on the theory of FRET, nanomedicine can be tactfully designed according to its different applications. The selection of donor and acceptor should be considered firstly. The spectral overlap between donor emission and acceptor excitation is a necessary condition for FRET and appropriate spectral overlap makes it easier and more sensitive to detect FRET signals. Some intelligent designs of FRET can also be achieved through proper donor/receptor selection in according with its applications in nanomedicine. For example, some liposoluble fluorophores could be used as FRET pairs for the study on nanomaterial-biomembrane interaction because of their diffusivity from nanomaterials to lipid membranes [46]. The sufficient tissue penetration of FRET signals is necessary for monitoring the biofate of nanocarriers *in vivo*. So, some near infrared fluorescent dyes (Cy 5.5, Cy 7.5) [118] or nanomaterials (UCNPs) [90] are more suitable to be selected as FRET pairs in the research. In addition to traditional FRET pairs, some special fluorophores with aggregation-caused quenching (ACQ) or aggregation-induced emission (AIE) properties are alternative in the design of FRET in nanomedicine. Some pioneering work has been conducted in this field [12,97].

The appropriate distance between donor and acceptor is an important guarantee for FRET to occur. The distance variation between donor and acceptor can directly changes FRET signals. The nano-size of nanomaterials makes it easier to keep the donor and the receptor close enough together. In the design of nanocarriers based on FRET, FRET pairs could be physically entrapped in nanocarriers or conjugated with nanocarriers or drugs covalently, then the FRET of drug-drug [51], drug-carrier [12,67] can be observed when nanocarriers are structured stably. When the structure of drug loading nanocarriers changes, the distance of FRET pair changes, resulting in the variation of FRET signals. This can be used in monitoring drug release and integrity of nanocarriers [51,118]. By labelling nanocarriers and environmental substances with FRET pairs respectively, FRET turns on when the donor and acceptor are close enough, and this strategy is frequently utilized in studies on nano-bio interaction [70,74]. It is worth mentioning that the FRET process is not limited on the intermolecular but also intramolecular FRET process. In this case, FRET occurs by connecting donor with acceptor in a molecular and the variation of distance of FRET pair can be implemented by breaking the linkers or changing molecular conformation [12,84,119].

The conversion strategy of FRET "on/off" should also be considered in the design of FRET nanosystems. FRET turns on when: (a) the existence of donor and acceptor; (b) the appropriate distance between donor and acceptor, and turns off when any of the conditions is not satisfied. Accordingly, numerous of methods of converting FRET "on/off" are design in applications of FRET in nanomedicine. Firstly, the conversion of FRET "on/off" can be implemented by destroying or recovering the donor-acceptor system. When nanocarriers containing FRET pair are exposed to environments *in vitro* or *in vivo*, the donor or acceptor can interact with some substances in the environment (e.g. H_2S [89], GSH [119]) and change its spectral properties, resulting in the conversion of FRET "on/off". This method is usually employed in trace substance detection or stimuli-responsive imaging and drug release. The variation of distance between donor and acceptor can also cause the conversion of FRET "on/off", so several methods based on this can be utilised in the design of FRET in nanomedicine. The physical diffusion of FRET pairs entrapped in nanocarriers can cause the separation of donor and acceptor, resulting in FRET turns off [46]. In addition, the structure variation of nanocarriers can change the distance between donor and acceptor and lead to the conversion of FRET signals, such as the assembling or disassembling of nanocarriers. It is often used to monitor the construction and integrity of nanocarriers *in vitro* and *in vivo* [51,111,118]. In some FRET systems designed in nanomedicine, the maintenance of distance between donor and acceptor relies on a proper linker. In these systems, the destruction or recovery of linker can cause the conversion of FRET signals (from "on" to "off" or from "off" to "on"). The type of linkers could be either chemical connection (e.g. chemical bonds, small molecular) [88] or biological connection (e.g. protein, nucleic acid) [98]. Besides, some design of FRET system based on macromolecule can also change the distance of FRET pair by conformational change, resulting in the conversion of FRET signals [84]. By combining with the construction of nanomaterials, the conversion of FRET signals can be more intelligently implemented. Nanocarriers constructed with stimuli-responsive materials can change their structures in different environments, which causes the conversion of FRET "on/off" [107]. This design strategy can be utilized in tumor imaging and monitoring nanomedicine intracellular transport. Also these stimuli-responsiveness can be involved in the design of linkers between donor

Fig. 3. FRET works in multiple stages of nanomedicine delivery process. (A) FRET as a versatile technology can be utilized throughout the whole studies of nanomedicines, from preparation and characterization to the biofate analysis including tissue distribution, cellular transport and molecular interaction with biomembranes (B) The construction and dynamics of nanomedicines can be characterized by FRET strategy. As an example, DNA conjugate micelles were fabricated. Functionalization of one DNA conjugate strand with a biorecognition ligand results in shielding of the ligand when in the micelles, while encoding of the DNA sequences with overhangs allows supramolecular unpacking by addition of a complementary strand and sequence-specific unshielding of the ligand. When the DNA strand was labeled with FRET probes, the molecular assembly/disassembly and 'on–off' switch of the recognition signal is visualized by FRET pair signaling, allowing direct and amplified readout of nucleic acid sequence recognition. Adapted with permission from [106]. Copyright (2014) Royal Society of Chemistry. (C) The biofate of nanomedicines can be sensitively monitored via the FRET effect among fluorescent labeled polymer materials. A pH-activatable micellar nanoprobes were prepared by using the PEO-b-(PR-r-TMR) copolymers as the schematic design. At pH>pKa of ammonium groups, the neutralized PR segments self-assemble into the micelle cores, leading to quenching of fluorophores by homo FRET mechanisms. Upon pH activation (pH<pKa), formation of charged ammonium groups results in micelle dissociation into unimers with a dramatic increase in fluorescence emission. The subcellular location showed that different nanoprobes could accurately indicate the alteration of pH microenvironments during the endocytosis process. Adapted with permission from [107]. Copyright (2011) John Wiley and Sons.

and acceptor [88] or conformational variation [101]. By conditions responsively varying linkers' situation and conformation, the conversion of FRET signals can be implemented. These design strategies have been widely utilized for trace substance detection *in vitro* and *in vivo*.

4. Intracellular fate of nanomedicines by FRET

When nanomedicines are administrated by various routes, the environment that nanomedicines encounter within the cells (e.g. cell surface proteins, endocytic organelles, and pH) is more dynamic and rigorous than that encountered *in vitro*. At the cellular level, nanomedicines firstly interact with cell membranes and are then taken up into the cells, transported in endosomes and different organelles, and finally transported across the cells. Even though some intact nanocarriers are internalised into cells, most of them may suffer from disassembly, degradation in lysosome, and releasing the drug in cytoplasm, which makes it hard for transcellular transport. It is well known that free drugs from disintegrated nanocarriers are different from drugs encapsulated in nanocarriers, which results in differences in cellular pharmacokinetic profiles. Therefore, the elucidation of the intracellular fate of nanomedicines is meaningful for the development of nanomedicines. Many characterisation approaches such as dynamic light scattering (e.g. particle size, distribution, and zeta potential measurements), microscopy (e.g. transmission electron microscope, AFM, and CLSM), and spectroscopy (e.g. ultraviolet–visible spectroscopy, Fourier transform infrared spectroscopy, and nuclear magnetic resonance) can investigate the overall structure of nanocarriers or individual components but not their integrity and structural changes. However, FRET is a very powerful technique to detect the static and dynamic characterisations of nanomedicines in cells (described in detailed in section 3). For this reason, FRET is widely applied to study the intracellular fate of nanomedicines, such as interaction with cell membranes, intracellular itinerary and co-localisation, intracellular integrity monitoring, and transcellular integrity monitoring.

4.1. Interaction with cell membrane

Interaction with cell membrane is the first step for nanomedicines during cellular internalisation. FRET is able to evaluate this process, helping to understand the mechanisms underlying cellular internalisation. Polymeric micelles are core–shell nanoparticles that have been widely used as drug delivery vehicles. When the polymeric micelles are close enough to the cell membrane, FRET can monitor whether micelles fuse with cell membranes or whether drug is released during the fusion process. Xiao and colleagues performed FRET to evaluate the cellular uptake and release of poly(ethylene glycol)-b-poly(D, L-lactic acid) (PEG-PLA) polymeric micelles incorporating Nile red (M-NIR) [120]. Fig. 4A depicts the phenomenon of FRET between the DAF (5-dodecanoylaminofluorescein)-inserted cell membrane (donor) and M-NIR (acceptor). To monitor the *in vitro* drug release of PEG-PLA micelles and verify whether the micelles can interact with cell membrane, A2780 human ovarian cancer cells were incubated with DAF, M-NIR, and their combination. The images of DAF, FRET, and Nile red channels were visualised and acquired using confocal microscope. Interestingly, the fluorescence emission of DAF increased in the DAF channel, and the fluorescence emission of Nile red similarly increased in the Nile red channel (Fig. 4B). On the contrary, with the combined stimulation of DAF and M-NIR, the fluorescence intensities of FRET and Nile red channels increased, whereas the fluorescence intensity of DAF channel reduced. Besides, the FRET ratios of all the randomly selected regions were elevated from 0 to approximately 0.5 over time (Fig. 4C). These results indicate that M-NIR interacted with the cell membrane and releases the drugs rapidly into the cell membrane.

In addition, Zou and colleagues have developed a FRET method for noninvasive *in vitro* monitoring of drug release from PEO-PS (poly (ethylene oxide)-block-polystyrene) nanoparticles [46]. To evaluate whether nanoparticles remain intact in the cell medium, the PEO-PS nanoparticles carrying two different lipophilic dyes (with DiO as donor and DiI as acceptor), at a close proximity of less than 10 nm, were synthesised. FRET signals are generated from the excessive accumulation of DiO and DiI in the cell membranes of MDA-MB-231 cells. The FRET ratio of PEO-PS nanoparticles is higher in the cell membranes than in the medium, indicating that DiO and DiI are rapidly released from PEO-PS nanoparticles into extracellular space. The higher FRET ratio in the cell membranes may be partially attributed to the excessive accumulation of the two free dyes on the cell surface and the closer proximity between them. Moreover, they also incorporated oleic acid-coated iron oxide nanoparticles into the PEO-PS nanoparticles to inhibit the release of unbound dyes, from the nanoparticles into medium, thus transferring more dyes for interaction with the cell membranes [46].

FRET is also often employed to identify the interactions between nanocarriers and cell surface proteins. For instance, Zhao et al. synthesised Ag nanoparticles conjugated with sgc8 aptamer (Apt-AgNPs) and employed FRET to detect the protein-specific cell surface sialylation [121]. CCRF-CEM cells were labelled with Cy5 and treated with Apt-Cy3-AgNPs, specifically tethered to the cell-membrane protein tyrosine kinase-7 (PTK7). Strong FRET signals were detected on the cells with PTK7, which signified the specificity of Apt-Cy3-AgNPs for PTK7 and thereby their utility for the imaging analysis of PTK7 expression sites on the cell surfaces.

4.2. Intracellular itinerary and co-localisation

The second step in nanoparticle internalisation is the endocytosis of nanomedicines into cells and transport across endosomes and different organelles. FRET can be used to track their itinerary in cells, which may help us to understand the fate of nanomedicines after cellular internalisation. After endocytosis, as the nanomedicines travel from early endosomes to late endosomes to lysosomes, they encounter a continuous pH change from 7.2 (extracellular environment), to 6.0-6.5 (early endosomes), to 5.0-5.5 (late endosomes), and finally 4.0-4.5 (lysosomes). In Wang's lab, they developed a series of pH-specific nanoparticles to investigate the functional range of organelles [122]. In the applications of drug delivery, endosomes are the first intracellular organelles encountered after nanocarriers are internalised into cells (endocytosis) [123]. Many nanocarriers are developed to release the therapeutic drugs in early endosomes and thus to get away from the degradation in lysosomes [124]. However, investigation of endosome/lysosome biology using the traditional approaches, suffer from undesirable effects encountered in acidic organelles. The use of FRET can be applied for evaluating the intracellular itinerary and localisation of nanocarriers in different organelles.

In a recent study, Chen et al. have utilised N-palmitoyl chitosan bearing a Cy5 moiety (Cy5-NPCS) to synthesise a pH-responsive nanocarrier for an efficient delivery of doxorubicin (DOX) to cancer cells [25]. In their research, at a pH ≥ 7, the donor (DOX) and the acceptor (Cy5) are in a close proximity for FRET to occur. At a low pH, the amine groups in Cy5-NPCS are protonated, resulting in the FRET pair to separate from each other. After treatment of HT1080 cells with Cy5-NPCS nanoparticles for 30 min, fluorescence is only observed in the first channel (Cy5), indicating high FRET efficiency in the caveolae/caveosomes (Fig. 5). After incubation for 1 h, the intensity of Cy5 markedly decreases with a weak fluorescence of DOX in the cytosol (the second channel in Fig. 5), suggesting the swelling of nanoparticles. At 4 h, no fluorescence of Cy5 was observed (the third channel in Fig. 5, FRET off) due to the trafficking of nanoparticles into the late endosomes/lysosomes (more acidic organelles). However, the strong signal of DOX was observed in the cytosol, indicating that DOX was released from Cy5-NPCS nanoparticles into the cytosol. Over time (12-24 h), DOX fluorescence was observed and accumulated in the cell nuclei. Taken together, the findings

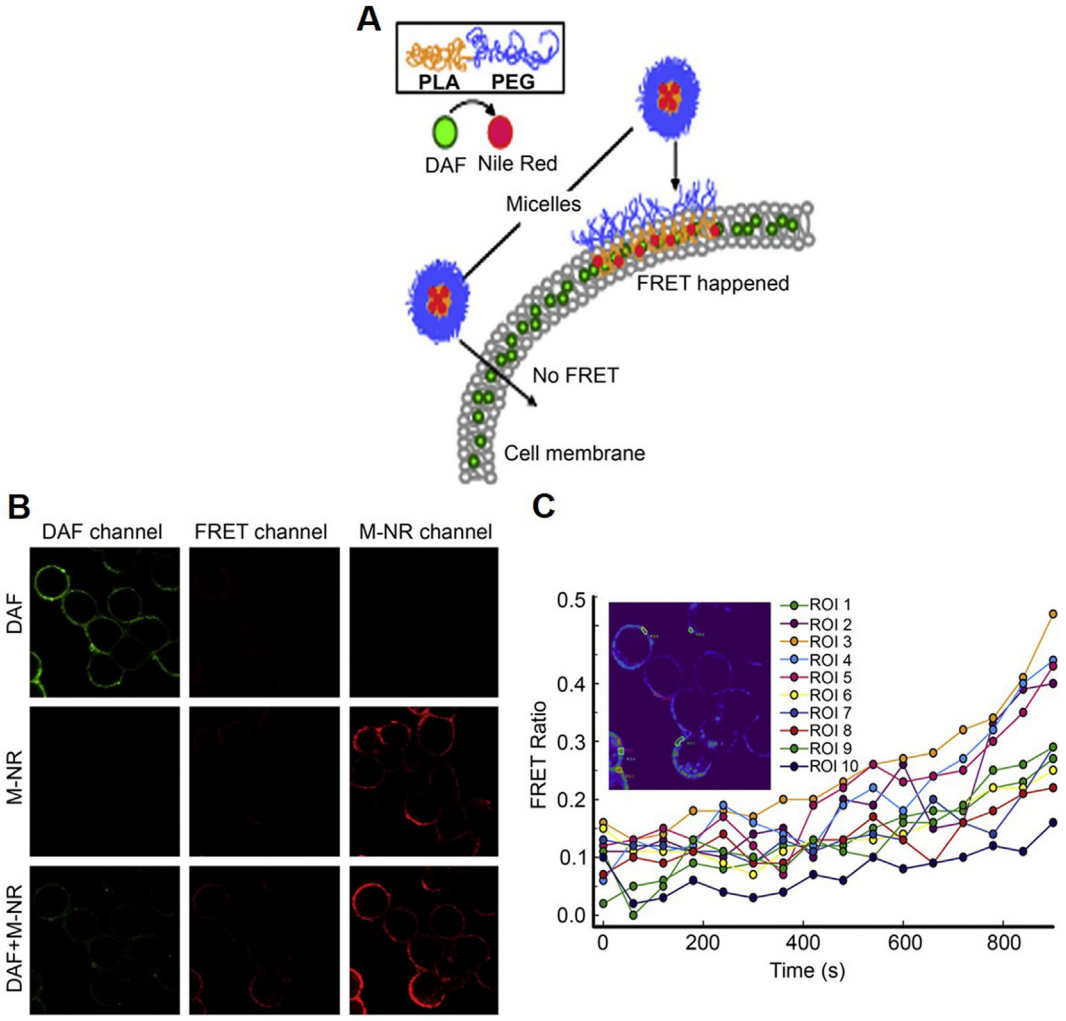

Fig. 4. The FRET signals analyzed using cell membrane labeled with DAF and polymeric micelles with core-loaded Nile red (M-NIR). (A) Illustration diagram of FRET between cell membrane containing DAF (donor) and PEG-PLA polymeric micelles loaded with Nile red (acceptor). FRET is triggered by the release of Nile red from the micelles onto the cell membrane, meanwhile the distance between the two dyes is close enough. (B) The images of FRET signals in A2780 cells treated with DAF, M-NIR and their combination. Top row: 1.4 mM DAF; middle row: 0.2 mg/ml M-NIR; and bottom row: 1.4 mM DAF followed by 0.2 mg/ml M-NIR. The intensities of DAF (excitation 488 nm; emission 520-550 nm), FRET (excitation 488 nm; emission 570-630 nm) and Nile red channels (excitation 543 nm; emission 570-630 nm) were visualized under confocal microscopy. (C) FRET ratios for the selected ROI from 1 to 10 of the cells with both DAF and M-NIR treatments. Adapted with permission from [120]. Copyright (2011) Elsevier.

suggested that DOX fluorescence is initially observed from the NPCS nanoparticles trafficking across the slightly acidified environment of the early endosomes. Subsequent to their transport into late endosomes/lysosomes, DOX was released into the cytosol and then steadily accumulated in the nuclei, resulting in cytotoxicity.

In order to improve biocompatibility as well as sensitivity of a FRET system, Chen et al. employed the CdZnSeS/ZnS alloy core/thick-shell QDs as donor for FRET-based applications [125]. The red fluorescence from FRET after excitation of the donor QDs was detected on the HeLa cell membrane, following treatment for 1 h. Additional FRET signals were observed after 4 h of treatment as the positively-charged sensor could augment cellular uptake and internalisation (Fig. 6A). Furthermore, huge yellow spots (merged green QDs donor fluorescence and red FRET acceptor fluorescence) were visualised, indicating that QDs-PEG-PDDLG/Cy3-HSA sensor remained almost intact after 4 h. As the rapid lysosomal escape ability is a key prerequisite for a prospective protein carrier, the fluorescence images of cells incubated with QDs-PEG-PDDLG were studied. Green, red, and blue colours correspond to fluorescence of QDs-PEG-PDDLG, lysosomes, and nuclei, respectively, whereas yellow regions designate the merged green QDs-PEG-PDDLG and red lysosomes. Following 2 h of treatment, the colocalisation of QDs-PEG-PDDLG with lysosomes was demonstrated by the yellow spots in the cell interior (Fig. 6B). As the incubation time increased (4 h), CLSM images displayed weak red fluorescence and dispersive green fluorescence with no yellow fluorescence, indicative of the escape ability of the carriers. The lysosomal escape of QDs-PEG-PDDLG could be attributed to the pH-dependent protonation of diethylenetriamine moieties in the polymer ligand side chains. Additionally, a biocompatible and nontoxic FRET probe was reported by Kulkarni and Jayakannan [126], wherein, a π-conjugated oligo-phenylenevinylene (OPV) fluorophore was selected as the FRET donor and conjugated with the PCL triblock copolymer. This copolymer self-assembled as <200 nm spherical NPs (FRET donor) and could encapsulate Nile red (FRET acceptor) to form the OPV-NR FRET probe, which was rapidly taken up by cancer cells and internalised in the cytoplasm and peri-nuclear environment [126]. Lee and colleagues developed a QD-FRET pair by attaching QDs to PEI and Cy5 to small interfering RNA (siRNA) [127]. When incubation with QDs-PEI/Cy5-siRNA complexes in human prostate carcinoma (PC-3) cells, QDs-PEI/Cy5-siRNA complexes were located in endosomes until 2 h treatment. After treatment for 2 h, Cy5-siRNA was dissociated from QDs-PEI/Cy5-siRNA complexes, and unpacked QDs-PEI and Cy5-siRNA were observed in the endosomal compartment. After treatment for 6 h, siRNA was completely released and sequestered in the cytoplasm.

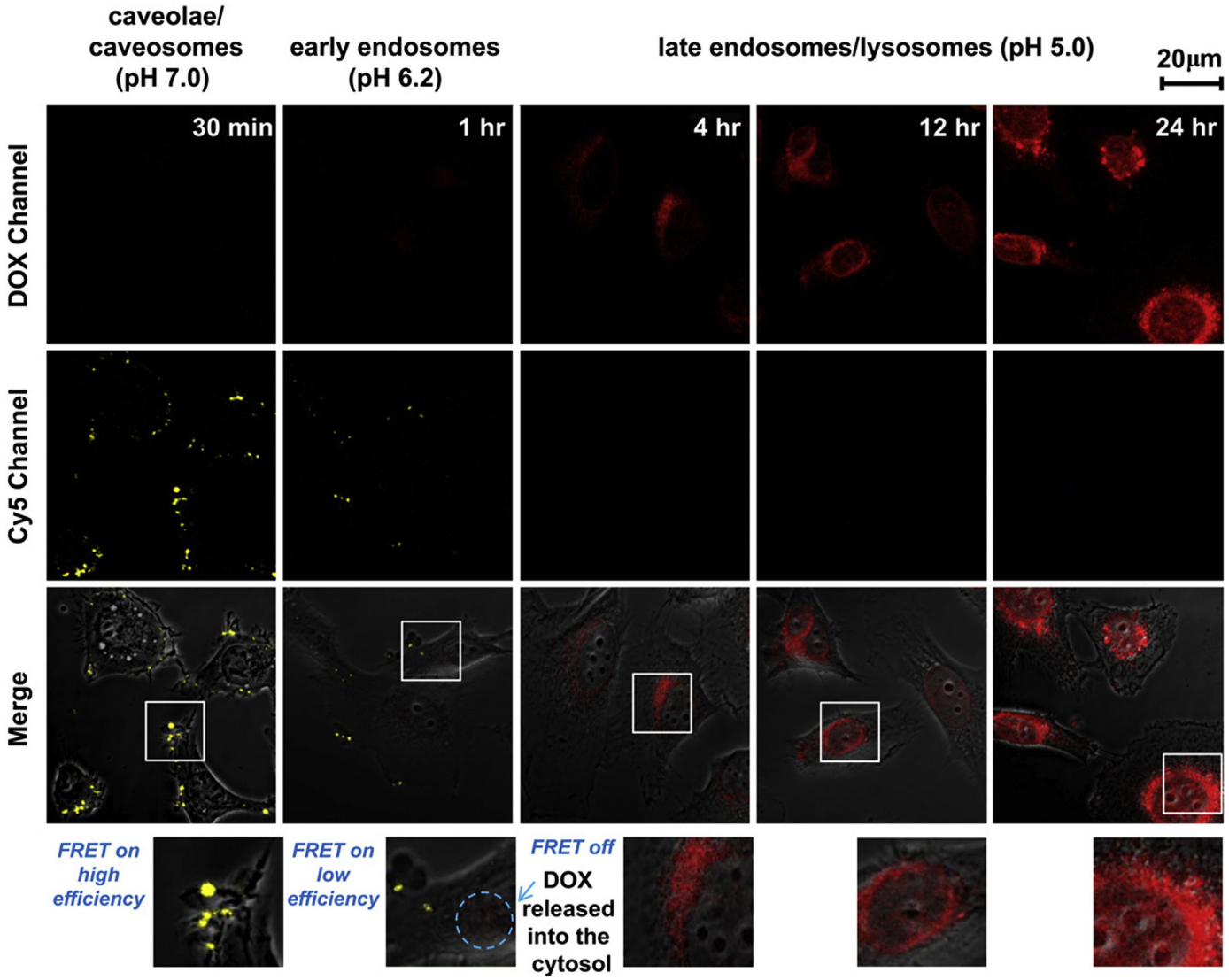

Fig. 5. Fluorescence images of HT1080 cells after treatment with DOX-loaded Cy5-NPCS nanoparticles. The optical window between 560-600 nm represents the fluorescence intensities of DOX (donor), whereas the optical window between 600-700 nm represents the fluorescence intensities of Cy5 (acceptor). Adapted with permission from [25]. Copyright (2011) Elsevier.

4.3. Intracellular integrity monitoring

After internalisation into cells, nanomedicines interact with different organelles (endosomes, lysosomes, endoplasmic reticulum, and Golgi apparatus etc.). Whether nanomedicines remain intact or dissociate in cells directly governs the efficacy of drugs. Most nanomedicines are designed to improve systemic circulation, to prevent drug release in cells or drug release from nanomedicines at inappropriate sites, as it also affects the treatment efficacy. FRET has also been introduced for intracellular integrity or release behaviour monitoring, based on the approximate distance needed for FRET to occur. Selected applications related to the intracellular integrity of nanocarriers, analysed by FRET, are listed in Table 4. The FRET fluorescence pairs are loaded into various nanocarriers (e.g. micelles, polymeric nanoparticles, nanocrystals, nanoemulsions, and mesoporous silica nanoparticles) and observed after treatment with cells. FRET pairs are primarily loaded into the hydrophobic domains of nanocarriers. While in some studies, one of the fluorophores is conjugated with the polymer and interacts with the other one in hydrophobic domains of nanocarriers. Among these studies, DiO/DiI FRET pair is most widely used for incorporation in the nanocarriers, possibly due to its stability and efficient energy transfer ability. Meanwhile, the *in vitro* FRET evaluation of nanomedicines is mainly performed on cell models including MDCK cells, Caco-2 cells, KB cells, MDA-MB-231 cancer cells, and HeLa cells. FRET signal is detected by different techniques, but most frequently by CLSM to monitor the intracellular behaviours.

Several studies have reported FRET analysis by loading both DiO and DiI into the micelle core, in order to assess the intracellular integrity, upon interaction with cells [41,42,128,129]. Under the conditions, where micelles are intact, FRET can be detected at the excitation wavelength of 484 nm (donor) and the emission wavelength of 565 nm (acceptor). Following the dissociation of micelles, an increased emission of donor at 501 nm and a reduced emission of acceptor at 565 nm are observed, indicating the longer distance between DiO and DiI. Our group has synthesised three amphiphilic polymers containing hydrophilic and hydrophobic blocks, namely, poly(ethyl ethylene phosphate)-co-poly(ε-caprolactone) (PEEP-PCL), poly(ethylene glycol)-co-poly(ε-caprolactone) (PEG-PCL), and poly(ethylene glycol)-(distearoylsnglycero-3-phosphoethanolaminen) (PEG-DSPE), in order to synthesise different micellar systems [42]. Additionally, we have evaluated the effects of the polymer structures on the mechanism of nanoparticle internalisation and transport across epithelial cells. Using FRET, we found that all the micellar systems are shown to be intact within 4 h.

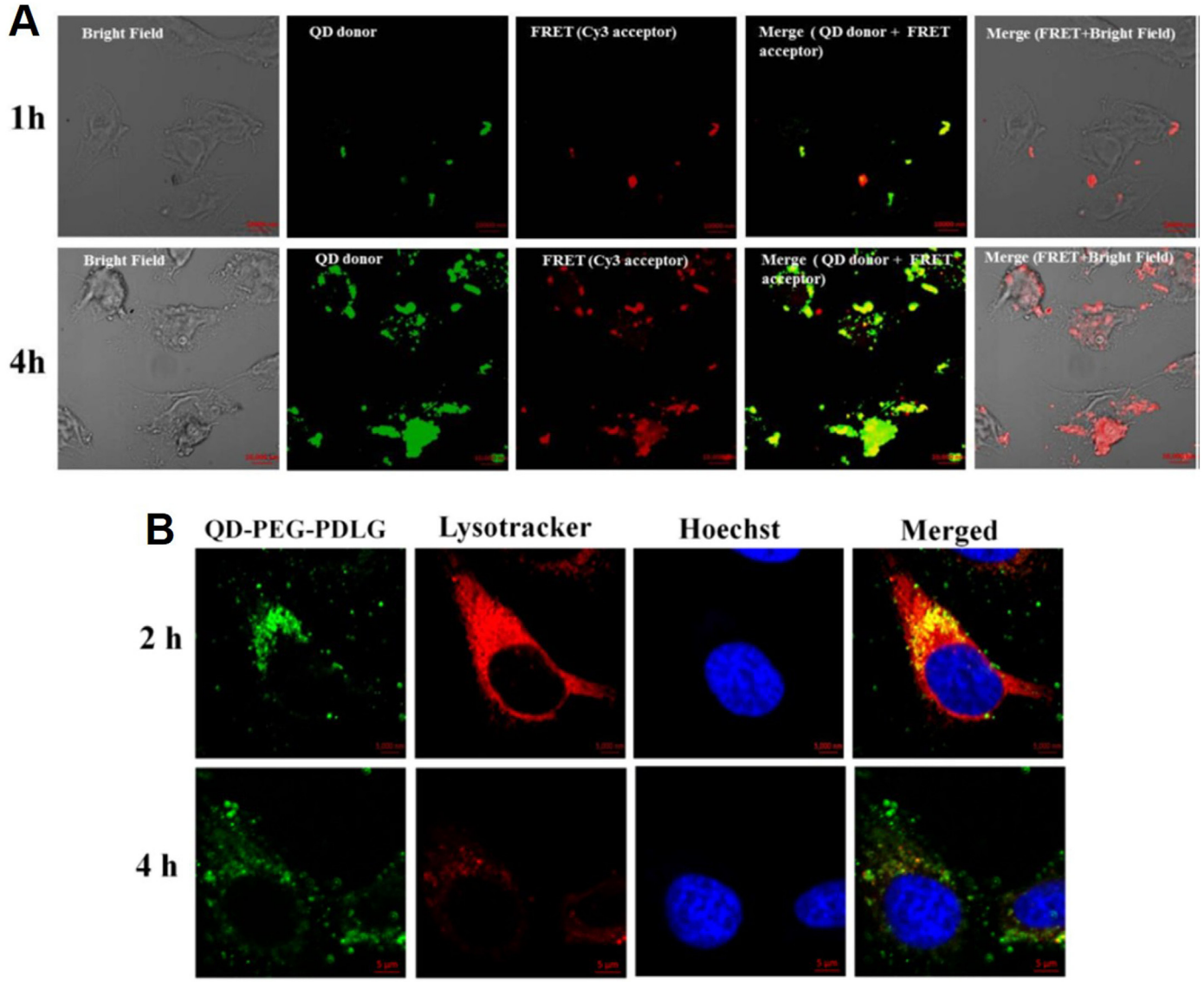

Fig. 6. (A) Fluorescence images of HeLa cells after treatment with QDs-PEG-PDDLG/HSA-Cy3 FRET sensors for 1 and 4 h. Left to right: bright field, donor QDs fluorescence, red-FRET fluorescence, merge images (QDs donor + Cy3 acceptor), and merge images (FRET + bright field). Scale bar: 10 μm. (B) Fluorescence images of HeLa cells after treatment with QDs-PEG-PDDLG for 2 and 4 h. Lysotracter Red and Hoechst were used to stain lysosomes and nuclei, respectively. The yellow fluorescence represents colocalization of QD-PEG-PDDLG (green) and lysosomes (red). Scale bar: 5 μm. Adapted with permission from [125]. Copyright (2016) American Chemical Society.

Furthermore, PEG-DSPE micelles demonstrate the most active and rapid transport, followed by PEG-PCL and PEEP-PCL, in the undifferentiated Madin-Darby canine kidney (MDCK) cells (for endocytosis and exocytosis analyses) and the differentiated MDCK monolayers (for transcytosis study).

In addition to intact micelles, stimuli-responsive nanocarriers have received increasing attention over the past decade, especially in the field of cancer therapy. For instance, Guo and colleagues have developed pH-triggered polymeric micelles for targeted anti-tumour drug delivery [119]. In the study, camptothecin (CPT) is transformed into $(CPT)_2$-ss-Mal dimer, and the FRET signals generated from the interaction between CPT molecules and reduction-labile maleimide thioether bond are used for intracellular monitoring of drug release. The blue fluorescence channels ($\lambda_{ex} = 370$ nm, $\lambda_{em} = 438$ nm) represent the fluorescence intensities of CPT (donor), whereas the green fluorescence channels ($\lambda_{em} = 550$ nm) represent the fluorescence intensities of Mal (acceptor). The reduced intracellular environment is expected to induce the breakage of maleimide thioether bond after cellular internalisation, and subsequently lead to the release of CPT from $(CPT)_2$-ss-Mal into the cells. Overall, this procedure can be self-assessed through FRET signals. As demonstrated in Fig. 7A, in the absence of CPT leakage, MDA-MB-231 cells exhibit an enhanced cellular uptake, as indicated by green fluorescence at 30 min. From 45 to 90 min, blue fluorescence is observed in the cells, instead of green fluorescence, suggesting that the CPT is released from the $(CPT)_2$-ss-Mal. A green fluorescence, of relatively low intensity, is detected in DA-TAT-PEG-PCL group at pH 7.4, but not PEG-PCL and TAT-PEG-PCL groups, indicating the cellular uptake of CPT from these micelles is relatively slow (Fig. 7B). However, at pH 6.8, DA-TAT-PEG-PCL micelles are significantly internalised and CPT is fully released within 2 h, which is similar to the strong blue fluorescence observed in TAT-PEG-PCL group. Additionally, the results of flow cytometry analysis confirm the pH-dependent endocytosis of DA-TAT-PEG-PCL into the cells. For DA-TAT-PEG-PCL group, the fluorescence intensity of CPT is comparatively higher at pH 6.8 than pH 7.4 (Fig. 7C). However, there are no significant differences in the fluorescence intensities of CPT at pH 7.4 and 6.8, in both PEG-PCL and TAT-PEG-PCL groups (Fig. 7C).

In addition, Pu and colleagues have synthesised N-palmitoyl chitosan (NPCS) bearing a hydrophobic Cy3 moiety (NPCS-Cy3) as a pH-responsive nanocarrier to enhance the uptake and delivery of curcumin

Table 4
A list of selected applications on intracellular fate of nanomedicines by FRET

FRET pair (donor/acceptor)	nanocarriers	Donor /acceptor location	Detection Apparatus	Cell lines	FRET signal	Ref.
DiO / DiI	PEEP-PCL, PEG-PCL and PEG-DSPE micelles	C / C	CLSM	MDCK cells	FRET signal can be observed in MDCK cells at 1h and 4h but disappeared at 8h.	[42]
	mPEG-PLGA nanoparticles	C / C	CLSM and microplate reader	MDCK cells, MDCK monolayer	The intracellular FRET ratio decreased from 0.87 to 0.79 after 2h, while in basolateral chamber ratio decreased to 0.53.	[28]
	nanocrystals	C / C	CLSM and microplate reader	MDCK cells, MDCK monolayer	The intracellular FRET ratio decreased from 0.92 to 0.63 after 1h, while in basolateral chamber ratio decreased to 0.36.	[5]
	PEG-PDLLA micelles	C / C	CLSM and luminescence spectrometer	KB cells	FRET signal outside the cell was strong, while inside was weak.	[128]
	nanoparticles	C / C	CLSM	MDA-MB-231 cancer cells	FRET ratios increased in cell membranes	[46]
DiI /DiD	lipid nanocapsules (LNCs) and nanoemulsions (LNEs)	C / C	CLSM	HEK293 (β3) cells (HEK293 cells transfected with human β3 integrin)	FRET ratio of LNCs group was higher than LNEs group	[44]
	lipid nanocapsules (LNCs) and nanoemulsions (NEs)	C / C	Fluorescence spectrophotometer	Caco-2 monolayer	FRET signal can be observed in basolateral chamber of LNCs group, while disappeared in NEs group.	[132]
Cy3 / Cy5	polymeric micelle	C / C	Flow cytometry	HuH-7 cells	FRET efficiency decreased with incubation time increase. And the FRET signal still existed after 24h.	[133]
	NA	P / P	CLSM and fluorescence spectrometer	A2780 ovarian cancer cells and NIH3T3 cells	FRET signal decreased in cancer cells from 4h – 24h, while remain stable in normal cells.	[47]
Coumarin / FITC	Mesoporous silica nanoparticles (MSNs)	P / P	CLSM	HeLa cells	FRET signal was negative corelated with the intracellular glutathione concentration	[134]
Curcumin / Cy3	chitosan polymeric nanoparticle	C / P	CLSM	RAW264.7 macrophages cells	FRET signal was strong at 15min and 1h but start to decrease after that. By 4h, the signal was almost diminished.	[27]
Doxorubicin / Cy5	chitosan polymeric nanoparticle	C / P	CLSM	Human fibrosarcoma (HT1080) cells	FRET signal was strong at 30min and start to decrease after 1h. after 4h, the signal could not be observed.	[25]
BODIPY1 / BODInD-Cl	mPEG-DSPE micelle	C / C	CLSM	Raw264.7 macrophages cells	FRET signal switched off when there was a high level of H_2S in cells.	[135]
Perylene / curcumin / 5,10,15,20-tetro (4-pyridyl) porphyrin	Curcumin nanoparticle	C / C / C	CLSM	A549 cells	FRET signal gradually decreased from 0.5h – 8h	[130]
Camptothecin (CPT) / maleimide thioether bond	PEG-PCL polymeric micelle	C / C	CLSM	MDA-MB-231 cells	FRET signal switched off under glutathione-triggered condition	[119]
BODIPY (558/568 nm) / BODIPY (630/650 nm) -X	polylactide based magnetic NPs	P / P	Fluorescent microscopy	Rat aortic smooth muscle cells (A 10) and BAECs cells	FRET signal decreased with the degradation status of nanoparticles	[136]
QDs (400/630 nm)/ Cy5.5	lipoprotein-based nanoparticles	C / C	fluorescence microscopy	J774A.1 macrophage	FRET signal can be observed within 10min, after that signal disappeared.	[137]
QDs (405/580 nm)/ Cy3	nanoparticles	C / C	CLSM	HeLa cells	FRET signal can be observed at 1h and 4h.	[125]
oligo-phenylenevinylene (OPV) fluorophore / Nile red (NIR)	PCL nanoparticle	P / C	CLSM and Cell analyzer	HeLa cells, breast cancer (MCF 7) cells and Wild type mouse embryonic fibroblasts cells	FRET signal can be observed in the aforementioned cells	[126]

a. C / C: both the donor and acceptor fluorescence were loaded in the carrier; C / P: donor was loaded in the carrier, and acceptor was conjugated with polymer on the carrier; P / C: donor was conjugated with polymer, and acceptor was loaded in carrier; P / P: both the donor and acceptor were conjugated with polymer.

[27]. The localisation of NPCS-Cy3 and the intracellular release of curcumin are detected by FRET. The findings suggest that the nanoparticles are disintegrated and curcumin is completely released at an intracellular level. Pu et al. fabricated redox-responsive polymer dots with disulfide cross-linked polymers to allow quenching, by loading BODIPY into the matrix [37]. The disulfide cross-links aided in the disintegration of the system by intracellular glutathione, resulting in fluorescence recovery of BODIPY and drug release. Zhang and coworkers developed a nanodrug self-delivered system without using any inert, for the purposes of diagnosis, treatment and monitoring the release of drugs into the cells [130]. In this system, a curcumin matrix was co-doped into the FRET pair of perylene (donor) and 5,10,15,20-tetro (4-pyridyl) porphyrin (acceptor), which served as an anticancer chemotherapeutic agent. From the FRET analysis, the obtained green fluorescence of curcumin molecules was quenched in the nanoparticle form and recovered upon its release into the tumour cells, offering real-time self-monitoring abilities. This self-monitored and self-delivered nanodrug system exhibits a broad application for the future treatment of cancers. Besides, Wu et al. designed lipoplexes and polyplexes for nuclei acid delivery and used QD-mediated FRET to evaluate intracellular integrity of lipoplexes and polyplexes [131]. In this study, QD605-amine and Cy5 labelled oligodeoxynucelotides (ODN, Cy5-GTI2040) were chosen as the PRET pair. After incubation with lipoplexes and polyplexes in KB cells for 4 h, lipoplexes and polyplexes were fully internalised into cells, and most of the lipoplexes and polyplexes remained intact. After 48 h post incubation, most of the lipoplexes and polyplexes broken up and little FRET-mediated Cy5 signal was detected.

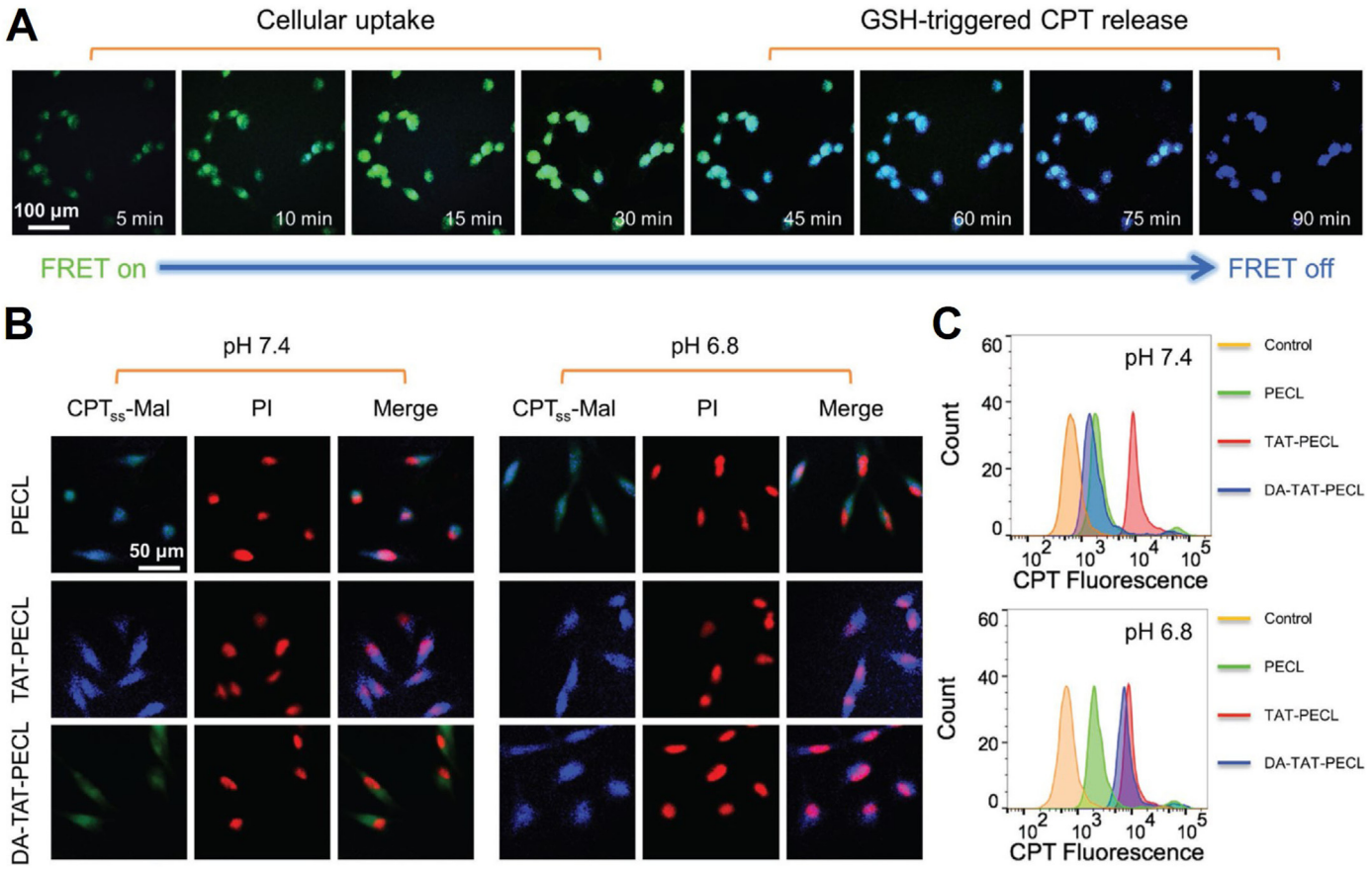

Fig. 7. (A) The images of glutathione-induced CPT release in the $(CPT)_2$-ss-Mal-treated MDA-MB-231 cell line. Green fluorescence represents the cellular uptake pathway of $(CPT)_2$-ss-Mal dimer, whereas blue fluorescence represents the release of CPT from the dimer. The pH-dependent uptake of CPT in the cells is analyzed using (B) fluorescence microscope and (C) flow cytometry. The cells are incubated for 2 h with DA-TAT-PEG-PCL, PEG-PCL and TAT-PEG-PCL micelles loaded with $(CPT)_2$-ss-Mal at different pH of 7.4 and 6.8. Propidium iodide (red-fluorescent) is used to stain the cell nuclei. Adapted with permission from [119]. Copyright (2017) John Wiley and Sons.

4.4. Transcellular Integrity Monitoring

There are many biological barriers *in vivo*, such as intestinal epithelial barriers, respiratory epithelial barriers, blood-brain barrier, and blood-eye barrier, which consist of closely connected epithelial monolayer. In order to deliver drugs into the targeted sites (like blood circulation, brain, and eyes), the drugs should not only be internalised into cells, but also transported across the epithelial monolayer. The nanomedicines must traverse these biological barriers in an intact form to maintain their properties and provide desirable efficacy. Therefore, it is essential to monitor the integrity of nanomedicines, during the transcellular transport. However, transcellular transport of nanomedicines through epithelial barrier is still largely unclear. Hence, further research is required to develop nanomedicines as well as to study their transcellular integrity. FRET signals can monitor the integrity of nanocarriers and calculate the amount of intact nanocarriers after transcellular transport.

In our previous study, FRET was used to measure the integrity of mPEG-PLGA (methoxy poly(ethylene glycol)-b-poly(lactic-co-glycolic acid)) nanoparticles transported transcellularly across MDCK epithelial cells [28]. The mPEG-PLGA nanoparticles were encapsulated with a DiO and DiI mixture in a 1:1 ratio (DiO/DiI-NPs), in order to determine their transportation ability across MDCK cell monolayers (Fig. 8A). The FRET signals of DiO/DiI-NPs diluted in acetone and water were measured at 420 nm excitation wavelength and 485-700 nm emission wavelengths. As shown in Fig. 8B, a high intensity of DiI signal (red curve) and FRET ratio of 0.89 were found after diluting the DiO/DiI-NPs in water. These positive results were probably due to the short distance between of DiO and DiI. In contrast, after dissolving DiO/DiI-NPs in acetone, the peak was shifted from 565 to 505 nm, suggesting that the FRET pair may be separated by acetone (green curve). Furthermore, the fluorescence intensities of DiO/DiI-NPs were measured in both apical and basolateral chambers. As shown in Fig. 8C, the initial ratio of FRET is 0.89 in the apical chamber which was reduced to 0.82 after incubation for 2 h, indicating that the nanoparticles remain intact in the cells. Meanwhile, in the basolateral chamber, the FRET signal was still present at a ratio of 0.53, suggesting that a proportion of intact nanoparticles was transported across the basolateral membrane.

To enhance the transportation of nanocarriers across the cells, a lipid covered saquinavir pure drug nanoparticle (Lipo@nanodrug) has been recently reported by synthesising the saquinavir nanoparticle with phospholipid bilayers [138]. Xia et al. have reported that the transcellular transport of Lipo@nanodrug is increased by 1.92- and 3.75-folds compared to pure nanodrug and coarse crystals, respectively. After reaching the target cells, Lipo@nanodrug was found in the Golgi apparatus and endoplasmic reticulum, and the transcytosis of Lipo@nanodrug may be induced in the intestinal epithelial cells. Dai et al. evaluated the integrity of liposomes and lipid disks while crossing the blood-brain barrier (BBB) and blood-brain tumour barrier (BBTB) *in vitro* [139]. FRET nanocarriers were prepared through encapsulation of DiO, DiI, and DiD into liposomes and lipid disks. It was observed that liposomes and lipid disks remain intact in the cytoplasm and cross the BBB with a ratio of 0.68% and 1.67%, respectively, whereas they cross the BBTB with a ratio of 2.31% and 8.32%, respectively. Collectively, a deep understanding on the transport mechanisms of the nanocarriers is required at the cellular, tissue, and systemic levels, in order to develop the better nanodrug delivery systems. In addition, the delivery efficiency and the

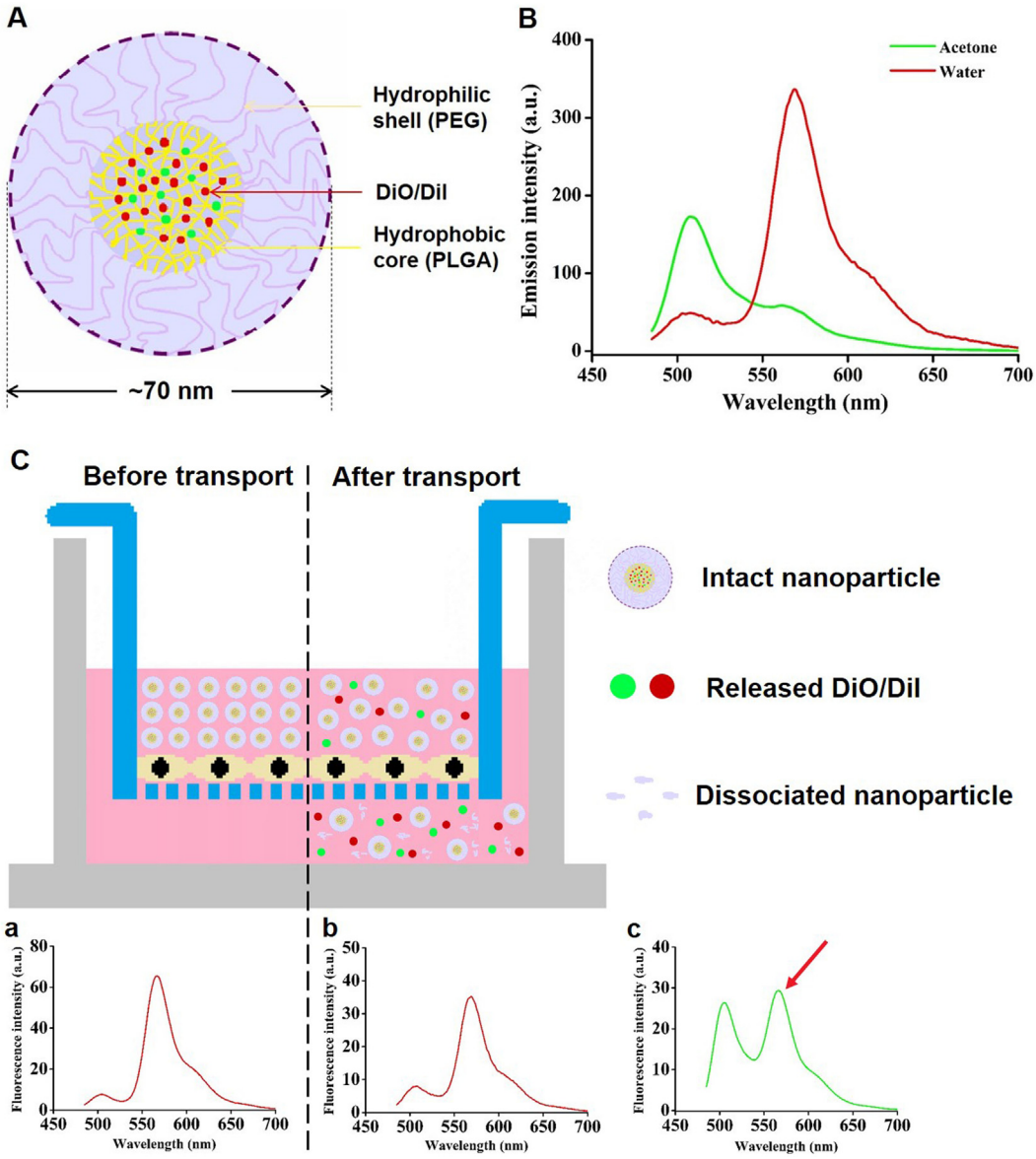

Fig. 8. (A) Schematic diagram showing the preparation of DiO/DiI-NPs. (B) Green curve represents the fluorescence spectrum of DiO/DiI-NPs diluted with 10-folds of acetone, whereas red curve indicates the DiO/DiI-NPs spectrum diluted in water. (C) The fluorescence intensities of DiO/DiI-NPs in both apical and basolateral chambers. (a) The spectrum of DiO/DiI-NPs in the apical chamber before the transportation, the spectra generated from both (b) apical and (c) basolateral chambers after 2 h of transportation. The occurrence FRET is indicated by red arrow. Adapted with permission from [28]. Copyright (2017) American Chemical Society.

cellular toxicity of nanoparticles are closely related to their capabilities of internalisation and intracellular transport across cellular monolayers.

5. *In vivo* fate of nanomedicines revealed by FRET

Despite the extensive *in vitro* studies performed on many novel nanomedicines, described in section 4, relatively little information has been revealed about the *in vivo* fate of nanomedicines including the integrity, bio-distribution, disassembly kinetics, and elimination etc., which are crucial to determine their *in vivo* bioactivity. As we known, the *in vivo* fate of nanomedicines mainly depends on their intrinsic properties such as composition, stability, drug release behaviour, compatibility, degradability, and their interactions with lipids, proteins, and cells within a microenvironment. The environment a nanomedicine encounters in living systems (e.g. multiple biological components, severe microenvironments, and biological barriers) is much more complex than that encountered *in vitro*, after a nanomedicine is delivered by different routes, especially for drugs loaded into novel functional nanocarriers for targeted delivery, prolonged circulation as well as for microenvironment responsive properties. Certain techniques (e.g. the dynamic light scattering) have been successfully utilised to monitor the dynamic size changes of nanoparticles *in vitro*, but their low sensitivity and interference from biological components still limit their applications *in vivo*. To circumvent this problem, as a non-invasive and real-time imaging technique, FRET has been widely utilised to evaluate and track nanomedicines including polymeric micelles, polymeric nanoparticles, and lipid-based nanoparticles in *in vivo* systems, as shown in Table 5. It is interesting to note that except normal and disease mice models, zebrafish has emerged as a new model to evaluate integrity of nanomedicines by FRET. The selection of FRET pairs such as DiD/DiR, Cy5.5/Cy7, Cy5.5/Cy7.5, and QD710/Cy7 are more specific *in vivo* than *in vitro*, and are only suitable to be used *in vivo* and imaged by IVIS Spectrum, as discussed in section 2.2 in detail. While for the DiO/DiI, Cy3.5/Cy5, and QD610/Cy5.5 FRET pairs, which are widely used in cells, they could also be used for imaging histologic sections by CLSM and superficial blood vessels *in vivo* by intravital CLSM. Nanomedicines are

administrated by tail vein injection, intraperitoneal injection, peritumoural injection, subcutaneous injection, and oral route, where FRET signals of biological samples including the whole body, organs, tumours, blood vessels, and plasma are imaged and analysed by IVIS Spectrum, CLSM, and spectrofluorometer. The appearance of FRET signal indicates that intact drug nanoparticles exist *in vivo*, while the FRET ratio changes with time suggesting the dynamic disassembly of drug with its nanocarriers. Depending on the selected FRET pairs and nanocarrier compositions, FRET-based technologies have been widely applied to track the *in vivo* fate of drug nanocarriers, to guide the development of nanomedicines.

5.1. In vivo imaging of FRET based nanocarriers

Compared with FRET imaging *in vitro* and at the cellular level, the requirements for FRET imaging *in vivo* are much more demanding and challenging, such as higher sensitivity, deeper tissue penetration, and less background fluorescence interference. While some FRET-based nanoparticles are very appropriate for imaging *in vivo* due to the advantage of nanoparticle-integrated FRET. Firstly, incorporation of a FRET pair inside nanoparticles is favourable for fluorescence resonance energy transfer and can be used to enhance fluorescence intensity *in vivo*, which distinguishes the integrity of nanocarriers from free fluorophore molecules, as well as monitors their dynamic disassembly by analysing FRET signal changes. Secondly, the FRET emission by dyes, such as DiD, DiR, Cy7, and Cy7.5 in the near infrared region can improve tissue penetration and reduce the auto-fluorescence. FRET generates a larger Stokes shift of the emission maxima, which also could minimise the crosstalk between excitation and emission, as well as reduce the background signal. Besides, FRET-based nanoparticles could protect fluorophores from interaction with biological components and getting rapidly cleared from the body, which leads to less quenching and allows long-term and sensitive tracking *in vivo*. Finally, nanoparticles preferentially accumulate at the tumour site via enhanced permeability and retention (EPR) effect, which helps in tumour imaging and diagnostic applications.

At present, FRET-based nanoparticles have been developed and applied for animal studies. Law's group synthesised DiD and DiR encapsulating, FRET-based PEG-PLGA polymeric nanoparticles for NIR and *in vivo* FRET imaging. These nanoparticles were brighter than quantum dots, stable in biological media, and demonstrated a potential for imaging applications [151]. Except the one-step FRET which occurs between two fluorophores, two steps or multiple FRET nanoparticles where FRET occurs sequentially between three or more fluorophores have also been applied for imaging *in vivo* [139,152]. It was also Law's group [152] which further developed a series of FRET PEG-PLGA polymeric nanoparticles with sequential and multiple FRET for multicolour and multiplexed imaging by encapsulation of a combination of DiO, DiI, DiD, and DiR in the core. The optimised nanoparticles Q7 (DiO: DiI: DiD: DiR=1:1:0.2:0.2) simultaneously emitted fluorescence at three different wavelengths (Red: 570 nm, Far red: 669 nm, NIR: 779 nm) for multicolour imaging via sequential and multiple FRET at λ_{ex} 485 nm (Fig. 9A). Three other optimised nanoparticles D6 (DiO: DiI: DiD: DiR=1:1:0:0), T3 (DiO: DiI: DiD: DiR=1:1:0.5:0), and M5 (DiO: DiI: DiD: DiR=1:0:0:0.05) emitted maximum fluorescence intensities at 570, 672, and 777 nm, respectively for multiplexed imaging upon excitation at 485 nm (Fig. 9B). When subcutaneously injected into the abdomen of mouse for whole-body imaging *in vivo*, T3 and M5 were 10 times brighter than the QDs (Fig. 9C and D). Furthermore, D6, T3, and M5 have been used together as a multiplexed platform for *in vivo* imaging with the calculated signal-to-noise ratios increasing in the following order: D6<T3<M5 (Fig. 9E and F). The multiple FRET nanoparticles could further be used to identify multiple cell types and tissue structures, as well as to image the delivery and biodistribution of drug nanocarriers.

In addition, the semiconducting polymer nanoparticles (SPNs) comprising a semiconducting polymer as donor and NIR as acceptor in the core, can be also used for FRET to improve the NIR quantum yield and enhance NIR fluorescence, which is a new class of optical nanomaterial for molecular imaging [153,154]. As well as the AIE dots, such as AIE-active polymer, as FRET donors were beneficial for the nanoparticle-based FRET systems [12,155]. Moreover, self-luminescing bioluminescence resonance energy transfer (BRET) which is analogous to FRET, enabled near-infrared imaging and cancer therapy *in vivo* without external light excitation, replacing the donor energy by a light-emitting protein, such as coelenterazine [156,157] and luminol [158]. Xiong et al further developed the BRET-FRET nanoparticles integrating BRET and FRET, which are well suited for lymph-node mapping and cancer imaging [159]. In the following part, we will systematically discuss the FRET-based nanoparticles to probe the fate of drug nanocarriers *in vivo*, including polymeric micelles, polymeric nanoparticles, and lipid-based nanoparticles.

5.2. The biofate of drug nanocarriers in vivo

5.2.1. Polymeric micelles

Polymeric micelles are ultrafine core/shell nanostructures (10-100 nm) which can be readily modified chemically and are an effective delivery system in cancer therapy. The amphiphilic block copolymers such as PEG-PLA, PEG-PCL, PEG-PLGA, and Pluronic block copolymers can self-assemble above their critical micellar concentration (CMC). Compared with conventional surfactant micelles, polymeric micelles have better kinetic and thermodynamic stability with a remarkably reduced CMC, and have a slower rate of dissociation, allowing retention of loaded drugs for a longer period. The hydrophilic block forms the shell layer of the micelles whereas the hydrophobic block forms their core. The hydrophilic shell layer such as PEG enhances systemic circulation and improves bio-distribution *in vivo*. However, all of these advantages of micellar carriers are dependent on their fate *in vivo*, especially their integrity and disassembly kinetics.

Compared with other static and stable nanoparticles, micelles possess a thermodynamically self-assembled structure, which could be changed to free monomers reversibly and inevitably after disintegration. When polymeric micelles enter into living system by intravenous injection, they are diluted rapidly by massive amount of blood and collide at high velocity. In addition, the interaction of lipids and protein assemblies in human plasma with polymeric micelles also could lead to the disintegration of nanoparticles and therefore drug release. As previous studies have shown, nanoparticles in biological fluids rapidly adsorbed lipids and proteins on their surface, forming the protein corona [160,161]. The so-called 'protein corona' largely determines the biofate of nanoparticles *in vivo* [162]. Simultaneously, these biological components also could destabilise the structure of nanoparticles, promoting an early disintegration and premature drug release before reaching the site of action [163]. For example, the lipoprotein *in vivo*, such as chylomicron (CM), low density lipoprotein (LDL), and very low density lipoprotein (VLDL) significantly disrupt the assembly structure of drug nanocarriers due to a similar amphiphilic nature [52].

At present, many FRET-based methods have been developed to reveal the integrity and mechanism of disassembly of polymeric micelles *in vivo*. Chen et al. investigated the self-assembly of PEG-PDLLA micelles, encapsulating DiO and DiI as a FRET pair in the core, *in vivo* by FRET [141]. At a close proximity of the FRET pair in the micellar core, *in vitro*, an efficient FRET signal was observed, and the FRET ratio was nearly 0.89. Once the PEG-PDLLA micelles were injected into the BALB/c mice, by tail vein injection, a sharp fall of FRET ratio to 0.39 was observed in the ear blood vasculature. The PEG-PDLLA micelles disintegrated rapidly and the lipophilic agent was released completely, in the blood stream, in an uncontrolled fashion. Besides, five components like red blood cells, albumin, α-, β-, and γ-globulins in blood were also tested, by FRET changes, in their experiments. It was revealed

Table 5
The applications of FRET for probing the fate of drug nanocarriers *in vivo*

Nanocarriers		Donor/ Accepter	Position [a]	Animal model	Delivery route	Test method	Sample	Initial FRET ratio	FRET ratio changes	Disassemble rate [b] (Integrity %)	Ref.
Polymeric micelles	PEG-PCL micelles	DiO/DiI	C/C	Zebrafish	Oral	CLSM	Intestine	0.47	1h: 0.75/4h 0.45	Rapid	[140]
	PEG-PDLLA micelles	DiO/DiI	C/C	Balb/C mice	Tail vein injection	Intravital CLSM	Ear blood vessels	0.89 0.92	15min:0.46/3h: 0.39 15min:0.58/1h:0.51/6h:0.42/12h:0.38	Rapid	[141] [43]
	PEG-PPLG Micelles	Cy5.5/Cy7.5	P/P C/P	Balb/C mice		*Ex vivo* IVIS	Blood	0.94 0.85	0 min: 0.8/72h: 0.5 0 min: 0.4/4h: 0.28	Slow Rapid	[142]
	PEG-CA_8 micelles	DiO/RB	C/P	Nude mice		Spectrofluorometer	Blood plasm	0.79	0 min:0.45/18 min:0.2	Rapid	[52]
	PEG-PCL micelles	Cy5/Cy5.5	P/P	Tumor-bearing mice			Blood plasm	0.83	15min: 0.57/30min:0.47/24h:0.33	Rapid	[143]
Polymeric NPs	mPEG-PLGA NPs	DiO/DiI	C/C	Zebrafish	Incubation	CLSM	Whole body	0.89	1h: 0.84/12h: 0.4/48h:0.32	slow	[28]
	C12 PEG-PLGA NPs OLA PEG-PLGA NPs PLGA PEG-PLGA NPs	Cy3.5/Cy5	C/C	Tumor-bearing nude mice	Tail vein injection	Intravital CLSM	Tumor vasculature	(A/D) 1	10min:0.1 10min:0.25 10min:0.65	Rapid Moderate Slow	[49]
	C12 PEG-PLGA NPs OLA PEG-PLGA NPs PLGA PEG-PLGA NPs	Cy5.5/Cy7				IVIS	Whole body		10min:0.18/1h:0.15 10min:0.35/1h:0.2 10min:1/1h:0.25	Rapid Moderate Slow	
	ROS responsive PEG-PPS NPs	DiO/DiI	C/C	C57 mice Sepsis mice	Intraperitoneal injection	*Ex vivo* IVIS	Organs	n/a	n/a significant decreased	Slow Rapid	[144]
	mPEG-$(Cys)_4$-PDLLA NPs			Balb/C mice	Tail vein injection	Intravital CLSM	Ear blood vessels Tumor	0.95	15min:0.84/1h:0.77/6h:0.58/12h:0.54 6h:0.31	Slow Rapid	[43]
	PEG-Cys_4-CA_8 NPs	DiO/RB	C/P	Nude mice	Tail vein injection	Spectrofluorometer	Blood plasm	0.84	0 min: 0.6/18 min: 0.35	Moderate	[52]
	Enzyme responsive NPs Enzyme non-responsive NPs	FAM/ RB	P/P	Nude mice	Tail vein injection	IVIS	Tumor	n/a	FRET signal: 8 days FRET signal: 1h	Cleared slowly Cleared rapidly	[145,146]
	pH responsive Polymer NPs	DOX/BTTPF	C/P	ICR mice	Tail vein injection	IVIS	Organs Tumors	n/a	FRET off FRET on	Disintegrated Integrated	[147]
	PEO-PS NPs Oleic acid-coated iron oxide PEO-PS NPs	DiD/DiR	C/C	nude mice		IVIS	Whole body	0.89	0min: 0.89/2h: 0.48 0min: 0.89/6h: 0.56	Rapid Slow	[46]
Lipid-based NPs	Lipid nanoparticles	DiI/DiD	C/C	Tumor-bearing nude mice	Tail vein injection	IVIS	Liver Tumor	(A/D) 0.5	(A/D)1h:0.313/5h:0.194/24h:0.111 (A/D)1h:0.307/5h:0.216/24h:0.172	46.7%/14.3%/0% 45%/20%/8.3%	[44]
						CLSM	Tumor		(A/D)1h:0.283/5h:0.146/24h:0.057	38.8%/11%/5.1%	
	Lipid nanoparticles	QD610/Cy5.5	C/P	nude mice	tail vein injection	Intravital CLSM	Tumor vasculature Tumor interstitium	n/a	0min: 0.5/30min: 0.47/2h: 0.41 0min: 0.5/30min: 0.52/2h: 0.46	Rapid	[62]
		QD710/Cy7				IVIS	Whole body		FRET signal decreased		
	Lipid nano-emulsion droplets	Cy5.5/Cy7.5	C/C	Healthy nude mice Tumor-bearing nude mice	Tail vein injection	IVIS	Tail vein Liver Tail vein Tumor	0.85	15min: 0.85/6h: 0.75 15min: 0.85/6h: 0.55/24h: 0.4 15min: 0.85/6h: 0.58 15min: 0.85/6h:0.4/24h: 0.25	100%/93% 100%/66%/20% 100%/70% 100%/40%/0%	[118]
	lipid nanoemulsions lipid nanocapsules PEG lipid nanocapsules	DiD/FP730-C18	C/C	nude mice	Tail vein injection	IVIS	Whole body	n/a	Imaging of FRET signal changes	Slow Rapid Moderate	[148]
	Liposomes	Pyro/Bchl	P/P	nude mice		IVIS	Whole body		Imaging of FRET signal changes	Slow	[149]
	Liposomes	DiO/DiI/DiD	C/C/C	Nude mice	Tail vein injection	IVIS CLSM	Brain Tumor	n/a	3-12h: FRET increased; 12-24h: FRET decreased	Integrated	[139]
	Lipid disks					IVIS CLSM	Brain Tumor				
Others	Thermosensitive PECT micelles hydrogel	FITC/RB	P/P	Nude mice	Subcutaneous injection	IVIS	Subcutaneous injection site	0.835	D1-D21:0.76	Slow	[150]
				Tumor-bearing nude mice	Intraperitoneal injection		Organs and tumor				
					Peritumoral injection	CLSM	Tumor Organs		Unchanged		
	Nanocrystals	C6/DiI	C/C	Zebrafish	Incubation	CLSM	Whole body	0.94	n/a	Integrated	[30]
	Pure drug nanoparticles	Cy5.5/Cy7.5	C/C	Nude mice	Tail vein injection	IVIS	liver	0.85	35min: 0.3/2h: 0.15	56%/10%	[50]

a. C/C: both the donor and acceptor were loaded in the carrier; C/P: donor was loaded in the carrier, and acceptor was conjugated with polymer on the carrier; P/C: donor was conjugated with polymer, and acceptor was loaded in carrier; P/P: both the donor and acceptor were conjugated with polymer.
b. The disassemble rate was judged according the conclusion in paper.

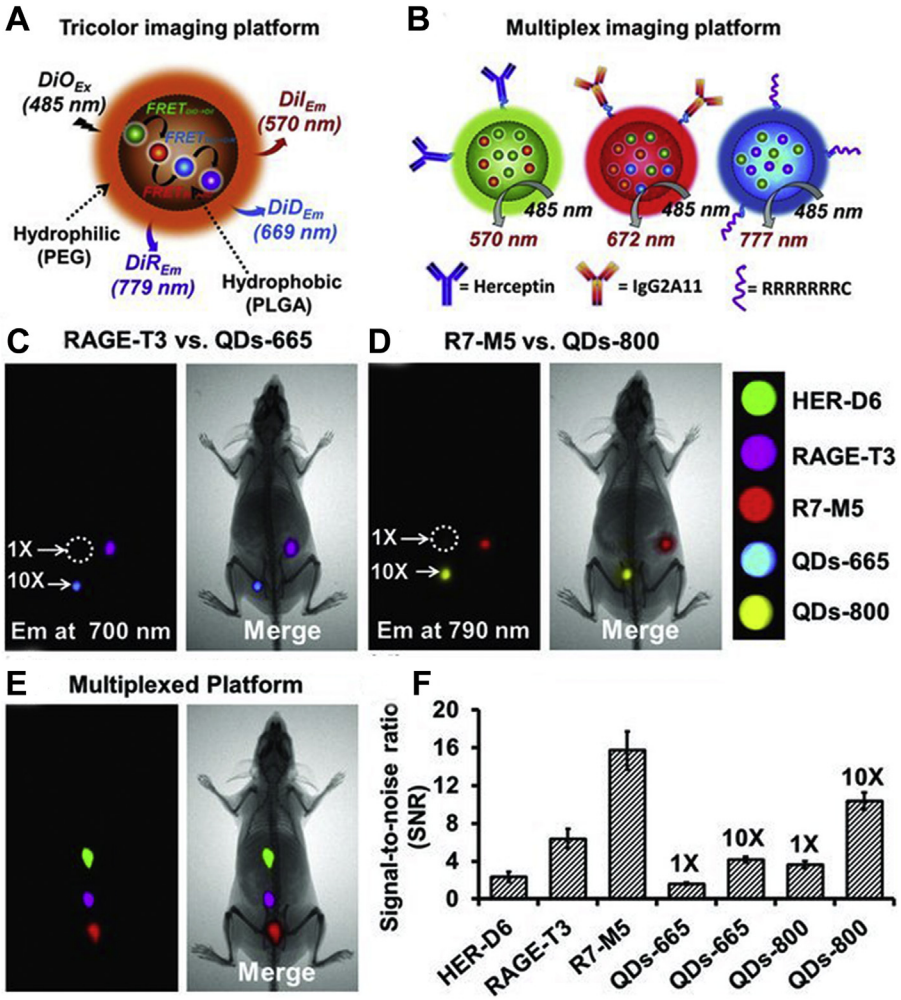

Fig. 9. *In vivo* multiplexed imaging of FRET based nanocarriers. The schematic representation of particles designed for (A) multicolor and (B) multiplex imaging. A comparison of (C) RAGE-T3 and (D) R7-M5 with the corresponding QDs-665 and QDs-800, respectively. (E) A merged FRET image and a merge FRET and X-ray image of a SCID mouse that was subcutaneously injected with HER-D6 (green), RAGE-T3 (magenta), and R7-M5 (red) particles (3.5×10^{11}) in deionized water (10μl) at different regions. Inset: The pseudo-color assigned for each particle. (F) A bar chart was plotted to compare the signal-to-noise ratio of different nanoparticles and QDs, where 1× and 10× are referred to 3.5×10^{11} and 3.5×10^{12} particles, respectively. Adapted with permission from [152]. Copyright (2013) John Wiley and Sons.

that α- and β-globulins are the main factors responsible for the disintegration of micelles in the blood stream. In addition, Li et al. [52,164] also demonstrated the easy and rapid disassembly of polymeric micelles in blood streams of mice (which reduced their anticancer effect *in vivo*) by FRET. For targeted polymeric micelles, the integrity and stability of micellar nanocarriers are essential for efficient drug delivery. Our group [140] has demonstrated, by FRET, that transferrin receptor-targeted 7 peptide-decorated DiO/DiI PEG-PCL micelles could be absorbed partially in an intact form across the small intestinal epithelial barrier in a visual zebrafish model, after oral administration (Fig. 10). The FRET ratio in the basolateral side of the intestine decreased after 2 h, which also confirmed that some micelles were disassembled during delivery into the body.

Since the hydrophobic FRET pair (DiO and DiI) can be together encapsulated into the core of micelles, as mentioned above, the behaviour of the polymers after being delivered into the body could not be monitored. Therefore, Morton and Zhao explored association of micellar unimers and unimer-drug association by FRET but with a different labelling position [142]. Two different FRET PEG-PPLG micelles have been formulated including the blank micelles and drug loaded micelles. The blank micelles were formulated by a mixture of PEG-PPLG-Cy5.5 and PEG-PPLG-Cy7, where the FRET pair was conjugated on each polymer respectively, (Fig. 11A) to probe the association of unimers in the blank micelles *in vivo*. The drug-loaded micelles were fabricated using PEG-PPLG-Cy7 to encapsulate Cy5.5 as the model drug and to probe the *in vivo* association of the unimer-drug (Fig. 11F). Two kinds of FRET PEG-PPLG micelles were observed with different FRET signal intensities distributed in the mice body, by IVIS, after administration via the tail vein (Fig. 11B and G). The FRET efficiency (FRET ratio) of the blank polymeric micelles in blood barely changed (between 50 and 85% for up to 72 h), and was much higher than drug-loaded polymeric micelles, the FRET efficiency of which was only 37%, after administration (Fig. 11D and I). Notably, the blank micelles had a longer circulation and slower clearance, *in vivo*, as shown in Fig. 11E and J. The biodistribution based on the FRET measurement demonstrated that most of the blank polymeric micelles remain intact in circulation after 24 h, while only a small amount was observed in the clearance organs, such as the liver, spleen, and kidneys. In contrast, the drug-loaded polymeric micelles had a stronger fluorescence signal in the clearance organs than in the circulation after 8 h. The drug-loaded micelles were easier to disassemble *in vivo* than blank micelles and were rapidly cleared from the circulation. Therefore, incorporation of drug in the micellar core had great influence on the stability of the micelles, where blank polymeric micelles actually were more stable than drug or fluorescent molecule-loaded micelles, *in vivo*.

What is the mechanism of clearance of polymeric micelles from the body? Do micelles clear as intact moieties or as unimers? Sun et al. [143] compared the *in vivo* behaviours of two different polymeric micelles

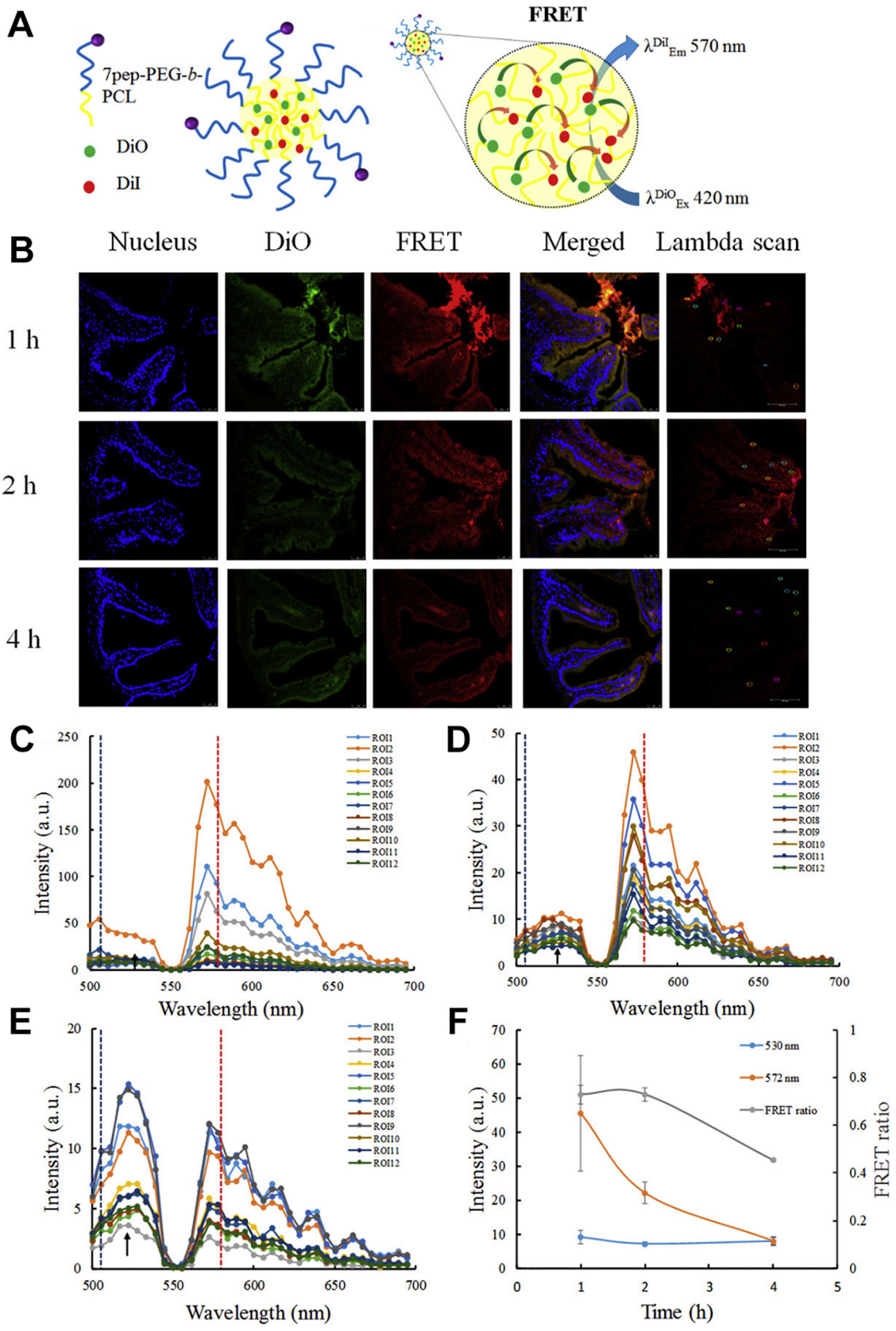
A
7pep-PEG-b-PCL
DiO
DiI
FRET
λDiIEm 570 nm
λDiOEx 420 nm
B
Nucleus
DiO
FRET
Merged
Lambda scan
1 h
2 h
4 h
C
Intensity (a.u.)
Wavelength (nm)
ROI1
ROI2
ROI3
ROI4
ROI5
ROI6
ROI7
ROI8
ROI9
ROI10
ROI11
ROI12
D
Intensity (a.u.)
Wavelength (nm)
E
Intensity (a.u.)
Wavelength (nm)
F
Intensity (a.u.)
FRET ratio
Time (h)
530 nm
572 nm
FRET ratio

using FRET technology: PEG-PCL micelles which are easy to disassemble and PEG-PS micelles which are highly stable with a glassy core and strong hydrophobicity of the PS block. The hydrophobic block tail end was conjugated with Cy5 and Cy5.5, as donor and acceptor for FRET (Fig. 12A). They found that the micellar stability affected their blood clearance. Once injected intravenously, the PEG-PCL micelles immediately disassembled into unimers by the blood shear and proteins (albumin), and were cleared rapidly from the blood stream and sequestered into the liver as unimers. While, the intact PEG-PS micelles were difficult to clear, which spread over the whole body and accumulated less in the liver but more in the spleen and tumour (Fig. 12B and D). Kupffer cells are resident macrophages in the liver, which are responsible for clearance of foreign substances in blood. After blocking the phagocytosis of liver macrophages by $GdCl_3$ pretreatment, PEG-PCL micelles also spread widely in the whole body and were largely distributed in the spleen, rather than the liver, which was very different from the $GdCl_3$-untreated mice. The $GdCl_3$ pretreatment did not significantly change the biodistribution of PEG-PS micelles (Fig. 12C and F). Therefore, it could be concluded that the Kupffer cells sequestered unimers rather than the micelles.

5.2.2. Polymeric nanoparticles

Polymeric nanoparticles are solid particles or particulate dispersions with a size in the range of 10-1000 nm, where the drug is encapsulated in the polymer matrix. The common polymers used for drug delivery are poly (lactic-co-glycolic acid) (PLGA), poly (lactic acid) (PLA), poly caprolactone (PCL), and poly (glycolic acid) (PGA), which are biocompatible and biodegradable *in vivo*. Compared with the polymeric micelles, polymeric nanoparticles possess a static and compact structure and are more stable *in vivo*. They are also grafted with hydrophilic molecules (e.g. PEG) to enhance their circulation *in vivo* or are modified with ligands for targeted drug delivery, as well as linked with functional groups for environment responsive drug release. FRET is widely used to investigate the disassembly kinetics and biodistribution of polymeric nanoparticles *in vivo*, especially for novel functional nanocarriers.

Although polymeric nanoparticles are more stable than polymeric micelles, similar to polymeric micelles, the incorporation of drug also significantly disrupts the stability and integrity of polymeric nanoparticles. Zhao et al. have illustrated, by FRET, that the improvement of drug-carrier compatibility significantly enhances the circulation stability and therapeutic effect of polymeric nanoparticles *in vivo* [49]. The Cy7-CA, Cy7-C12 to Cy7-OLA with increasing hydrophobicity or Cy7-$PLGA_{2k}$ with higher miscibility as acceptor and Cy5.5-PLGA as donor were encapsulated into PEG-PLGA nanoparticles for whole body imaging by IVIS; while Cy5-X (X= C12, OLA, or $PLGA_{2k}$) and Cy3.5-PLGA were used to investigate the drug release kinetics in the vasculature in real time by intravital CLSM on a window chamber mouse model. All three model drugs exhibited a burst in drug release with a sharp FRET ratio reduction at the beginning. The dissociation rates of drug-carrier followed the order: C12> OLA> $PLGA_{2k}$, which is in the same order of their hydrophobicity and miscibility. They further demonstrated that either improving the miscibility or increasing the hydrophobicity of drug resulted in stronger drug-carrier associations and slower drug release in circulation, enhanced drug delivery efficiency in tumour, and improved antitumour effects. Therefore, the properties of drug-carrier, like hydrophobicity and miscibility, could significantly influence the stability, drug release, delivery efficiency, and therapeutic effect of drug nanocarriers *in vivo*. Interestingly, our previous work has utilised a visible and dynamic zebrafish model [28] with FRET to demonstrate that small-sized mPEG-PLGA nanoparticles were gradually dissociated with time. And the mPEG–PLGA nanoparticles of Schisantherin A enhanced the blood-brain barrier delivery efficiency and anti-parkinsonian activity.

FRET has also been widely used to monitor the dynamic changes of environment responsive functional polymeric nanoparticles *in vivo*. For instance, polymeric nanoparticles crosslinked by disulfide bonds have been used to stabilise nanomedicine in circulation and control drug release in reductive environment in cancer cells, as demonstrated perfectly by FRET [43,52]. Lee et al. [43] synthesised DOX mPEG-$(Cys)_4$-PDLLA nanoparticles (DS), crosslinked by disulfide bonds, and investigated their fate *in vivo* by FRET imaging and compared their anti-tumour activity with self-assembled non-crosslinked mPEG-PDLLA micelles (SA) (Fig. 13A). The DiO and DiI were encapsulated into the core to monitor the integrity and drug release kinetics of SA and DS NPs by FRET imaging in the blood vessels of the ear lobes after tail vein injection. As shown in Fig. 13B, the FRET ratio of SA micelles in bloodstream rapidly decreased, indicating that polymeric micelles were easy to disassemble in bloodstreams and lost their drug contents. In contrast, the FRET ratio of DS NPs in bloodstream slowly decreased due to the stabilisation by disulfide bond crosslinking (Fig. 13C). However, in the reductive environment of tumour cells, that have high glutathione (GSH) concentration, the FRET ratio also rapidly decreased to 0.31 at 6 h (Fig. 13D and E). In addition, DS NPs remained intact with a strong FRET signal in tumour free tissues, like liver, spleen, lung, and kidney (Fig. 13F). The blood-stable and tumour-adaptable DS NPs significantly enhanced the long circulation and anti-cancer effect of the drug *in vivo*, which inhibited tumour growth in mice (Fig. 13G and H). FRET analysis showed that the DS nanoparticles were stable in blood and retained the drug contents in the NP core during circulation *in vivo*, then disassociated and triggered drug release in response to the high GSH levels in cancer cells. Except for the GSH responsive disulfide bond crosslinked polymeric nanoparticles, pH [147], reactive oxygen species (ROS) [144], and enzyme [145,146] responsive polymeric nanoparticles and thermosensitive hydrogels [150] were also evaluated by FRET to verify their environment responsive drug release properties and biodistribution. Therefore, these series of FRET methods are powerful for probing the biofate of drug nanocarriers.

5.2.3. Lipid-based nanocarriers

Due to the low toxicity, good biocompatibility, biodegradability, and drug encapsulation capability, lipid-based nanocarriers are widely used as potential carriers for drug delivery. These generally include lipid nanoparticles, lipid nano-emulsions, lipid nano-capsules, and liposomes. Although many lipid-based drug nanocarriers have been applied in clinic, such as liposomes, emulsions, and solid lipid nanoparticles, the understanding of their biofate *in vivo* is still very poor. At present, some studies have been carried out to reveal the biofate of lipid-based nanocarriers by FRET, which would help to guide the development of lipid-based drug nanocarriers.

Compared with polymeric nanoparticles, lipid-based nanocarriers are relatively soft and friable, especially in the presence of rapid blood streams and in the presence of all kinds of physical interactions with lipids, proteins, and enzymes under *in vivo* environments. Because of the fact that lipid-based nanocarriers can exchange components with lipids and proteins, they are easily degraded by enzymes *in vivo* [165]. Zhao et al. developed QD-based lipid nanoparticles for a FRET-based

Fig. 10. Integrity of PEG-PCL polymeric micelles in the intestine of adult zebrafish by FRET after oral administration. (A) Diagram of the FRET 7pep-DiO–DiI-Micelle and reported their integrity by change in their emission; (B) Confocal fluorescence microscopy analysis of the intestine of adult zebrafish after oral administration of 7pep–DiO–DiI–micelle at 1, 2, and 4 h. DiO and FRET channel were observed using excitation wavelength of 488 nm. Emission wavelengths between 500 and 530 were used for DiO channel imaging. Emission wavelengths between 580 and 650 nm were used for FRET channel imaging. The excitation wavelength of confocal lambda scan was 488 nm and λ-scan range was from 500 to 700 nm. Scale bar: 25 and 50 μm. (C–E) Spectral analysis of 12 ROIs at 1, 2, and 4 h; arrows indicate λ DiO_{em} (530 nm). (F) Monitoring of fluorescence of micelles during the intestinal absorption. Emission intensities of donor (530 nm) and acceptor (572 nm) and FRET ratios were shown as the mean from the ROIs. Adapted with permission from [140]. Copyright (2018) American Chemical Society.

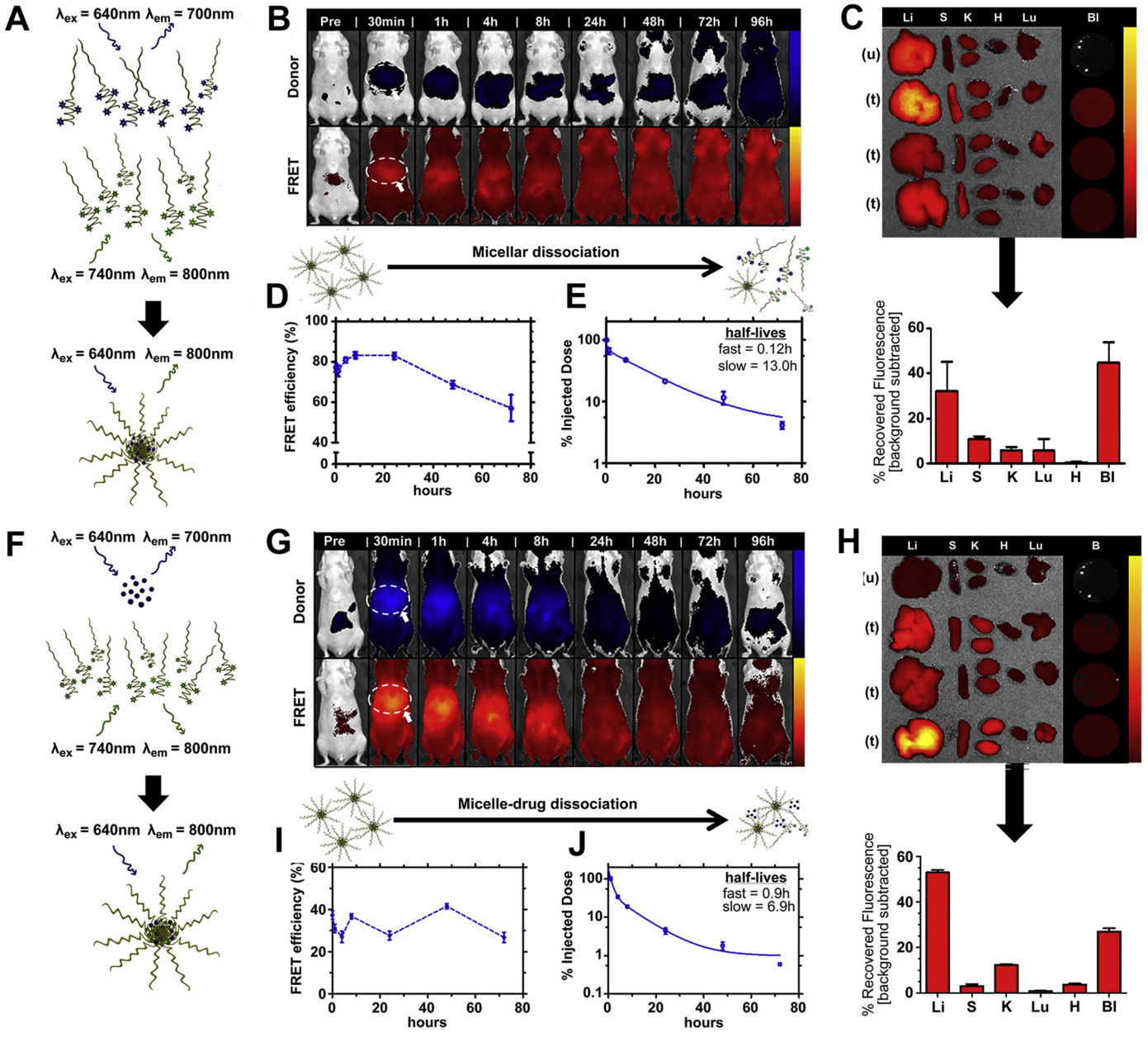

Fig. 11. Biological behaviour of blank and drug-loaded micelle formulations *in vivo* by FRET. (A) FRET blank micelles prepared on the basis of independently fluorophore conjugated unimers mixed in equivalent ratio and (F) drug-loaded micelles on the basis of fluorophore-conjugated unimers with an encapsulated FRET pair as model drug. The biodistribution of FRET (B) blank micelles and (G) drug-loaded micelles in whole body of mice imaged using IVIS imaging. Top row corresponds to the donor fluorescent channel, $\lambda_{ex} = 640$ nm, $\lambda_{em} = 700$ nm; bottom row corresponds to FRET fluorescent channel, $\lambda_{ex} = 640$ nm, $\lambda_{em} = 800$ nm. Liver association is identified (circle and arrow) in the first image displayed post-systemic administration for reference. Biodistribution of (C) blank micelles after 24 h and (H) drug-loaded micelles after 8 h ($n = 3$). Liver (Li), Spleen (S), Kidneys (K), Heart (H), Lungs (Lu), and Blood (Bl) extracted for each FRET micelle treatment and an untreated control for autofluorescence background. Below the image is quantification of recovered fluorescence (units of radiant efficiency) following background subtraction of autofluorescence from the untreated control. FRET efficiency of (D) blank micelles and (I) drug-loaded micelles in circulation as a function of time (determined from live-animal bleeds following systemic administration). Initial FRET efficiency reported as that obtained immediately following doping of blood collected from an untreated animal with the micelle formulation. Data represents mean ± SEM. Circulation profile of FRET (E) blank micelles and (J) drug-loaded micelles, displaying percent of injected dose fluorescence recovered as a function of time. Adapted with permission from [142]. Copyright (2014) Elsevier.

monitoring of the disassembly kinetics of self-assembled lipid nanoparticles in real time, by *in vivo* FRET imaging after intravenous administration [62]. The QDs were coated with dye-DMPE and PEG-DSPE monolayers. Two kinds of FRET lipid nanoparticles were synthesised for IVIS and CLSM imaging, respectively. The QD710-Cy7-PEG lipid NPs were used for whole body live imaging using a Xenogen IVIS Spectrum imaging system. The FRET signal was observed in the whole body and the NPs accumulated in the tumour as early as 30 min post-injection. The quenching of FRET emission and de-quenching of QDs in the tumour site and *ex vivo* organs revealed the disassociation of Cy7-lipid from QDs. The Cy7-lipids were mostly taken up by the kidneys and liver for subsequent renal clearance. In addition, the lipid NPs were also drained from the tumour and migrated to inguinal lymph nodes, within minutes, and disassembled gradually after injecting into the periphery of solid tumours in nude mice. Then, the QD cores were retained in the inguinal lymph nodes and lipids were excluded which subsequently underwent renal clearance. To study the disassembly kinetics of lipid NPs in tumour blood vessels and tumour interstitium, by intravital CLSM, they synthesised another FRET-based lipid NPs, QD610-Cy5.5-PEG, with absorption at a shorter wavelength. Their study showed that most of the QD610-Cy5.5-PEG lipid-NPs were disassembled in the blood circulation after the initial 2 h, with the

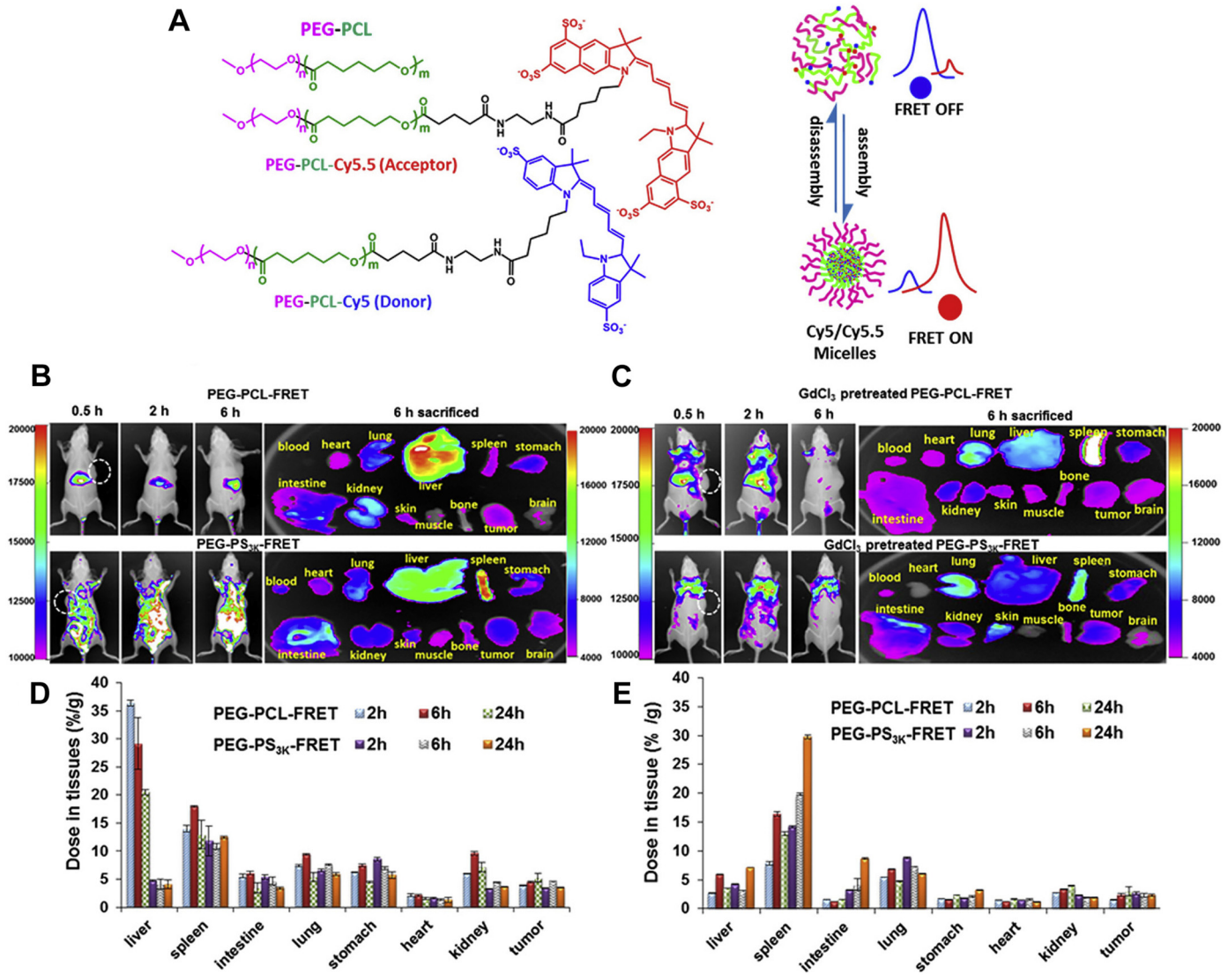

Fig. 12. *In vivo* behaviours of two different polymeric micelles (PEG-PCL and PEG-PS) by FRET. Design and working principle of the FRET micelles, (A) PEG-PCL with its PCL end conjugated with a FRET pair of Cy5 (donor) or Cy5.5 (acceptor). The *in vivo* imaging (B, C) and biodistribution (D, E) of PEG-PCL (or PS)-FRET i.v. injected in tumor-bearing nude mice without (B, D) or with (C, E) $GdCl_3$ pretreatment. (B) Mice were i.v. injected with PEG-PCL-FRET at 10 mg/kg and imaged at 0.5, 2, and 6 h and then sacrificed and dissected, and (D) the polymer concentration in each tissue was analyzed. (C) Mice were i.v. administered with $GdCl_3$ at 15 mg/kg at 48, 24, and 6 h prior to the injection of the polymer solution and then (E) analyzed as in (D). Data are reported as the mean (SD) for triplicate samples. The imaging was taken by the FRET fluorescence (Ex/Em = 640 nm/720 nm). Adapted with permission from [143]. Copyright (2018) American Chemical Society.

dissociation half-life of around 42 min. The disassembled QDs and Cy5.5-lipids were observed, obviously, in the tumour interstitium at 48 h. Therefore, the self-assembled lipid nanoparticles were concluded to be structurally dynamic, and that they dissociated in circulation through lipid exchange after intravenous administration.

Laine et al. systematically compared the behaviour of lipid nanoemulsions (LNEs), conventional lipid nanocapsules (LNCs), and one-step PEGylated stealth LNCs (OS LNCs) *in vivo* by FRET imaging [148]. The OS LNCs and LNEs exhibited a different biodistribution and a long circulation time with good structural stability for several hours, post-injection, compared with conventional LNCs. Especially the LNEs remained intact and stable in plasma for 24 h. Thus, lipid nanoemulsions are more stable in circulation than lipid nanoparticles, which is contrary to the common opinion that lipid nanoemulsions, as liquid systems, should not be stable enough after delivery into the body. In addition, FRET was also applied to monitor the integrity, disassembly kinetics, and delivery of liposomes [139,149]. Dai et al. demonstrated, by a two-step FRET, that liposomes and lipid disks traversed the blood–brain barrier (BBB) and the blood–brain tumour barrier (BBTB) in an intact form. In these experiments, DiO, DiI, and DiD were loaded into liposomes and lipid disks. The *ex vivo* and immune-histochemical FRET imaging suggested that liposomes and disks could traverse the BBB and BBTB *in vivo* in an intact form.

Notably, FRET has been used to quantify the integrity of drug nanocarriers *in vivo* [44,50,118]. Bouchaala and Mercier quantified the integrity of drug nanocarriers directly in blood circulation and tumour of living mice by FRET ratiometric imaging for the first time [118]. As the donor and acceptor respectively, Cy5.5 and Cy7.5 were encapsulated in the core of lipid nanoemulsions, which were prepared by the spontaneous emulsification of Labrafac WL and Cremophor ELP (Fig. 14A). Before quantitative analysis of the integrity of lipid nanoemulsions, it is required to calibrate the FRET ratio (A/(A+D)) response to the integrity (%) of lipid nanoemulsions, in the same imaging setup, *in vivo* (Fig. 14 B and C). Based on the calibration results, the FRET ratio images obtained in living mice, directly correlated with the integrity of lipid nanoemulsions *in vivo*. A strong FRET signal was observed in the tumour site by IVIS imaging after systemic administration, indicating that intact lipid nanoemulsions extensively accumulated in the tumour site

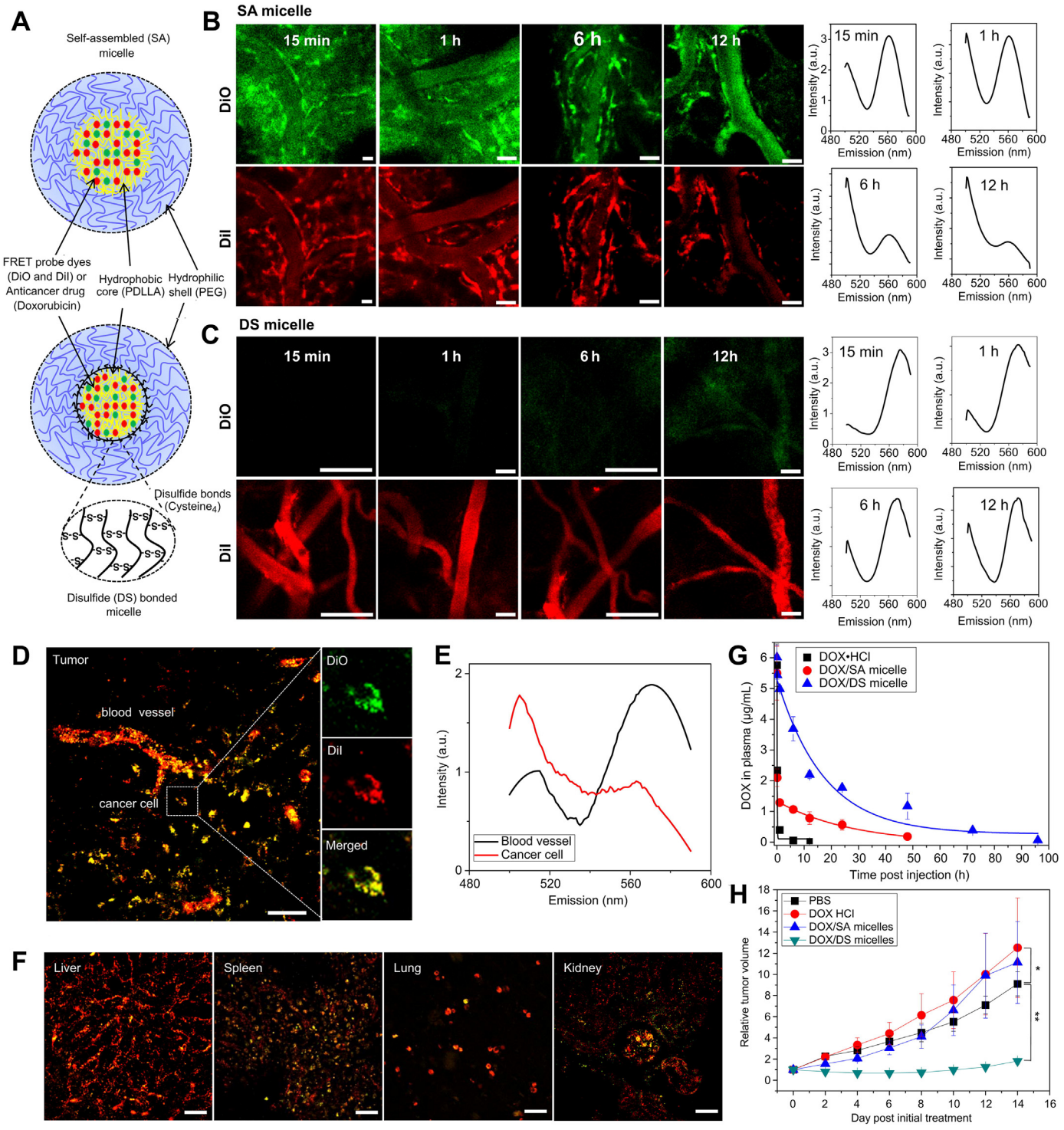

Fig. 13. Monitored the dynamic changes and biodistribution of SA and DS nanoparticels by FRET in vivo, and prolonged blood retention time and enhanced antitumor effects of DOX via DS micelles. (A) Schematic illustrations of self-assembled (SA) and disulfide (DS) bonded micelles with FRET dyes (DiO and DiI) or doxorubicin (DOX). In vivo real-time FRET imaging of blood vessels in mouse ears after i.v. injection of (B) SA or (C) DS FRET micelles. The green and red colors represent DiO and DiI signals (scale bar: 40 μm). Fluorescence spectra (right) of FRET micelles in the blood vessels were measured at different time points. The excitation was 488 nm. (D) Confocal FRET image of M109 tumor tissue at 6 h after i.v. injection of DS FRET micelles. The figure is the merged image of DiO (green) and DiI (red) channels. The yellow color indicates overlapped signals from both FRET dyes. (Scale bar: 40μm). High-magnification image (right image) of a single cancer cell with DiO (green), DiI (red), and merged channels are shown. (E) Fluorescence spectra of DS FRET micelles in blood vessel and cancer cell were measured. (F) FRET images of other tissues (liver, spleen, lung, and kidney). (Scale bar: 40 μm). (G) Blood retention kinetics of DOX·HCl, DOX loaded in SA and DS micelles in mice. DOX·HCl (at 4 mg/kg), DOX/SA and DOX/DS micelles (at 4 mg DOX equiv/kg) were intravenously injected. The data were fitted with a one-compartment model ($y = Ae^{(-x/t)} + y_0$) for DOX·HCl and DOX/DS micelle groups or a two-compartment model ($y = A_1e^{(-x/t1)} + A_2e^{(-x/t2)} + y_0$) for DOX/SA micelle group. Data are expressed as means ± SEM (n = 5). (H) Relative tumor volume (the ratio of tumor volume to initial size before treatment) for M109 tumor as a function of time. DOX·HCl (2 mg/kg), DOX/SA, and DOX/DS micelles (2 mg DOX Equiv/kg) were intravenously injected at Day 0 and 4. Data are expressed as means ± SEM (n = 6 - 8). *P > 0.1; **P < 0.005. Adapted with permission from [43]. Copyright (2012) Elsevier.

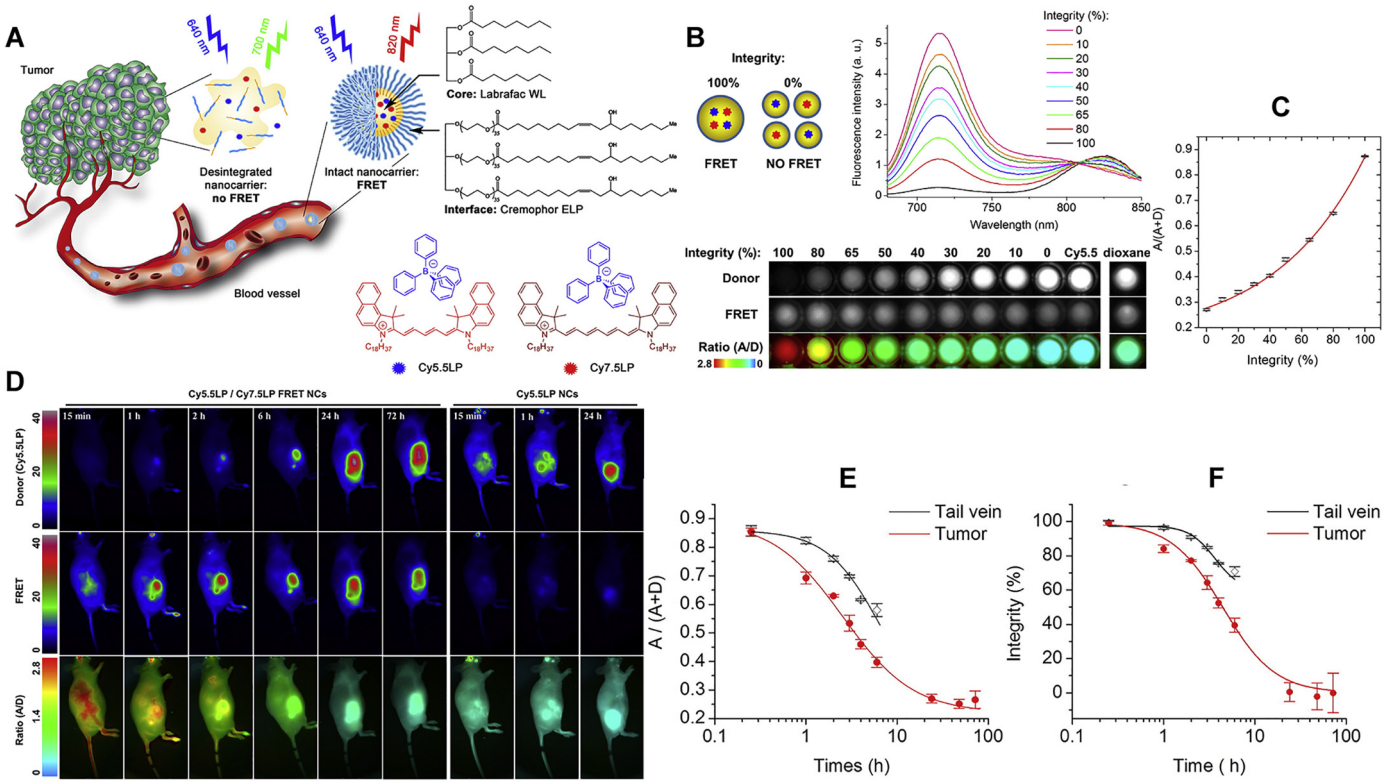

Fig. 14. Quantified integrity of lipid nanoemulsions in bloodstream and tumor by near-infrared ratiometric FRET imaging in living mice. (A) Concept of FRET nanocarriers reported on their integrity by change in their emission color. Chemical structures of oil Labrafac WL (medium chain triglyceride) and Cremophor ELP (PEGylated surfactant), as well as lipophilic cyanine 5.5 and 7.5 dyes (Cy5.5LP and Cy7.5LP) with their bulky hydrophobic counterions are showed. (B) Calibration of ratiometric *in vivo* images using mixtures of intact FRET nanocarriers with nanocarriers containing separately donor and acceptor at low concentration. The mixing is done to preserve the same concentration of dyes: 100% integrity corresponds to FRET nanocarriers (1% of Cy5.5LP and 1% of Cy7.5LP) diluted in PBS 1000-fold from the original formulation, while 0% integrity corresponds to a mixture of nanocarriers containing separately donor (0.1% of Cy5.5LP) and acceptor (0.1% Cy7.5LP), both diluted at 100-fold in PBS. The latter mixture models the disintegrated nanocarriers, where donor and acceptor separate and get diluted in the tissue. Fluorescence images of these mixtures acquired with the *in vivo* imaging set-up: donor (Cy5.5LP) channel (upper panels), acceptor (Cy7.5LP) FRET channel (middle panels), and the acceptor/donor ratio images (lower panels). Nanocarriers containing only donor dye (Cy5.5LP) and FRET NCs diluted 1000-fold in dioxane (second model of the complete disintegration) are also shown. (C) Calibration curve of A/(A + D) ratio vs the level of integrity of nanocarriers obtained based on data in (B) panel (n = 3). (D) FRET imaging of tumor-bearing nude mice at different times after injected with NIR-FRET lipid nanocarriers (1% of Cy5.5LP and Cy7.5LP each) or control nanocarriers with donor dye only (1% of Cy5.5LP dye). Upper panels present intensity images of the Cy5.5LP channel (700 nm), middle panels present images of Cy7.5LP channel (820 nm), while the lower panels present ratiometric images (acceptor/donor). The excitation wavelength was 630 nm. (E, F) Analysis of the A/(A + D) ratio (E) and integrity (F) of nanocarriers in different regions of tumor-bearing mice as a function of post-administration time. Three mice were analyzed, the error bars represent the standard error of the mean (n=3). Adapted with permission from [118]. Copyright (2016) Elsevier.

(Fig. 14D). A quantitative analysis of FRET imaging showed that 71% of the lipid nanoemulsions was intact in the blood circulation, 6 h post tail-vein injection, while only 40% were intact in the tumours (Fig. 14E and F). It also demonstrated that the lipid nanoemulsions synthesised only from oil (medium chain triglycerides) and a surfactant (Cremophor® ELP) maintained their integrity in blood stream for hours and showed remarkably efficient accumulation in tumours.

In summary, these FRET-based methods have demonstrated the biofate of different drug nanocarriers. The self-assembled polymeric micelles are relatively easy to disassemble and lose their drug content rapidly after systemic administration, which leads to a rapid clearance from the body. As a result, disassembly of polymeric micelles undoubtedly will influence drug delivery and therapeutic efficiency, especially for the targeted and functionalised polymeric micelles. Furthermore, the premature drug release of anti-cancer drugs may increase the non-specific toxicity to healthy organs. The main clearance mechanism of polymeric micelles from blood was that they were sequestered into the liver as unimers. Compared to polymeric micelles, polymeric nanoparticles and lipid-based nanoparticles were more stable, especially the environment responsive polymeric nanoparticles, which could achieve controlled drug release. Moreover, compatibility of drug with carriers is another important factor affecting stability, which needs to be considered in the future. Therefore, these *in vivo* biofate studies of drug nanocarriers will be helpful to develop *in vivo* stable and controlled release drug nanocarriers with long circulation to enhance drug delivery and therapeutic efficiency.

6. Conclusion and future perspective

Despite the emerging applications of nanomedicine for diagnosis and treatment, the intracellular fate of nanomedicines is largely unknown with respect to: a) whether nanomedicine disintegrates before internalisation into cells; b) whether nanomedicines retain their integrity after uptake into cells; and c) whether nanomedicines are transported across the epithelial barrier. Therefore, the loading of FRET pairs into nanocarriers or conjugating FRET pairs with polymers to form nanocarriers, has been widely used to address intracellular fate of drug nanocarriers, including interaction with cell membrane, intracellular itinerary and co-localisation, intracellular integrity monitoring, and transcellular integrity monitoring. Apart from intracellular integrity studies, FRET-based techniques can also track the *in vivo* delivery and biodistribution of drug nanocarriers, monitor their stability, integrity, and disassembly kinetics by non-invasive and real-time imaging. Since the *in vivo* environment that nanomedicines encounter is more dynamic and rigorous than that encountered *in vitro* when nanomedicines interact with cells, the ideal FRET pairs are expected

with high fluorescence intensity and good tissue penetration, good biocompatibility and selectivity, low toxicity and high intracellular targeting. Compared with other fluorescence labelling techniques which are always on, FRET technology can distinguish the intact nanoparticles from disassembled nanoparticles with high sensitivity, as well as monitor disassembly kinetics of nanoparticles by changes in FRET signals. In clinical study, FRET-based bioassays have been extensively reviewed for their application for cancer biomarker determination in patients [166], where commonly utilized fluorescent organic dye molecules are usually replaced by functional fluorescent nanoprobes. For example, Wang and his co-workers has reported a polymer-based FRET approach to quantify DNA methylation levels of colon cancer-related genes in a Chinese population, which has demonstrated high accuracy and sensitivity for both colon cancer detection (86.3 and 86.7%) and for differential diagnosis (97.5 and 94%) [167]. However, no much clinical study of FRET technique for biofate study of nanomedicines have been reported so far. The new direction of bioluminescence resonance energy transfer (BRET) application in photodynamic therapy is to develop self-illuminating nanoparticles for both imaging and therapy for potential clinical translation in the future. For example, Zhang's group has synthesized a novel polymeric conjugate with a luminescent donor and a fluorescent acceptor for in-vivo luminescence imaging and photodynamic therapy in deep tissues. The microenvironment in inflammatory sites or in the tumour further trigger BRET to generate singlet oxygen to kill cancer cells [158]. Besides cancer therapy, Wang's group has reported a new modality activated by chemical molecules through BRET process to produce reactive oxygen species (ROS) for antifungal activities [168]. We believe that with more collaborations and efforts of multidiscipline scientists in chemistry, biological science and medical doctors to overcome limited depth of tissue penetration, external irradiation, poor targeting ability and biocompatibility of the FRET-based nanoparticles, FRET-based technique has bright clinical translation potential in cancer diagnosis and therapy as well as for other disease in the future.

Although FRET-based approaches have many advantages towards the evaluation of drug nanocarriers *in vivo*, there are still some limitations. Firstly, the lipophilic fluorescent dyes of FRET pairs released from the FRET nanoparticles may generate FRET again when they are 'accumulated' in intracellular cell membranes or same organs, which may lead to misjudgement in the integrity and disassembly kinetics of drug nanocarriers in quantification, because the FRET ratio is no longer proportional to the nanoparticle integrity. Therefore, strategies of covalently labelling hydrophilic dyes to FRET nanoparticles may be more reliable. Secondly, for IVIS FRET imaging, the difference in the penetration depth for different wavelengths of light would affect the precision of quantitative analysis. Furthermore, IVIS imaging can only detect the overall surface fluorescence but not that in the deep tissues. Therefore, FRET technology still needs further modifications to become a reliable approach and to increase its *in vivo* applications.

In the future, more reliable, sensitive, and selective covalent FRET pairs or conjugated pairs with polymers are required to reduce the interference from the biological ingredients, and to enhance optical penetration capabilities to detect structural changes of nanomedicines in deep tissues. For complementary and validation purposes, other methods reviewed in this theme issue are encouraged to compare with FRET-based methods to reveal intracellular and *in vivo* fate for the same drug nanocarriers in different animal models. Moreover, more clinical translational research should be performed to elucidate integrity and biofate of nanomedicines but not limited to cancer biomarker determination to further expand application of FRET-based techniques. Combined with FRET approach, Zebrafish has potential to become a new visible model providing information on integrity and biofate of nanomedicines in circulation and organs after incubation, oral delivery or injection, which will provide a fast and dynamic platform for nanomedicine development before extensive trials in rodents.

Acknowledgements

This work was financially supported through grants from the National Natural Science Foundation of China (No. 81528021, 81872809), the Guangdong Provincial Natural Science Foundation of China (2018A030310623), and a research grant from the University of Macau (MYRG2017-00200-ICMS), and the National Basic Research Program of China (2015CB932100). Authors would like to thank Dr. Ruibing Wang in University of Macau and Dr. Xiang Yi for their very helpful discussions.

References

[1] R. Juliano, Nanomedicine: is the wave cresting? Nat. Rev. Drug Discov. 12 (2013) 171–172.
[2] J. Bourquin, A. Milosevic, D. Hauser, R. Lehner, F. Blank, A. Petri-Fink, B. Rothen-Rutishauser, Biodistribution, clearance, and long-term fate of clinically relevant nanomaterials, Adv. Mater. 30 (2018), 1704307.
[3] D.M. Charron, G. Zheng, Nanomedicine development guided by FRET imaging, Nano Today 18 (2018) 124–136.
[4] N.T. Chen, S.H. Cheng, C.P. Liu, J.S. Souris, C.T. Chen, C.Y. Mou, L.W. Lo, Recent advances in nanoparticle-based Forster resonance energy transfer for biosensing, molecular imaging and drug release profiling, Int. J. Mol. Sci. 13 (2012) 16598–16623.
[5] T. Chen, C. Li, Y. Li, X. Yi, S.M. Lee, Y. Zheng, Oral delivery of a nanocrystal formulation of schisantherin a with improved bioavailability and brain delivery for the treatment of Parkinson's disease, Mol. Pharm. 13 (2016) 3864–3875.
[6] G. Bunt, F.S. Wouters, FRET from single to multiplexed signaling events, Biophys. Rev. 9 (2017) 119–129.
[7] X. Hu, J. Zhang, Z. Yu, Y. Xie, H. He, J. Qi, X. Dong, Y. Lu, W. Zhao, W. Wu, Environment-responsive aza-BODIPY dyes quenching in water as potential probes to visualize the in vivo fate of lipid-based nanocarriers, Nanomedicine 11 (2015) 1939–1948.
[8] X. Hu, X. Dong, Y. Lu, J. Qi, W. Zhao, W. Wu, Bioimaging of nanoparticles: the crucial role of discriminating nanoparticles from free probes, Drug Discov. Today 22 (2017) 382–387.
[9] Y. Xie, B. Shi, F. Xia, J. Qi, X. Dong, W. Zhao, T. Li, W. Wu, Y. Lu, Epithelia transmembrane transport of orally administered ultrafine drug particles evidenced by environment sensitive fluorophores in cellular and animal studies, J. Control. Release 270 (2018) 65–75.
[10] Y.F. Wang, T. Zhang, X.J. Liang, Aggregation-induced emission: lighting up cells, revealing life! Small 12 (2016) 6451–6477.
[11] X. Xue, Y. Zhao, L. Dai, X. Zhang, X. Hao, C. Zhang, S. Huo, J. Liu, C. Liu, A. Kumar, Spatiotemporal drug release visualized through a drug delivery system with tunable aggregation-induced emission, Adv. Mater. 26 (2014) 712–717.
[12] C. Wang, Z. Wang, X. Zhao, F. Yu, Y. Quan, Y. Cheng, H. Yuan, DOX loaded aggregation-induced emission active polymeric nanoparticles as a fluorescence resonance energy transfer traceable drug delivery system for self-indicating cancer therapy, Acta Biomater. 85 (2019) 218–228.
[13] T. Förster, Zwischenmolekulare energiewanderung und fluoreszenz, Ann. Phys. 437 (1948) 55–75.
[14] L. Ma, F. Yang, J. Zheng, Application of fluorescence resonance energy transfer in protein studies, J. Mol. Struct. 1077 (2014) 87–100.
[15] H. Sahoo, Förster resonance energy transfer – a spectroscopic nanoruler: principle and applications, J Photochem Photobiol C: Photochem Rev 12 (2011) 20–30.
[16] T. Ha, T.H. Enderle, D.F. Ogletree, D.S. Chemla, P.R. Selvin, S. Weiss, Probing the interaction between two single molecules: fluorescence resonance energy transfer between a single donor and a single acceptor, Proc. Natl. Acad. Sci. U. S. A. 93 (1996) 6264–6268.
[17] P. Wu, L. Brand, Resonance energy transfer: methods and applications, Anal. Biochem. 218 (1994) 1–13.
[18] A.J.P. Teunissen, C. Perez-Medina, A. Meijerink, W.J.M. Mulder, Investigating supramolecular systems using Forster resonance energy transfer, Chem. Soc. Rev. 47 (2018) 7027–7044.
[19] D.W. Piston, G.J. Kremers, Fluorescent protein FRET: the good, the bad and the ugly, Trends Biochem. Sci. 32 (2007) 407–414.
[20] J.F. Lovell, J. Chen, M.T. Jarvi, W.G. Cao, A.D. Allen, Y. Liu, T.T. Tidwell, B.C. Wilson, G. Zheng, FRET quenching of photosensitizer singlet oxygen generation, J. Phys. Chem. B 113 (2009) 3203–3211.
[21] J.A. Broussard, K.J. Green, Research techniques made simple: methodology and applications of Forster resonance energy transfer (FRET) microscopy, J. Invest. Dermatol. 137 (2017) e185–e191.
[22] M. Kuscu, O.B. Akan, Coverage and throughput analysis for FRET-based mobile molecular sensor/actor nanonetworks, Nano Communication Networks 5 (2014) 45–53.
[23] B. Hochreiter, A.P. Garcia, J.A. Schmid, Fluorescent proteins as genetically encoded FRET biosensors in life sciences, Sensors (Basel) 15 (2015) 26281–26314.
[24] J. Garcia-Amoros, S. Tang, Y. Zhang, E.R. Thapaliya, F.M. Raymo, Self-assembling nanoparticles of amphiphilic polymers for in vitro and in vivo FRET imaging, Top. Curr. Chem. 370 (2016) 29–59.

[25] K.J. Chen, Y.L. Chiu, Y.M. Chen, Y.C. Ho, H.W. Sung, Intracellularly monitoring/imaging the release of doxorubicin from pH-responsive nanoparticles using Förster resonance energy transfer, Biomaterials 32 (2011) 2586–2592.
[26] C.H. Lee, S.H. Cheng, I.P. Huang, J.S. Souris, C.S. Yang, C.Y. Mou, L.W. Lo, Intracellular pH-responsive mesoporous silica nanoparticles for the controlled release of anticancer chemotherapeutics, Angew. Chem. Int. Ed. Eng. 49 (2010) 8214–8219.
[27] H.L. Pu, W.L. Chiang, B. Maiti, Z.X. Liao, Y.C. Ho, M.S. Shim, E.Y. Chuang, Y. Xia, H.W. Sung, Nanoparticles with dual responses to oxidative stress and reduced pH for drug release and anti-inflammatory applications, ACS Nano 8 (2014) 1213–1221.
[28] T. Chen, C. Li, Y. Li, X. Yi, R. Wang, S.M. Lee, Y. Zheng, Small-sized mPEG-PLGA nanoparticles of schisantherin A with sustained release for enhanced brain uptake and anti-Parkinsonian activity, ACS Appl. Mater. Interfaces 9 (2017) 9516–9527.
[29] E. De Filippo, A.C. Schiedel, P. Manga, Interaction between G protein-coupled receptor 143 and tyrosinase: implications for understanding ocular albinism type 1, J. Invest. Dermatol. 137 (2017) 457–465.
[30] Y. Li, X. Miao, T. Chen, X. Yi, R. Wang, H. Zhao, S.M. Lee, X. Wang, Y. Zheng, Zebrafish as a visual and dynamic model to study the transport of nanosized drug delivery systems across the biological barriers, Colloids Surf. B: Biointerfaces 156 (2017) 227–235.
[31] R. Roy, S. Hohng, T. Ha, A practical guide to single-molecule FRET, Nat. Methods 5 (2008) 507–516.
[32] M. Levitus, S. Ranjit, Cyanine dyes in biophysical research: the photophysics of polymethine fluorescent dyes in biomolecular environments, Q. Rev. Biophys. 44 (2011) 123–151.
[33] A.S. Klymchenko, R. Kreder, Fluorescent probes for lipid rafts: from model membranes to living cells, Chem. Biol. 21 (2014) 97–113.
[34] T. Kowada, H. Maeda, K. Kikuchi, BODIPY-based probes for the fluorescence imaging of biomolecules in living cells, Chem. Soc. Rev. 44 (2015) 4953–4972.
[35] D. Mendez-Gonzalez, E. Lopez-Cabarcos, J. Rubio-Retama, M. Laurenti, Sensors and bioassays powered by upconverting materials, Adv. Colloid Interf. Sci. 249 (2017) 66–87.
[36] J. Saha, A.D. Roy, D. Dey, D. Bhattacharjee, A. Hu, Role of quantum dot in designing FRET based sensors, Materials Today: Proceedings 5 (2018) 2306–2313.
[37] Y.K. Kim, J.E. Lee, B. Ryplida, C.A. Choi, Z.A.I. Mazrad, G. Lee, S. Lee, I. In, J.H. Jeong, S.Y. Park, Redox-responsive FRET-based polymer dot with BODIPY for fluorescence imaging-guided chemotherapy of tumor, Eur. J. Pharm. Biopharm. 132 (2018) 200–210.
[38] F. Yan, Z. Bai, Y. Chen, F. Zu, X. Li, J. Xu, L. Chen, Ratiometric fluorescent detection of copper ions using coumarin-functionalized carbon dots based on FRET, Sensors Actuators B Chem. 275 (2018) 86–94.
[39] Y. Wu, S. Huang, F. Zeng, J. Wang, C. Yu, J. Huang, H. Xie, S. Wu, A ratiometric fluorescent system for carboxylesterase detection with AIE dots as FRET donors, Chem. Commun. 51 (2015) 12791–12794.
[40] W. Zhong, X. Zeng, J. Chen, Y. Hong, L. Xiao, P. Zhang, Photoswitchable fluorescent polymeric nanoparticles for rewritable fluorescence patterning and intracellular dual-color imaging with AIE-based fluorogens as FRET donors, Polym. Chem. 8 (2017) 4849–4855.
[41] T. Chen, Y. Li, C. Li, X. Yi, R. Wang, S.M. Lee, Y. Zheng, Pluronic P85/F68 micelles of baicalein could interfere with mitochondria to overcome MRP2-mediated efflux and offer improved anti-Parkinsonian activity, Mol. Pharm. 14 (2017) 3331–3342.
[42] C. Yu, B. He, M.H. Xiong, H. Zhang, L. Yuan, L. Ma, W.B. Dai, J. Wang, X.L. Wang, X.Q. Wang, Q. Zhang, The effect of hydrophilic and hydrophobic structure of amphiphilic polymeric micelles on their transport in epithelial MDCK cells, Biomaterials 34 (2013) 6284–6298.
[43] S.Y. Lee, S. Kim, J.Y. Tyler, K. Park, J.X. Cheng, Blood-stable, tumor-adaptable disulfide bonded mPEG-(Cys)4-PDLLA micelles for chemotherapy, Biomaterials 34 (2013) 552–561.
[44] J. Gravier, L. Sancey, S. Hirsjarvi, E. Rustique, C. Passirani, J.P. Benoit, J.L. Coll, I. Texier, FRET imaging approaches for in vitro and in vivo characterization of synthetic lipid nanoparticles, Mol. Pharm. 11 (2014) 3133–3144.
[45] D. Li, J. Zhuang, Y. Yang, D. Wang, J. Yang, H. He, W. Fan, A. Banerjee, Y. Lu, W. Wu, L. Gan, J. Qi, Loss of integrity of doxorubicin liposomes during transcellular transportation evidenced by fluorescence resonance energy transfer effect, Colloids Surf. B: Biointerfaces 171 (2018) 224–232.
[46] P. Zou, H. Chen, H.J. Paholak, D. Sun, Noninvasive fluorescence resonance energy transfer imaging of in vivo premature drug release from polymeric nanoparticles, Mol. Pharm. 10 (2013) 4185–4194.
[47] J. Yang, R. Zhang, D.C. Radford, J. Kopecek, FRET-trackable biodegradable HPMA copolymer-epirubicin conjugates for ovarian carcinoma therapy, J. Control. Release 218 (2015) 36–44.
[48] X. Wei, R. Dong, D. Wang, T. Zhao, Y. Gao, P. Duffy, X. Zhu, W. Wang, Supramolecular fluorescent nanoparticles constructed via multiple non-covalent interactions for the detection of hydrogen peroxide in cancer cells, Chemistry 21 (2015) 11427–11434.
[49] Y. Zhao, F. Fay, S. Hak, J. Manuel Perez-Aguilar, B.L. Sanchez-Gaytan, B. Goode, R. Duivenvoorden, C. de Lange Davies, A. Bjorkoy, H. Weinstein, Z.A. Fayad, C. Perez-Medina, W.J. Mulder, Augmenting drug-carrier compatibility improves tumour nanotherapy efficacy, Nat. Commun. 7 (2016), 11221.
[50] F. Cayre, S. Mura, B. Andreiuk, D. Sobot, S. Gouazou, D. Desmaele, A.S. Klymchenko, P. Couvreur, In vivo FRET imaging to predict the risk associated with hepatic accumulation of squalene-based prodrug nanoparticles, Adv. Healthc. Mater. 7 (2018), 1700803.
[51] M. Miteva, K.C. Kirkbride, K.V. Kilchrist, T.A. Werfel, H. Li, C.E. Nelson, M.K. Gupta, T.D. Giorgio, C.L. Duvall, Tuning PEGylation of mixed micelles to overcome intracellular and systemic siRNA delivery barriers, Biomaterials 38 (2015) 97–107.
[52] Y. Li, M.S. Budamagunta, J. Luo, W. Xiao, J.C. Voss, K.S. Lam, Probing of the assembly structure and dynamics within nanoparticles during interaction with blood proteins, ACS Nano 6 (2012) 9485–9495.
[53] T.A. Werfel, C. Swain, C.E. Nelson, K.V. Kilchrist, B.C. Evans, M. Miteva, C.L. Duvall, Hydrolytic charge-reversal of PEGylated polyplexes enhances intracellular unpackaging and activity of siRNA, J. Biomed. Mater. Res. A 104 (2016) 917–927.
[54] P. Zou, S.T. Stern, D. Sun, PLGA/liposome hybrid nanoparticles for short-chain ceramide delivery, Pharm. Res. 31 (2014) 684–693.
[55] J.A. Broussard, B. Rappaz, D.J. Webb, C.M. Brown, Fluorescence resonance energy transfer microscopy as demonstrated by measuring the activation of the serine/threonine kinase Akt, Nat. Protoc. 8 (2013) 265–281.
[56] A. Margineanu, J.J. Chan, D.J. Kelly, S.C. Warren, D. Flatters, S. Kumar, M. Katan, C.W. Dunsby, P.M. French, Screening for protein-protein interactions using Forster resonance energy transfer (FRET) and fluorescence lifetime imaging microscopy (FLIM), Sci. Rep. 6 (2016), 28186.
[57] E.S. Butz, M. Ben-Johny, M. Shen, P.S. Yang, L.J. Sang, M. Biel, D.T. Yue, C. Wahl-Schott, Quantifying macromolecular interactions in living cells using FRET two-hybrid assays, Nat. Protoc. 11 (2016) 2470–2498.
[58] M. Baumdick, M. Gelleri, C. Uttamapinant, V. Beranek, J.W. Chin, P.I.H. Bastiaens, A conformational sensor based on genetic code expansion reveals an autocatalytic component in EGFR activation, Nat. Commun. 9 (2018) 3847.
[59] R. Kreder, K.A. Pyrshev, Z. Darwich, O.A. Kucherak, Y. Mely, A.S. Klymchenko, Solvatochromic nile red probes with FRET quencher reveal lipid order heterogeneity in living and apoptotic cells, ACS Chem. Biol. 10 (2015) 1435–1442.
[60] Y. Wang, K. Zhou, G. Huang, C. Hensley, X. Huang, X. Ma, T. Zhao, B.D. Sumer, R.J. DeBerardinis, J. Gao, A nanoparticle-based strategy for the imaging of a broad range of tumours by nonlinear amplification of microenvironment signals, Nat. Mater. 13 (2014) 204–212.
[61] Y. Wang, C. Wang, Y. Li, G. Huang, T. Zhao, X. Ma, Z. Wang, B.D. Sumer, M.A. White, J. Gao, Digitization of endocytic pH by hybrid ultra-pH-sensitive nanoprobes at single-organelle resolution, Adv. Mater. 29 (2017) 1603794.
[62] Y. Zhao, I. van Rooy, S. Hak, F. Fay, J. Tang, L. Davies Cde, M. Skobe, E.A. Fisher, A. Radu, Z.A. Fayad, C. de Mello Donega, A. Meijerink, W.J. Mulder, Near-infrared fluorescence energy transfer imaging of nanoparticle accumulation and dissociation kinetics in tumor-bearing mice, ACS Nano 7 (2013) 10362–10370.
[63] S. Mura, J. Nicolas, P. Couvreur, Stimuli-responsive nanocarriers for drug delivery, Nat. Mater. 12 (2013) 991–1003.
[64] K. Katagiri, Y. Imai, K. Koumoto, T. Kaiden, K. Kono, S. Aoshima, Magnetoresponsive on-demand release of hybrid liposomes formed from Fe3O4 nanoparticles and thermosensitive block copolymers, Small 7 (2011) 1683–1689.
[65] V.A. Huu, J. Luo, J. Zhu, J. Zhu, S. Patel, A. Boone, E. Mahmoud, C. McFearin, J. Olejniczak, C. de Gracia Lux, J. Lux, N. Fomina, M. Huynh, K. Zhang, A. Almutairi, Light-responsive nanoparticle depot to control release of a small molecule angiogenesis inhibitor in the posterior segment of the eye, J. Control. Release 200 (2015) 71–77.
[66] J. Li, X. Yu, Y. Wang, Y. Yuan, H. Xiao, D. Cheng, X. Shuai, A reduction and pH dual-sensitive polymeric vector for long-circulating and tumor-targeted siRNA delivery, Adv. Mater. 26 (2014) 8217–8224.
[67] C.K. Wong, A.J. Laos, A.H. Soeriyadi, J. Wiedenmann, P.M. Curmi, J.J. Gooding, C.P. Marquis, M.H. Stenzel, P. Thordarson, Polymersomes prepared from thermoresponsive fluorescent protein-polymer bioconjugates: capture of and report on drug and protein payloads, Angew. Chem. Int. Ed. Eng. 54 (2015) 5317–5322.
[68] H. Akita, A. Kudo, A. Minoura, M. Yamaguti, I.A. Khalil, R. Moriguchi, T. Masuda, R. Danev, K. Nagayama, K. Kogure, H. Harashima, Multi-layered nanoparticles for penetrating the endosome and nuclear membrane via a step-wise membrane fusion process, Biomaterials 30 (2009) 2940–2949.
[69] J. Shi, P.W. Kantoff, R. Wooster, O.C. Farokhzad, Cancer nanomedicine: progress, challenges and opportunities, Nat. Rev. Cancer 17 (2017) 20–37.
[70] M.H. Kathawala, S.P. Khoo, T. Sudhaharan, X. Zhao, J.S.C. Loo, S. Ahmed, K.W. Ng, Fluorescence techniques used to measure interactions between hydroxyapatite nanoparticles and epidermal growth factor receptors, Biotechnol. J. 10 (2015) 171–179.
[71] E.M. Galvez, J. Pardo, Quantum dot bioconjugates: emerging tools with great potential to study protein interactions and dynamics by FRET, Int. J. Biomed. Nanosci. Nanotechnol. 2 (2011) 55–74.
[72] L. Wang, R. Yan, Z. Hao, L. Wang, J. Zeng, J. Bao, X. Wang, Q. Peng, Y. Li, Fluorescence resonant energy transfer biosensor based on upconversion-luminescent nanoparticles, Angew. Chem. Int. Ed. 44 (2005) 6054–6057.
[73] J. Shi, C. Chan, Y. Pang, W. Ye, F. Tian, J. Lyu, Y. Zhang, M. Yang, A fluorescence resonance energy transfer (FRET) biosensor based on graphene quantum dots (GQDs) and gold nanoparticles (AuNPs) for the detection of mecA gene sequence of Staphylococcus aureus, Biosens. Bioelectron. 67 (2015) 595–600.
[74] J. Barauskas, C. Cervin, M. Jankunec, M. Spandyreva, K. Ribokaite, F. Tiberg, M. Johnsson, Interactions of lipid-based liquid crystalline nanoparticles with model and cell membranes, Int. J. Pharm. 391 (2010) 284–291.
[75] B. He, Y. Shi, Y. Liang, A. Yang, Z. Fan, L. Yuan, X. Zou, X. Chang, H. Zhang, X. Wang, W. Dai, Y. Wang, Q. Zhang, Single-walled carbon-nanohorns improve biocompatibility over nanotubes by triggering less protein-initiated pyroptosis and apoptosis in macrophages, Nat. Commun. 9 (2018) 2393.
[76] G. Chen, I. Roy, C. Yang, P.N. Prasad, Nanochemistry and nanomedicine for nanoparticle-based diagnostics and therapy, Chem. Rev. 116 (2016) 2826–2885.
[77] I.L. Medintz, H.T. Uyeda, E.R. Goldman, H. Mattoussi, Quantum dot bioconjugates for imaging, labelling and sensing, Nat. Mater. 4 (2005) 435–446.
[78] S. Wilhelm, Perspectives for upconverting nanoparticles, ACS Nano 11 (2017) 10644–10653.

[79] F. Wang, R. Deng, J. Wang, Q. Wang, Y. Han, H. Zhu, X. Chen, X. Liu, Tuning upconversion through energy migration in core-shell nanoparticles, Nat. Mater. 10 (2011) 968–973.
[80] S.H.C. Askes, S. Bonnet, Solving the oxygen sensitivity of sensitized photon upconversion in life science applications, Nat. Rev. Chem. 2 (2018) 437–452.
[81] H. Li, H. Hu, D. Xu, Silver decahedral nanoparticles-enhanced fluorescence resonance energy transfer sensor for specific cell imaging, Anal. Chem. 87 (2015) 3826–3833.
[82] G. Hong, S.M. Tabakman, K. Welsher, H. Wang, X. Wang, H. Dai, Metal-enhanced fluorescence of carbon nanotubes, J. Am. Chem. Soc. 132 (2010) 15920–15923.
[83] B.M. Luby, D.M. Charron, C.M. MacLaughlin, G. Zheng, Activatable fluorescence: From small molecule to nanoparticle, Adv. Drug Deliv. Rev. 113 (2017) 97–121.
[84] F. Li, Y. Huang, Q. Yang, Z. Zhong, D. Li, L. Wang, S. Song, C. Fan, A graphene-enhanced molecular beacon for homogeneous DNA detection, Nanoscale 2 (2010) 1021–1026.
[85] I.L. Medintz, A.R. Clapp, H. Mattoussi, E.R. Goldman, B. Fisher, J.M. Mauro, Self-assembled nanoscale biosensors based on quantum dot FRET donors, Nat. Mater. 2 (2003) 630–638.
[86] T.T. Ruckh, C.G. Skipwith, W.D. Chang, A.W. Senko, V. Bulovic, P.O. Anikeeva, H.A. Clark, Ion-switchable quantum dot Forster resonance energy transfer rates in ratiometric potassium sensors, ACS Nano 10 (2016) 4020–4030.
[87] J. Qian, C. Wang, X. Pan, S. Liu, A high-throughput homogeneous immunoassay based on Forster resonance energy transfer between quantum dots and gold nanoparticles, Anal. Chim. Acta 763 (2013) 43–49.
[88] Z. Ding, J. Tan, G. Feng, Z. Yuan, C. Wu, X. Zhang, Nanoscale metal-organic frameworks coated with poly(vinyl alcohol) for ratiometric peroxynitrite sensing through FRET, Chem. Sci. 8 (2017) 5101–5106.
[89] Y. Ma, C. Zhang, P. Yang, X. Li, L. Tong, F. Huang, J. Yue, B. Tang, A CuO-functionalized NMOF probe with a tunable excitation wavelength for selective detection and imaging of H2S in living cells, Nanoscale 10 (2018) 15793–15798.
[90] M. Zhao, B. Li, P. Wang, L. Lu, Z. Zhang, L. Liu, S. Wang, D. Li, R. Wang, F. Zhang, Supramolecularly engineered NIR-II and upconversion nanoparticles in vivo assembly and disassembly to improve bioimaging, Adv. Mater. 30 (2018), e1804982.
[91] Z. Yang, K.Y. Loh, Y.T. Chu, R. Feng, N.S.R. Satyavolu, M. Xiong, S.M.N. Huynh, K. Hwang, L. Li, H. Xing, X. Zhang, Y.R. Chemla, M. Gruebele, Y. Lu, Optical control of metal ion probes in cells and zebrafish using highly selective DNAzymes conjugated to upconversion nanoparticles, J. Am. Chem. Soc. (2018) 17656–17665.
[92] W. Hu, Q. Chen, H. Li, Q. Ouyang, J. Zhao, Fabricating a novel label-free aptasensor for acetamiprid by fluorescence resonance energy transfer between NH2-NaYF4: Yb, Ho@SiO2 and Au nanoparticles, Biosens. Bioelectron. 80 (2016) 398–404.
[93] Q. Long, H. Li, Y. Zhang, S. Yao, Upconversion nanoparticle-based fluorescence resonance energy transfer assay for organophosphorus pesticides, Biosens. Bioelectron. 68 (2015) 168–174.
[94] S. Mayilo, M.A. Kloster, M. Wunderlich, A. Lutich, T.A. Klar, A. Nichtl, K. Kurzinger, F.D. Stefani, J. Feldmann, Long-range fluorescence quenching by gold nanoparticles in a sandwich immunoassay for cardiac troponin T, Nano Lett. 9 (2009) 4558–4563.
[95] C.C. Huang, H.T. Chang, Selective gold-nanoparticle-based "turn-on" fluorescent sensors for detection of mercury(II) in aqueous solution, Anal. Chem. 78 (2006) 8332–8338.
[96] Q. Yu, P. Gao, K.Y. Zhang, X. Tong, H. Yang, S. Liu, J. Du, Q. Zhao, W. Huang, Luminescent gold nanocluster-based sensing platform for accurate H2S detection in vitro and in vivo with improved anti-interference, Light Sci. Appl. 6 (2017), e17107.
[97] F. Wen, Y. Dong, L. Feng, S. Wang, S. Zhang, X. Zhang, Horseradish peroxidase functionalized fluorescent gold nanoclusters for hydrogen peroxide sensing, Anal. Chem. 83 (2011) 1193–1196.
[98] Q. Zeng, Q. Li, W. Ji, X. Bin, J. Song, Highly sensitive homogeneous immunoassays based on construction of silver triangular nanoplates-quantum dots FRET system, Sci. Rep. 6 (2016), 26534.
[99] A. Ahmad, K. Kern, K. Balasubramanian, Selective enhancement of carbon nanotube photoluminescence by resonant energy transfer, Chemphyschem 10 (2009) 905–909.
[100] V. Biju, T. Itoh, Y. Baba, M. Ishikawa, Quenching of photoluminescence in conjugates of quantum dots and single-walled carbon nanotube, J. Phys. Chem. B 110 (2006) 26068–26074.
[101] H. Chang, L. Tang, Y. Wang, J. Jiang, J. Li, Graphene fluorescence resonance energy transfer aptasensor for the thrombin detection, Anal. Chem. 82 (2010) 2341–2346.
[102] J.H. Jung, D.S. Cheon, F. Liu, K.B. Lee, T.S. Seo, A Graphene Oxide Based Immunobiosensor for Pathogen Detection, Angew. Chem. Int. Ed. 49 (2010) 5708–5711.
[103] G. Pagona, A.S.D. Sandanayaka, Y. Araki, J. Fan, N. Tagmatarchis, G. Charalambidis, A.G. Coutsolelos, B. Boitrel, M. Yudasaka, S. Iijima, O. Ito, Covalent functionalization of carbon nanohorns with porphyrins: nanohybrid formation and photoinduced electron and energy transfer, Adv. Funct. Mater. 17 (2007) 1705–1711.
[104] S. Zhu, S. Han, L. Zhang, S. Parveen, G. Xu, A novel fluorescent aptasensor based on single-walled carbon nanohorns, Nanoscale 3 (2011) 4589–4592.
[105] T. Förster, 10th Spiers Memorial Lecture. Transfer mechanisms of electronic excitation, Diss. Faraday Soc. 27 (1959) 7–17.
[106] J.P. Magnusson, F. Fernandez-Trillo, G. Sicilia, S.G. Spain, C. Alexander, Programmed assembly of polymer-DNA conjugate nanoparticles with optical readout and sequence-specific activation of biorecognition, Nanoscale 6 (2014) 2368–2374.
[107] K. Zhou, Y. Wang, X. Huang, K. Luby-Phelps, B.D. Sumer, J. Gao, Tunable, ultrasensitive pH-responsive nanoparticles targeting specific endocytic organelles in living cells, Angew. Chem. Int. Ed. 50 (2011) 6109–6114.
[108] A.O. Moughton, R.K. O'Reilly, Noncovalently connected micelles, nanoparticles, and metal-functionalized nanocages using supramolecular self-assembly, J. Am. Chem. Soc. 130 (2008) 8714–8725.
[109] S. Mandal, J. Kuchlyan, D. Banik, S. Ghosh, C. Banerjee, V. Khorwal, N. Sarkar, Ultrafast FRET to study spontaneous micelle-to-vesicle transitions in an aqueous mixed surface-active ionic-liquid system, Chemphyschem 15 (2014) 3544–3553.
[110] Q. Zhang, D. Dehaini, Y. Zhang, J. Zhou, X. Chen, L. Zhang, R.H. Fang, W. Gao, L. Zhang, Neutrophil membrane-coated nanoparticles inhibit synovial inflammation and alleviate joint damage in inflammatory arthritis, Nat. Nanotechnol. 13 (2018) 1182–1190.
[111] Y.T. Sato, K. Umezaki, S. Sawada, S.A. Mukai, Y. Sasaki, N. Harada, H. Shiku, K. Akiyoshi, Engineering hybrid exosomes by membrane fusion with liposomes, Sci. Rep. 6 (2016), 21933.
[112] J.C. Azcarate, S.A. Diaz, J.A. Fauerbach, F. Gillanders, A.A. Rubert, E.A. Jares-Erijman, T.M. Jovin, M.H. Fonticelli, ESIPT and FRET probes for monitoring nanoparticle polymer coating stability, Nanoscale 9 (2017) 8647–8656.
[113] S. Ganta, H. Devalapally, A. Shahiwala, M. Amiji, A review of stimuli-responsive nanocarriers for drug and gene delivery, J. Control. Release 126 (2008) 187–204.
[114] S.J. Seo, M. Chen, H. Wang, M.S. Kang, K.W. Leong, H.W. Kim, Extra- and intracellular fate of nanocarriers under dynamic interactions with biology, Nano Today 14 (2017) 84–99.
[115] L.A. Lane, X. Qian, A.M. Smith, S. Nie, Physical chemistry of nanomedicine: understanding the complex behaviors of nanoparticles in vivo, Annu. Rev. Phys. Chem. 66 (2015) 521–547.
[116] S.Y. Lee, S. Kim, J.Y. Tyler, K. Park, J.X. Cheng, Blood-stable, tumor-adaptable disulfide bonded mPEG-(Cys)(4)-PDLLA micelles for chemotherapy, Biomaterials 34 (2013) 552–561.
[117] J. Sun, F. Cui, R. Zhang, Z. Gao, J. Ji, Y. Ren, F. Pi, Y. Zhang, X. Sun, Comet-like Heterodimers "gold nanoflower @graphene quantum dots" probe with FRET "Off" to DNA circuit signal "On" for sensing and imaging microRNA in vitro and in vivo, Anal. Chem. 90 (2018) 11538–11547.
[118] R. Bouchaala, L. Mercier, B. Andreiuk, Y. Mely, T. Vandamme, N. Anton, J.G. Goetz, A.S. Klymchenko, Integrity of lipid nanocarriers in bloodstream and tumor quantified by near-infrared ratiometric FRET imaging in living mice, J. Control. Release 236 (2016) 57–67.
[119] X. Guo, L. Wang, K. Duval, J. Fan, S. Zhou, Z. Chen, Dimeric drug polymeric micelles with acid-active tumor targeting and FRET-traceable drug release, Adv. Mater. 30 (2018) 1705436.
[120] L. Xiao, X. Xiong, X. Sun, Y. Zhu, H. Yang, H. Chen, L. Gan, H. Xu, X. Yang, Role of cellular uptake in the reversal of multidrug resistance by PEG-b-PLA polymeric micelles, Biomaterials 32 (2011) 5148–5157.
[121] T. Zhao, T. Li, Y. Liu, Silver nanoparticle plasmonic enhanced förster resonance energy transfer (FRET) imaging of protein-specific sialylation on the cell surface, Nanoscale 9 (2017) 9841–9847.
[122] C. Wang, Y. Wang, Y. Li, B. Bodemann, T. Zhao, X. Ma, G. Huang, Z. Hu, R.J. DeBerardinis, M.A. White, J. Gao, A nanobuffer reporter library for fine-scale imaging and perturbation of endocytic organelles, Nat. Commun. 6 (2015) 8524.
[123] L. Rajendran, H.J. Knolker, K. Simons, Subcellular targeting strategies for drug design and delivery, Nat. Rev. Drug Discov. 9 (2010) 29–42.
[124] A.E. Nel, L. Madler, D. Velegol, T. Xia, E.M. Hoek, P. Somasundaran, F. Klaessig, V. Castranova, M. Thompson, Understanding biophysicochemical interactions at the nano-bio interface, Nat. Mater. 8 (2009) 543–557.
[125] H.Y. Yang, Y. Fu, M.S. Jang, Y. Li, J.H. Lee, H. Chae, D.S. Lee, Multifunctional Polymer Ligand Interface CdZnSeS/ZnS Quantum Dot/Cy3-Labeled Protein Pairs as Sensitive FRET Sensors, ACS Appl. Mater. Interfaces 8 (2016) 35021–35032.
[126] B. Kulkarni, M. Jayakannan, Fluorescent-tagged biodegradable polycaprolactone block copolymer FRET probe for intracellular bioimaging in cancer cells, ACS Biomaterials Science & Engineering 3 (2017) 2185–2197.
[127] H. Lee, I.K. Kim, T.G. Park, Intracellular trafficking and unpacking of siRNA/quantum dot-PEI complexes modified with and without cell penetrating peptide: confocal and flow cytometric FRET analysis, Bioconjug. Chem. 21 (2010) 289–295.
[128] H. Chen, S. Kim, L. Li, S. Wang, K. Park, J.X. Cheng, Release of hydrophobic molecules from polymer micelles into cell membranes revealed by Forster resonance energy transfer imaging, Proc. Natl. Acad. Sci. U. S. A. 105 (2008) 6596–6601.
[129] S. Zhao, W. Dai, B. He, J. Wang, Z. He, X. Zhang, Q. Zhang, Monitoring the transport of polymeric micelles across MDCK cell monolayer and exploring related mechanisms, J. Control. Release 158 (2012) 413–423.
[130] J. Zhang, Y.C. Liang, X. Lin, X. Zhu, L. Yan, S. Li, X. Yang, G. Zhu, A.L. Rogach, P.K. Yu, P. Shi, L.C. Tu, C.C. Chang, X. Zhang, X. Chen, W. Zhang, C.S. Lee, Self-monitoring and self-delivery of photosensitizer-doped nanoparticles for highly effective combination cancer therapy in vitro and in vivo, ACS Nano 9 (2015) 9741–9756.
[131] Y. Wu, Y.P. Ho, Y. Mao, X. Wang, B. Yu, K.W. Leong, L.J. Lee, Uptake and intracellular fate of multifunctional nanoparticles: a comparison between lipoplexes and polyplexes via quantum dot mediated Forster resonance energy transfer, Mol. Pharm. 8 (2011) 1662–1668.
[132] E. Roger, J.C. Gimel, C. Bensley, A.S. Klymchenko, J.P. Benoit, Lipid nanocapsules maintain full integrity after crossing a human intestinal epithelium model, J. Control. Release 253 (2017) 11–18.
[133] N. Yoshinaga, T. Ishii, M. Naito, T. Endo, S. Uchida, H. Cabral, K. Osada, K. Kataoka, Polyplex micelles with phenylboronate/gluconamide cross-linking in the core exerting promoted gene transfection through spatiotemporal responsivity to intracellular pH and ATP concentration, J. Am. Chem. Soc. 139 (2017) 18567–18575.
[134] J. Lai, B.P. Shah, E. Garfunkel, K.B. Lee, Versatile fluorescence resonance energy transfer-based mesoporous silica nanoparticles for real-time monitoring of drug release, ACS Nano 7 (2013) 2741–2750.

[135] C. Zhao, X. Zhang, K. Li, S. Zhu, Z. Guo, L. Zhang, F. Wang, Q. Fei, S. Luo, P. Shi, H. Tian, W.H. Zhu, Forster resonance energy transfer switchable self-assembled micellar nanoprobe: ratiometric fluorescent trapping of endogenous H2S generation via fluvastatin-stimulated upregulation, J. Am. Chem. Soc. 137 (2015) 8490–8498.
[136] J.E. Tengood, I.S. Alferiev, K.H. Zhang, I. Fishbein, R.J. Levy, M. Chorny, Real-time analysis of composite magnetic nanoparticle disassembly in vascular cells and biomimetic media, Proc. Natl. Acad. Sci. U. S. A. 111 (2014) 4245–4250.
[137] T. Skajaa, Y.M. Zhao, D.J. van den Heuvel, H.C. Gerritsen, D.P. Cormode, R. Koole, M.M. van Schooneveld, J.A. Post, E.A. Fisher, Z.A. Fayad, C.D. Donega, A. Meijerink, W.J.M. Mulder, Quantum dot and Cy5.5 labeled nanoparticles to investigate lipoprotein biointeractions via Forster resonance energy transfer, Nano Lett. 10 (2010) 5131–5138.
[138] D. Xia, Y. He, Q. Li, C. Hu, W. Huang, Y. Zhang, F. Wan, C. Wang, Y. Gan, Transport mechanism of lipid covered saquinavir pure drug nanoparticles in intestinal epithelium, J. Control. Release 269 (2018) 159–170.
[139] T. Dai, K. Jiang, W. Lu, Liposomes and lipid disks traverse the BBB and BBTB as intact forms as revealed by two-step Förster resonance energy transfer imaging, Acta Pharm. Sin. B 8 (2018) 261–271.
[140] Y. Li, X. Song, X. Yi, R. Wang, S.M. Lee, X. Wang, Y. Zheng, Zebrafish: A visual model to evaluate the biofate of transferrin receptor-targeted 7peptide-decorated coumarin 6 micelles, ACS Appl. Mater. Interfaces 9 (2017) 39048–39058.
[141] H. Chen, S. Kim, W. He, H. Wang, P.S. Low, K. Park, J.X. Cheng, Fast release of lipophilic agents from circulating PEG-PDLLA micelles revealed by in vivo Forster resonance energy transfer imaging, Langmuir 24 (2008) 5213–5217.
[142] S.W. Morton, X. Zhao, M.A. Quadir, P.T. Hammond, FRET-enabled biological characterization of polymeric micelles, Biomaterials 35 (2014) 3489–3496.
[143] X. Sun, G. Wang, H. Zhang, S. Hu, X. Liu, J. Tang, Y. Shen, The blood clearance kinetics and pathway of polymeric micelles in cancer drug delivery, ACS Nano 12 (2018) 6179–6192.
[144] G. Chen, H.Z. Deng, X. Song, M.Z. Lu, L. Zhao, S. Xia, G.X. You, J.X. Zhao, Y.L. Zhang, A.J. Dong, H. Zhou, Reactive oxygen species-responsive polymeric nanoparticles for alleviating sepsis-induced acute liver injury in mice, Biomaterials 144 (2017) 30–41.
[145] C.E. Callmann, C.V. Barback, M.P. Thompson, D.J. Hall, R.F. Mattrey, N.C. Gianneschi, Therapeutic enzyme-responsive nanoparticles for targeted delivery and accumulation in tumors, Adv. Mater. 27 (2015) 4611–4615.
[146] M.P. Chien, M.P. Thompson, C.V. Barback, T.H. Ku, D.J. Hall, N.C. Gianneschi, Enzyme-directed assembly of a nanoparticle probe in tumor tissue, Adv. Mater. 25 (2013) 3599–3604.
[147] J.C. Yu, Y.L. Chen, Y.Q. Zhang, X.K. Yao, C.G. Qian, J. Huang, S. Zhu, X.Q. Jiang, Q.D. Shen, Z. Gu, pH-Responsive and near-infrared-emissive polymer nanoparticles for simultaneous delivery, release, and fluorescence tracking of doxorubicin in vivo, Chem. Commun. 50 (2014) 4699–4702.
[148] A.L. Laine, J. Gravier, M. Henry, L. Sancey, J. Bejaud, E. Pancani, M. Wiber, I. Texier, J.L. Coll, J.P. Benoit, C. Passirani, Conventional versus stealth lipid nanoparticles: Formulation and in vivo fate prediction through FRET monitoring, J. Control. Release 188 (2014) 1–8.
[149] K.K. Ng, M. Takada, C.C. Jin, G. Zheng, Self-sensing porphysomes for fluorescence-guided photothermal therapy, Bioconjug. Chem. 26 (2015) 345–351.
[150] P. Huang, H. Song, Y. Zhang, J. Liu, Z. Cheng, X.J. Liang, W. Wang, D. Kong, J. Liu, FRET-enabled monitoring of the thermosensitive nanoscale assembly of polymeric micelles into macroscale hydrogel and sequential cognate micelles release, Biomaterials 145 (2017) 81–91.
[151] A. Wagh, S.Y. Qian, B. Law, Development of biocompatible polymeric nanoparticles for in vivo NIR and FRET imaging, Bioconjug. Chem. 23 (2012) 981–992.
[152] A. Wagh, F. Jyoti, S. Mallik, S. Qian, E. Leclerc, B. Law, Polymeric nanoparticles with sequential and multiple FRET cascade mechanisms for multicolor and multiplexed imaging, Small 9 (2013) 2129–2139.
[153] H. Zhu, Y. Fang, X. Zhen, N. Wei, Y. Gao, K.Q. Luo, C. Xu, H. Duan, D. Ding, P. Chen, K. Pu, Multilayered semiconducting polymer nanoparticles with enhanced NIR fluorescence for molecular imaging in cells, zebrafish and mice, Chem. Sci. 7 (2016) 5118–5125.
[154] M. Palner, K. Pu, S. Shao, J. Rao, Semiconducting polymer nanoparticles with persistent near-infrared luminescence for in vivo optical imaging, Angew. Chem. Int. Ed. Eng. 54 (2015) 11477–11480.
[155] X. Han, D.E. Liu, T. Wang, H. Lu, J. Ma, Q. Chen, H. Gao, Aggregation-induced-emissive molecule incorporated into polymeric nanoparticulate as FRET donor for observing doxorubicin delivery, ACS Appl. Mater. Interfaces 7 (2015) 23760–23766.
[156] M.K. So, C. Xu, A.M. Loening, S.S. Gambhir, J. Rao, Self-illuminating quantum dot conjugates for in vivo imaging, Nat. Biotechnol. 24 (2006) 339–343.
[157] N. Kosaka, M. Mitsunaga, S. Bhattacharyya, S.C. Miller, P.L. Choyke, H. Kobayashi, Self-illuminating in vivo lymphatic imaging using a bioluminescence resonance energy transfer quantum dot nano-particle, Contrast Media Mol. Imaging 6 (2011) 55–59.
[158] X. Xu, H. An, D. Zhang, H. Tao, Y. Dou, X. Li, J. Huang, J. Zhang, A self-illuminating nanoparticle for inflammation imaging and cancer therapy, Sci. Adv. 5 (2019) eaat2953.
[159] L. Xiong, A.J. Shuhendler, J. Rao, Self-luminescing BRET-FRET near-infrared dots for in vivo lymph-node mapping and tumour imaging, Nat. Commun. 3 (2012) 1193.
[160] G. Caracciolo, Liposome-protein corona in a physiological environment: challenges and opportunities for targeted delivery of nanomedicines, Nanomedicine 11 (2015) 543–557.
[161] S. Tenzer, D. Docter, J. Kuharev, A. Musyanovych, V. Fetz, R. Hecht, F. Schlenk, D. Fischer, K. Kiouptsi, C. Reinhardt, K. Landfester, H. Schild, M. Maskos, S.K. Knauer, R.H. Stauber, Rapid formation of plasma protein corona critically affects nanoparticle pathophysiology, Nat. Nanotechnol. 8 (2013) 772–781.
[162] M.P. Monopoli, C. Aberg, A. Salvati, K.A. Dawson, Biomolecular coronas provide the biological identity of nanosized materials, Nat. Nanotechnol. 7 (2012) 779–786.
[163] S. Kim, Y. Shi, J.Y. Kim, K. Park, J.X. Cheng, Overcoming the barriers in micellar drug delivery: loading efficiency, in vivo stability, and micelle-cell interaction, Expert Opin. Drug. Del. 7 (2010) 49–62.
[164] Y. Li, K. Xiao, J. Luo, W. Xiao, J.S. Lee, A.M. Gonik, J. Kato, T.A. Dong, K.S. Lam, Well-defined, reversible disulfide cross-linked micelles for on-demand paclitaxel delivery, Biomaterials 32 (2011) 6633–6645.
[165] P.M. Bummer, Physical chemical considerations of lipid-based oral drug delivery–solid lipid nanoparticles, Crit. Rev. Ther. Drug Carrier Syst. 21 (2004) 1–20.
[166] P. Das, A. Sedighi, U.J. Krull, Cancer biomarker determination by resonance energy transfer using functional fluorescent nanoprobes, Anal. Chim. Acta 1041 (2018) 1–24.
[167] Q. Yang, Y. Dong, W. Wu, C. Zhu, H. Chong, J. Lu, D. Yu, L. Liu, F. Lv, S. Wang, Detection and differential diagnosis of colon cancer by a cumulative analysis of promoter methylation, Nat. Commun. 3 (2012) 1206.
[168] H. Yuan, H. Chong, B. Wang, C. Zhu, L. Liu, Q. Yang, F. Lv, S. Wang, Chemical molecule-induced light-activated system for anticancer and antifungal activities, J. Am. Chem. Soc. 134 (2012) 13184–13187.